EA-77-A-01-6010-10
Distribution Category UC-90g

DEVELOPMENT, TESTING AND EVALUATION OF MHD-MATERIALS

Quarterly Report

for the period October - December 1977

H. P. R. Frederikse, T. Negas and S. J. Schneider

Inorganic Materials Division
Institute for Materials Research
National Bureau of Standards
Washington, D.C. 20234

Date Published: December 31, 1977

PREPARED FOR THE UNITED STATES
DEPARTMENT OF ENERGY

Under Contract No. EA-77-A-01-6010

TABLE OF CONTENTS

ABSTRACT

During this quarter work continued on preparation for the U-02 Phase III materials test to be held in Moscow early in 1978. Westinghouse Research and Development Laboratories held two Proof tests as precursors for this experiment. Two monitors from NBS were present for each test. Pre-test electrical conductivities and x-ray diffraction data on all candidate materials has been completed.

The post test characterization of the materials tested in the first proof test for U-02 Phase III has been completed and the final report issued. Analysis for materials in the second proof test is nearly completed.

A comprehensive program has started to determine the chemical and electro-chemical reactions involved at the boundaries between molten (and solid) slag and various electrode materials at different temperatures.

Electrodes of design based partly on the results of these experiments are being constructed for future tests at AVCO.

Further progress has been made on the seed-slag interaction problem including especially the relation between melt composition and temperature in partially crystallized slags.

The effect on viscosity caused by changes in concentration of each oxide of a five component slag at 1600 and 1300 °C are shown. Viscosity vs. temperature relationships are shown for slags from fly ash of a power plant at Bow, New Hampshire and slag from coal from the Montana Rosebud seam.

Vapor pressure measurements of K over a K_2O-SiO_2-Al_2O_3 glass having an SiO_2/Al_2O_3 weight ratio of 5 indicate an enhanced K_2O activity down to 20 w/o K_2O; measurements over a glass having an SiO_2/Al_2O_3 ratio of 2 show reduced activity as compared to K_2O-SiO_2 solution.

Diffusion of iron from iron containing electrode materials appears to be less in the insulator magnesium aluminate than in pure MgO under identical laboratory conditions.

Some 60 materials were analyzed by XRD. These materials included those submitted by industrial firms and other governmental laboratories as well as materials under study in the NBS materials program.

Two new activities were started in the first quarter of the new Fiscal Year (1978).

a. A beginning was made with the establishment of a center which will provide information on MHD materials and readily available data on their properties for design and operational purposes. Reports from various MHD contractors have been reviewed for the purpose of defining the requirements for a computer based data system to be used in the Data Center for MHD Materials. The assessment of downstream materials is part of the center activities. In the evaluation studies, the use of the unified numbering system (UNS) for metal alloy is described and an update of the requirement, test results and material recommendations for steam superheater tubing is given.

b. We have also started the construction of a hot corrosion test rig for the evaluation of candidate materials for the steam superheater tubing under conditions that simulate the environment in the downstream section.

OBJECTIVES AND SCOPE OF WORK

The overall objective of this program is to obtain chemical and physical definition of high temperature materials which have shown promise for use in coal-fired open-cycle MHD power systems. Major problem areas in which investigations will be concentrated are:

1. Characterization of coal slag and its effects on system components and performance at prototype temperatures.

2. Development of electrode materials which provide adequate performance over extended periods of time.

3. Insulating materials which limit thermal losses and are resistant to prolonged thermal and erosion effects.

4. Preheater materials which can withstand the operating modes of separately and directly fired operation.

5. Seed recovery methods from slag which are technically and economically feasible.

6. Phase equilibria and diffusion rates of seed in slag and the corrosive action of combination on system components and materials.

7. Durability of prototype MHD sub-systems.

The program is designed to contribute to the solution of these problems by providing much needed data on candidate materials and by evaluating test samples and structures that have been subjected to real or simulated MHD conditio The activities are grouped under six tasks:

G. Program Management Coordination (Assisting ERDA in coordination, planning and review of the various MHD-Materials Development Programs).

H. U-02 Materials Testing and Characterization (Coordination of U-02 Test Activities, Phase I). (Terminated June 30, 1976).

I. Operational Design Properties (viscosity, electrical conductivity, vaporization).

J. Corrosion by Seed and Slag (phase equilibria, diffusion).

K. Materials Testing and Characterization (test coordination, pre- and post-test analysis).

L. Assessment of Steam Plant Components (corrosion resistance of metals and alloys).

SUMMARY OF ACCOMPLISHMENTS (OCTOBER-DECEMBER 1977)
(Completed Milestones-See Work Plan FY 1978)

The results obtained during this first quarter (FY 78) are presented in terms of the projected milestones of the NBS-ERDA (DoE) Contract.

TASK I. 6. Measured viscosities of several slags furnished by MHD contractors.

9. Measured electrical conductivities of new promising electrode materials.

12. Measured K pressure over melts in the K_2O-SiO_2-Al_2O_3 system in the temperature range 1473-1873 K.

TASK J. 18. Determined electrochemical reaction processes of electrode materials ($LaCrO_3$, Pt) with seed/slag.

22. Conducted diffusion studies of iron containing spinel electrode-$MgAl_2O_4$ insulator sandwiches without electric field.

TASK K. 26. Monitored and proof tests of Phase III-U-02 electrode materials at Westinghouse R&D Laboratory, October 10, 11 and Nov. 17, 18.

27a. Phase III-U-02 proof test 1 pre- and post-test materials characterization completed.

b. Post-test analysis on MIT slagging electrode test completed.

TASK L. 30. Updated assessment of materials for the steam heat exchanger tubes to include new and promising alloys.

TALKS AND PUBLICATIONS

Phase Equilibria and Crystal Chemistry Related to Seed-Slag Reactions Under MHD Conditions. The System K_2O:Al_2O_3:Fe_2O_3:SiO_2, R. S. Roth, University of Wyoming, Laramie, Wyoming, Nov. 10, 1977. (Paper will be published later).

The System K_2O-Al_2O_3-Fe_2O_3-SiO_2. Part II, Crystal Chemistry of Phases on Joins $KFeO_2$-SiO_2 and $KAlSiO_2$-$KFeSiO_2$, R. S. Roth. Annual meeting of Geological Soc. of Am., Seattle, WA, Nov. 9, 1977.

Magnetic Susceptibility of Cerium Tantalate Compounds, G. A. Candela, A. H. Kahn, T. Negas, C. L. McDaniel, 13th Rare Earth Research Conf., Oglebay Park, Wheeling, WV, Oct. 1977.

Phase Relationships and Crystal Chemistry of Compounds Containing Cerium Oxide, R. S. Roth, T. Negas, H. S. Parker, D. B. Minor, C. D. Olson, C. Skarda, 13th Rare Earth Research Conf., Oglebay Park, Wheeling, WV, Oct. 1977.

Crystal Chemistry and Oxidation-Reduction of Phases in Rare Earth Tantalate-Niobate Systems., R. J. Cava, T. Negas, R.S. Roth, H. S. Parker, D. B. Minor and C. D. Olson, 13th Rare Earth Research Conf., Oglebay Park, Wheeling, WV, Oct. 1977.

Rare Earth Ceramics for MHD Power Generators, H. P. R. Frederikse, W. R. Hosler, and T. Negas, 13th Rare Earch Research Conf., Oglebay Park, Wheeling, WV, Oct. 1977.

SUMMARY OF PROGRESS

Task G. Program Management and Coordination (S. J. Schneider)

S. J. Schneider and other NBS staff participated in assorted DoE arranged or sanctioned program review/coordination meetings, briefings and technical conferences. These included:

1. U.S.-U.S.S.R. Technology Working group meeting, November 1977, Washington, D. C., S. J. Schneider.

2. U.S.-U.S.S.R. Steering Committee meeting, December 1977, Moscow. S. J. Schneider.

3. Montana Tech and MSU Program Review, December 1977, Butte and Bozeman, Montana. S. J. Schneider, T. Negas.

4. First International Meeting on Coal Conversion and Utilization, October 1977, at NBS, Gaithersburg, MD. (NBS was co-sponsor and host for conference; this involved meeting arrangements, program planning and lecture presentation).

5. 13th Rare Earth Research Conf., Oglebay Park, Wheeling, WV, Oct. 1977. H. Frederikse, T. Negas, R. Roth, G. Candela, D. Minor.

In addition, NBS hosts a number of visitors from MHD contractors and others interested in MHD. A noteworthy visit to NBS was made by Dr. J. P. Coutures, C.N.R.S., France. Dr. Coutures described his materials work especially that pertaining to his interaction with the IVTAN, USSR.

The conclusions and recommendations resulting from these meetings and other DoE assigned activities are reflected in reports to DoE, through direct consultation with DoE staff or through documents published elsewhere.

As part of NBS involvement in Phase III U-02 materials test, NBS monitored two proof tests at Westinghouse and performed post test analysis of exposed samples. Also NBS planned and performed an electrode test at AVCO (Mark VI, slagging). Results of these tests are documented elsewhere in this report.

T. Negas attended meeting at Westinghouse Research and Development Center to decide on electrodes to be utilized in Phase III U-02 test.

Task I. OPERATIONAL DESIGN PROPERTIES

1. Viscosity of Coal Slags (W. Capps and D. A. Kauffman, Inorganic Glass Secti

Introduction

Because of the increasing number of contractors involved in the development of open cycle, coal-fired MHD, and because of the increasing emphasis on two selected coals, a part of this task has concentrated on developing a means of predicting viscosity of coal slags as functions of ash analyses and temperature. Special attention has been given to the two selected coals, Montana Rosebud Seam and Illinois #6 Seam coals.

Slag Preparation and Viscosity Measurements

a. A series of synthetic slags was prepared, based on a large number of ash analyses available from Rosebud and Illinois #6 coals. Viscosity was measured on each composition from approximately 1600 C down to the onset of crystallization. These data are being used to develop a mathematical model suitable for the prediction of viscosity of slags from these two coals as functions of composition and temperature. Some of the results have been presented in previous reports as they have become available. Figure 1 shows at a glance the effect that each oxide has on the viscosity at 1600 C as the oxide is added to or subtracted from the reference or base slag composition. Figure 2 shows the viscosity-composition relationships for these same melts at 1300 C. There is noticeably less data at 1300 C than at 1600. The reason is that crystallization had commenced at 1300 C for many of these compositions and therefore no viscosity data was taken.

b. Viscosity of a power plant flyash from a New Hampshire coal was measured at the request of AVCO-Everett Labs. See Fig. 3, Curve 1.

c. Viscosity of a power plant flyash from a Montana Rosebud Seam coal was measured at the request of AVCO-Everett Labs. See Fig. 3, Curve 2.

d. A sample of the New Hampshire flyash was added to K_2CO_3 and remelted. The resulting slag composition was 80% flyash and 20% by weight of K_2O representing a seeded slag. This was prepared for W. R. Hosler and A. J. Armstrong for electrical conductivity measurements at NBS.

Future Plans

Viscosity data of the systematically varied series of synthetic coal slags will be used to find the best of several mathematical models for predictic of viscosity from coal ash analyses.

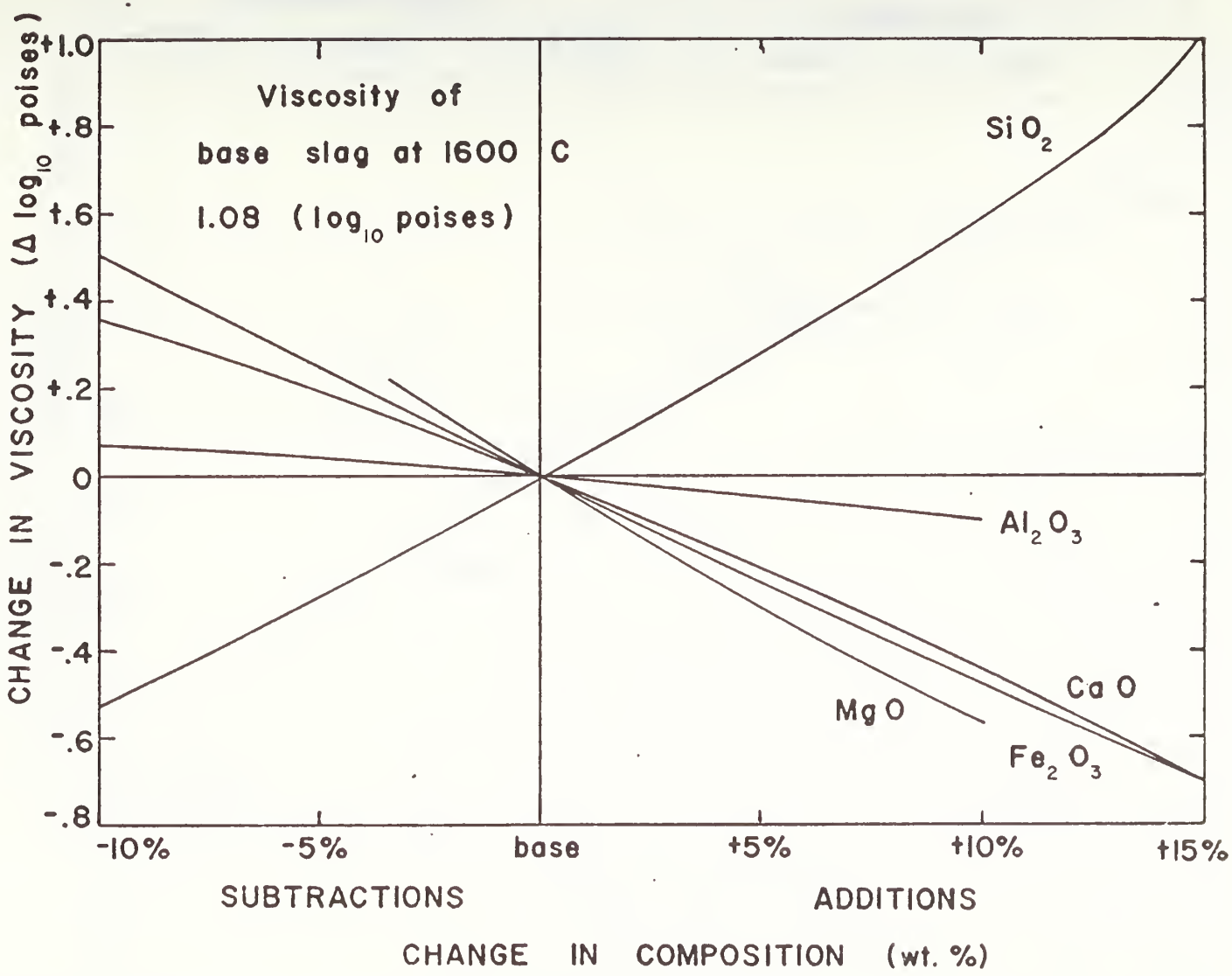

Fig. 1. The Effect of Change of Concentration of Each Oxide on the Viscosity of Base Slag K-884 at 1600 C.(47.8% SiO_2,21.8% Al_2O_3,16.6% Fe_2O_3, 10.6% CaO,3.3% MgO)

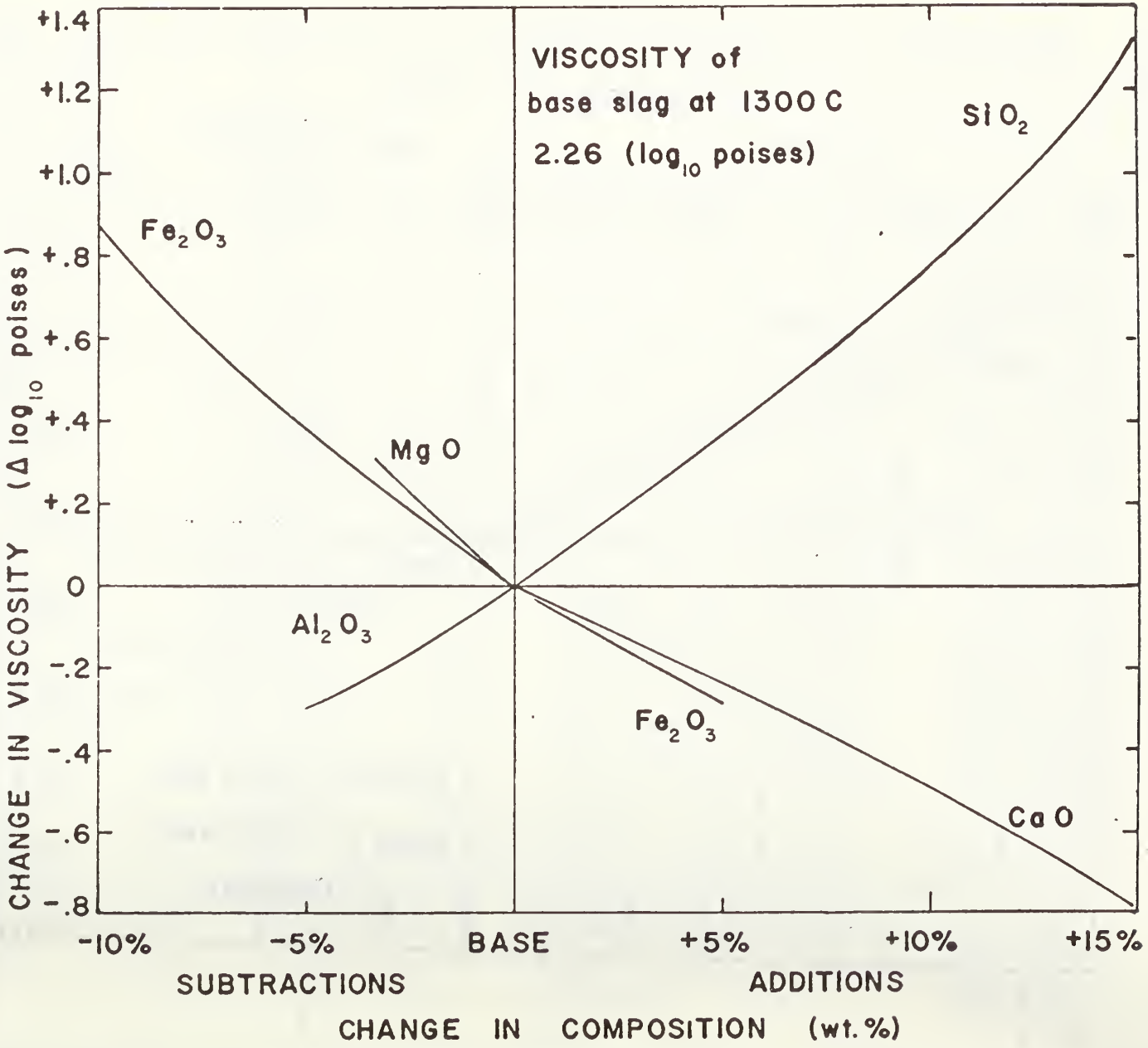

Fig. 2. The Effect of Change of Concentration of Each Oxide on the Viscosity of Base Slag

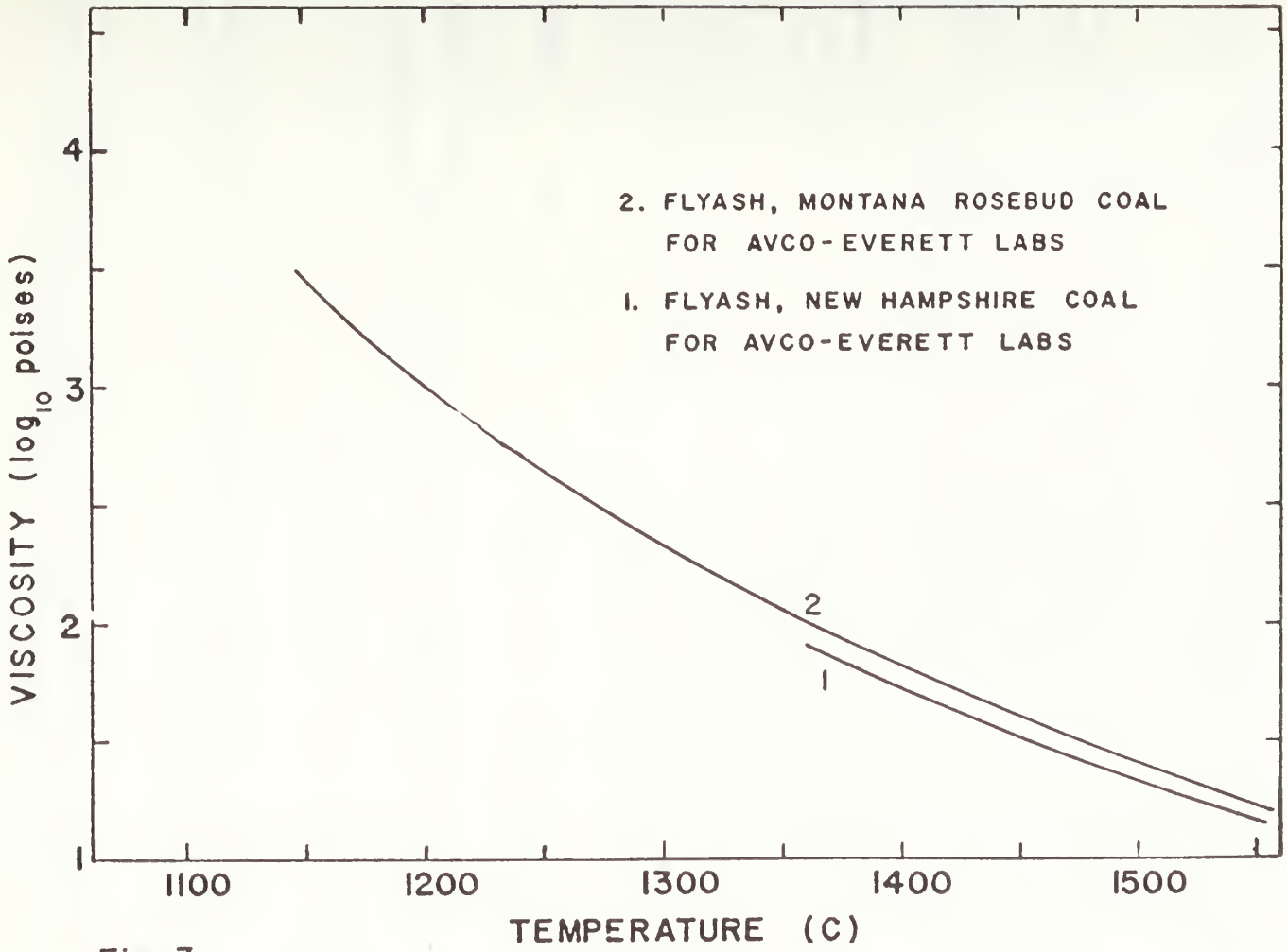
2. FLYASH, MONTANA ROSEBUD COAL
FOR AVCO-EVERETT LABS
1. FLYASH, NEW HAMPSHIRE COAL
FOR AVCO-EVERETT LABS
2
1
VISCOSITY (log10 poises)
4
3
2
1
1100
1200
1300
1400
1500
TEMPERATURE (C)

Fig. 3.

2. Electrical Conductivity (W. R. Hosler and A. J. Armstrong)

Introduction

The electrical conductivity of materials for both electrodes and insulators is an important parameter in designing electrode systems for MHD power generation. Generally, conductivities less than $0.1\ (\text{ohm cm})^{-1}$ will cause a considerable amount of joule heating in those materials used for electrodes. Insulating materials must have low conductivity at high temperatures to prevent current leakage down the channel due to the induced Hall voltage.

A number of samples have been sent to NBS from outside firms for conductivity measurements. In addition, NBS has designed and procured from outside vendors some materials of possible use as MHD electrodes. All measurements reported here are done using a four probe d.c. technique. They are done isothermally at temperatures between room temperatures and 1700 °C, and under several partial pressures of oxygen. At each temperature an attempt is made to establish equilibrium between the surrounding gas and the sample (oxidation-reduction).

$SrZrO_3$. Four samples have been received from H. U. Anderson of AT Research, Rolla, Missouri in which various amounts of La and Cr were substituted into $SrZrO_3$. The electrical conductivities of two of these samples were reported in our previous Quarterly Report (see pp. 17 and 18). The electrical conductivities of the remaining two samples in this series have been measured (see Figs. 1 and 2). In general, the result of increasing the amount of La and Cr was to increase the overall electrical conductivity and to increase the effect of the partial pressure of oxygen on the electrical conductivity.

Two composite (two phase) samples were received from H. U. Anderson of AT research (see Figs. 3 and 4).

Of all the samples based on $SrZrO_3$ one composition shows promise as an MHD electrode. The composite sample of composition 50% $Sr_{.9}Zr_{.9}La_{.1}Cr_{.1}O_3$ + 50% $Sr_{.1}Zr_{.1}La_{.9}Cr_{.9}O_3$ (see Fig. 4) displayed sufficient electrical conductivity for MHD use over a wide range of temperature with little oxygen dependency.

NAFF 41. A sample of composition 4 $NiAl_2O_4$ + 1 Fe_3O_4 was prepared by Trans Tech Gaithersburg, MD. This sample has been measured (see Fig. 5) and found to possess sufficient electrical conductivity for MHD use only at elevated temperatures (above 800 °c).

$LaCrO_3$ + .05 Mg. A sample of magnesia stabilized lanthanum chromite was received from General Refractories. Its electrical conductivity is shown in Fig. 6. This material appears to be useful for MHD purposes down to very low temperatures (below 100 °C).

$YFeO_3$ + 5% $CaZrO_3$. A sample of $YeFeO_3$ doped with $CaZrO_3$ was prepared by Trans Tech. The electrical conductivity of this material has been measured as a function of temperature and oxygen partial pressure (see

Figs. 7 and 8). XRD measurements show a foreign peak in the pattern due to unstabilized phase of ZrO_2. Other work involving nonstoichiometric $YFeO_3$(Ca) materials and $YFeO_3$(Ca) + $CaZrO_3$ is in progress.

Bow, New Hampshire Coal Slag. Fly ash from the Bow, New Hampshire power plant was obtained from Mr. S. Petty of AVCO. The electrical conductivity is shown in Figure 9. This slag is unseeded. Measurements on the seeded material will be done in the future. This data was taken using a new four probe technique developed for obtaining four probe conductivity data on slags above the melting temperature. In this technique, powdered slag is placed in an Al_2O_3 closed end tube which has four platinum probes, sealed by peening platinum sponge around the wires, spaced along the side of tube near the closed end. When the melting temperature of the slag is exceeded, the liquid slag flows and fills the bottom of the Al_2O_3 tube. From the data shown in Figure 9, it is apparent that the electrical conductivity (without K) is low even at 1300 °C. It should also be pointed out that these data were taken using instantaneous current voltage application to avoid electrochemical reactions between platinum and slag described elsewhere in the report. Polarization voltages begin immediately when current is drawn during the measurement; therefore, this data should be taken as somewhat qualitative. New methods of measurement are under investigation.

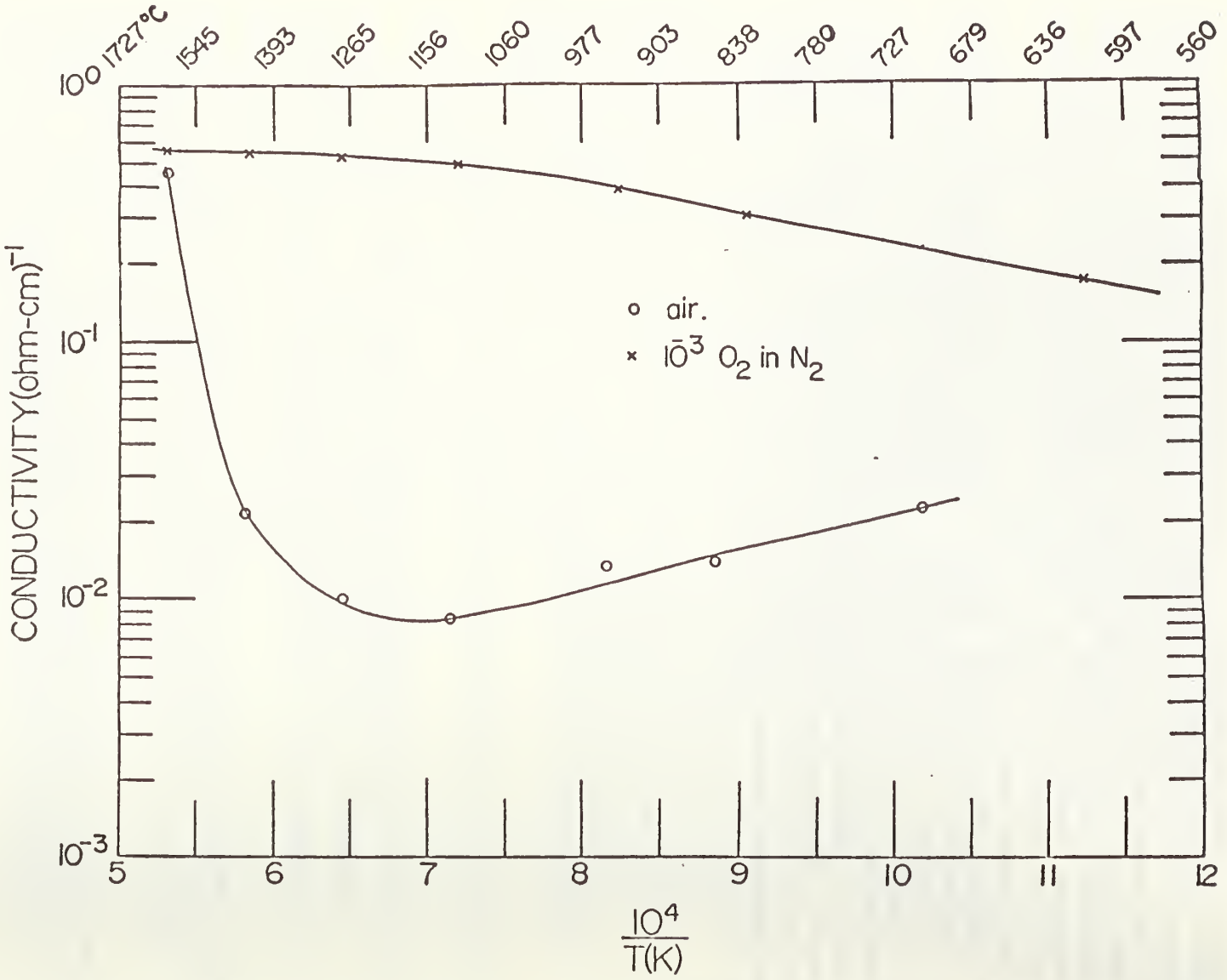

Fig. 1.Electrical conductivity of $Sr_{0.9}La_{0.1}Zr_{0.7}Cr_{0.3}O_3$ as a function of temperature at several partial pressures of oxygen. Sample prepared at AT Research. No details on preparation were submitted.

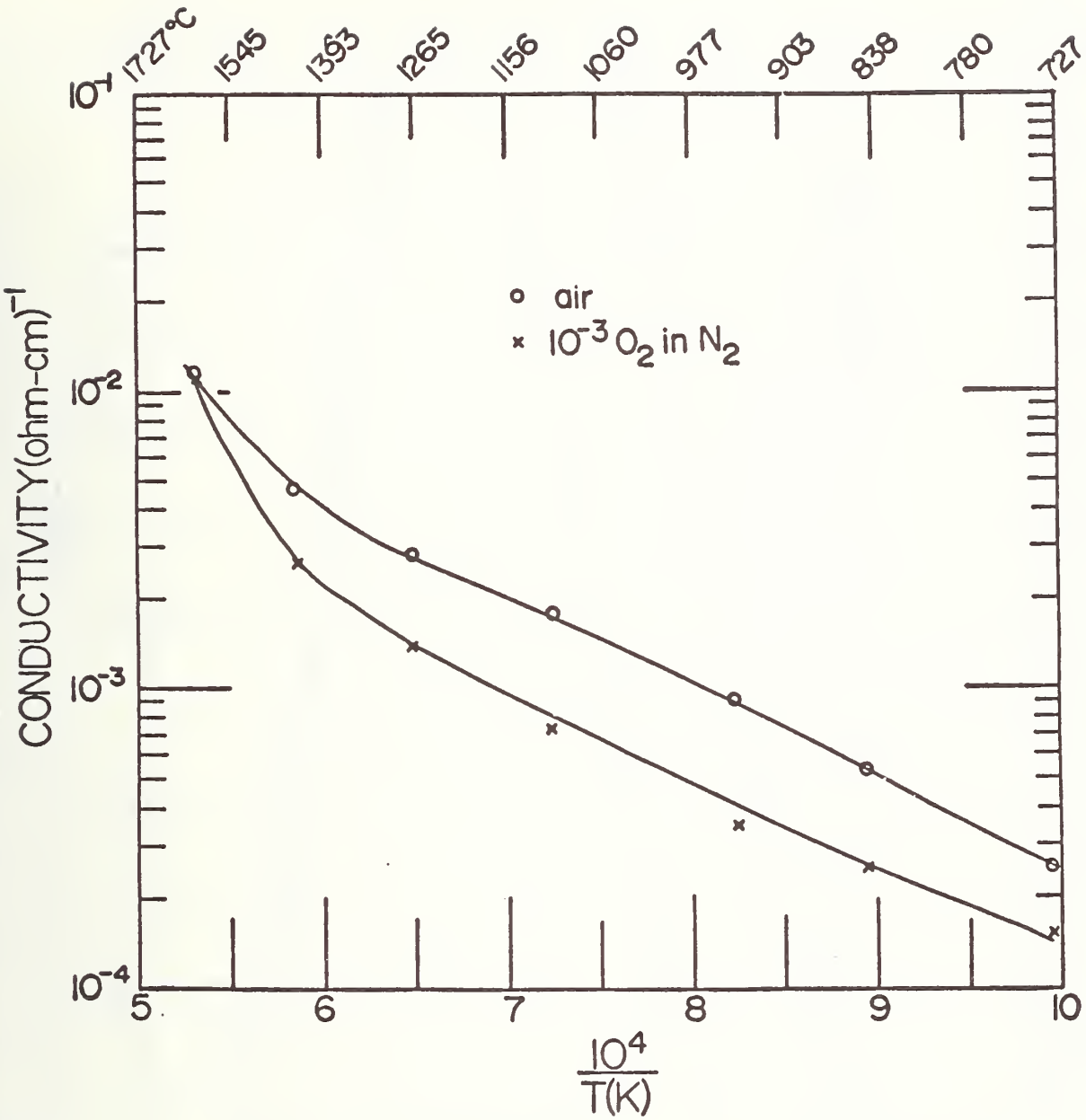

Fig. 2.

Electrical conductivity of $Sr_{.9}La_{.1}Zr_{.9}Cr_{.1}O_3$ as a function of temperature at several partial presures of oxygen. Sample prepared by A T Research by H. Anderson. No preparation data supplied. Measurements made at NBS.

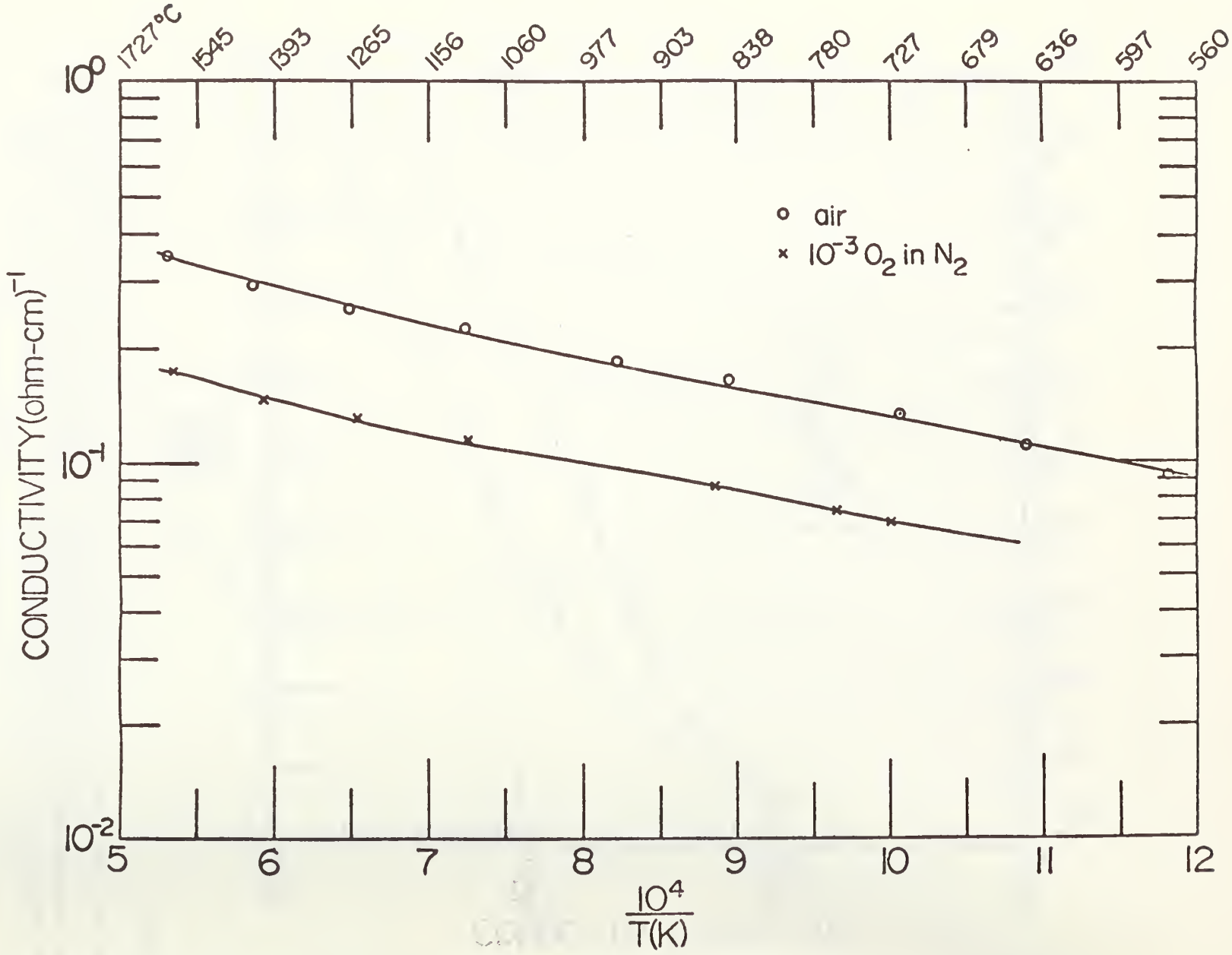

Fig. 3. Electrical conductivity of $Sr_{.9}La_{.1}Zr_{.7}Cr_{.3}O_3$ + $Sr_{.1}Zr_{.1}La_{.9}Cr_{.9}O_3$ as a function of air at several partial pressures of oxygen in nitrogen. Sample [illegible]

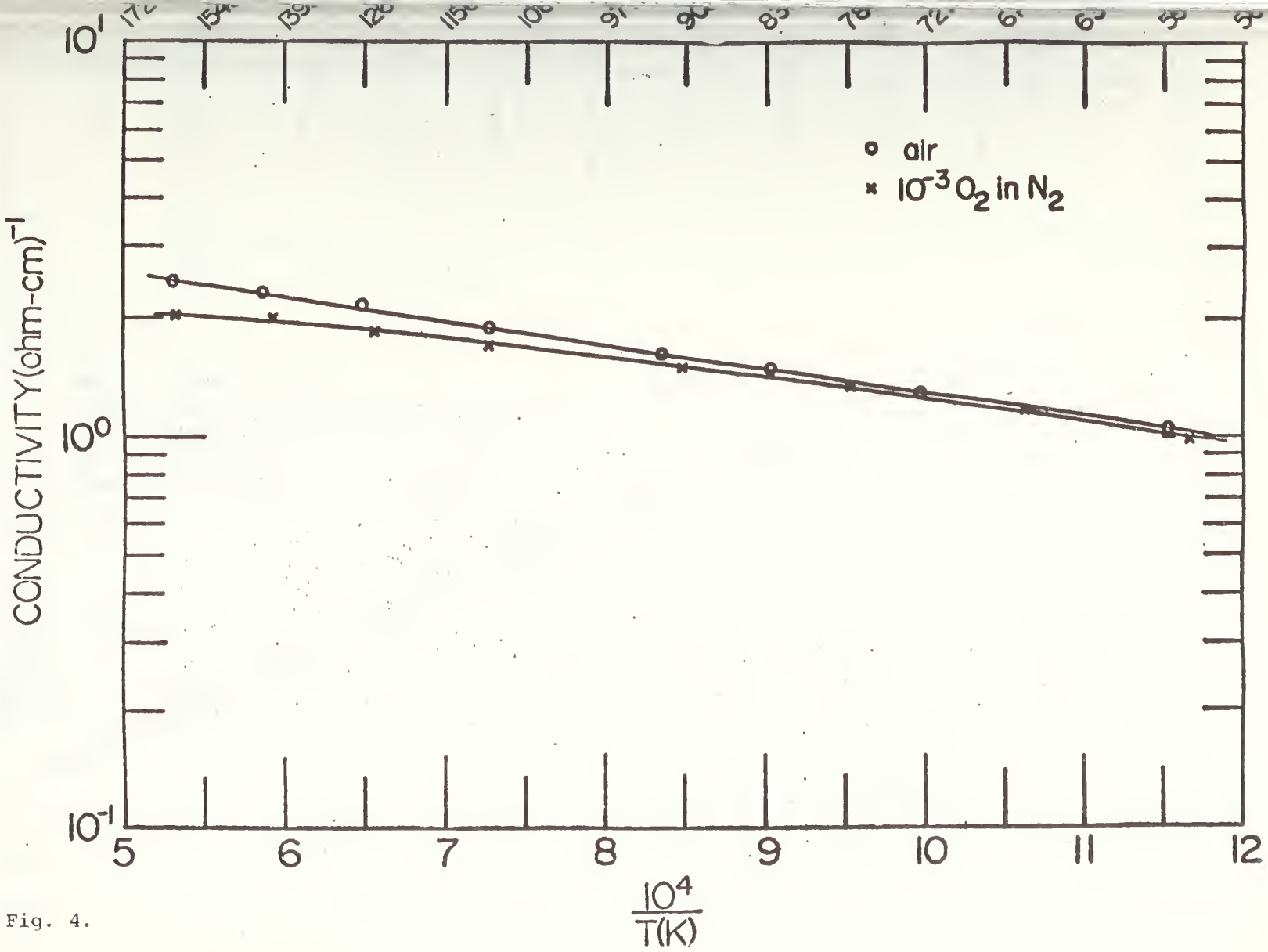

Fig. 4.

Electrical conductivity of $Sr_{0.9}Zr_{0.9}La_{0.1}Cr_{0.1}O_3$ + $Sr_{0.1}Zr_{0.1}La_{0.9}Cr_{0.9}O_3$ as a function of temperature at several pressures of oxygen. The conductivity in air at 354 °C and 25 °C is 0.57 and 0.028 (ohm cm)$^{-1}$ respectively. In 10^{-3} atmos. partial pressure of oxygen in nitrogen σ = .64 (ohm cm)$^{-1}$ at 410 °C and 0.032 at 25 °C. Samples prepared by H. Anderson, A T Research.

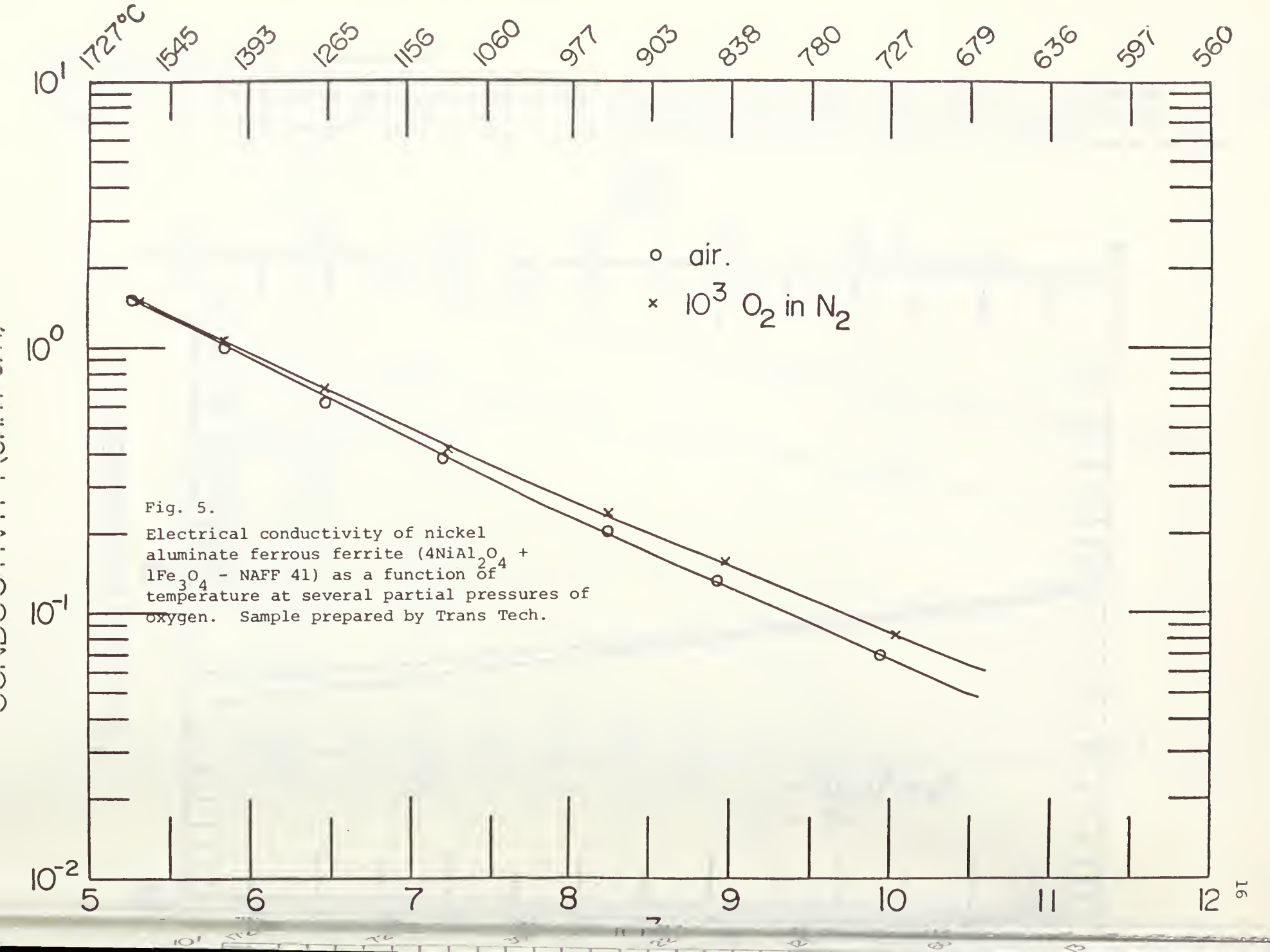

Fig. 5.
Electrical conductivity of nickel aluminate ferrous ferrite ($4NiAl_2O_4$ + $1Fe_3O_4$ - NAFF 41) as a function of temperature at several partial pressures of oxygen. Sample prepared by Trans Tech.

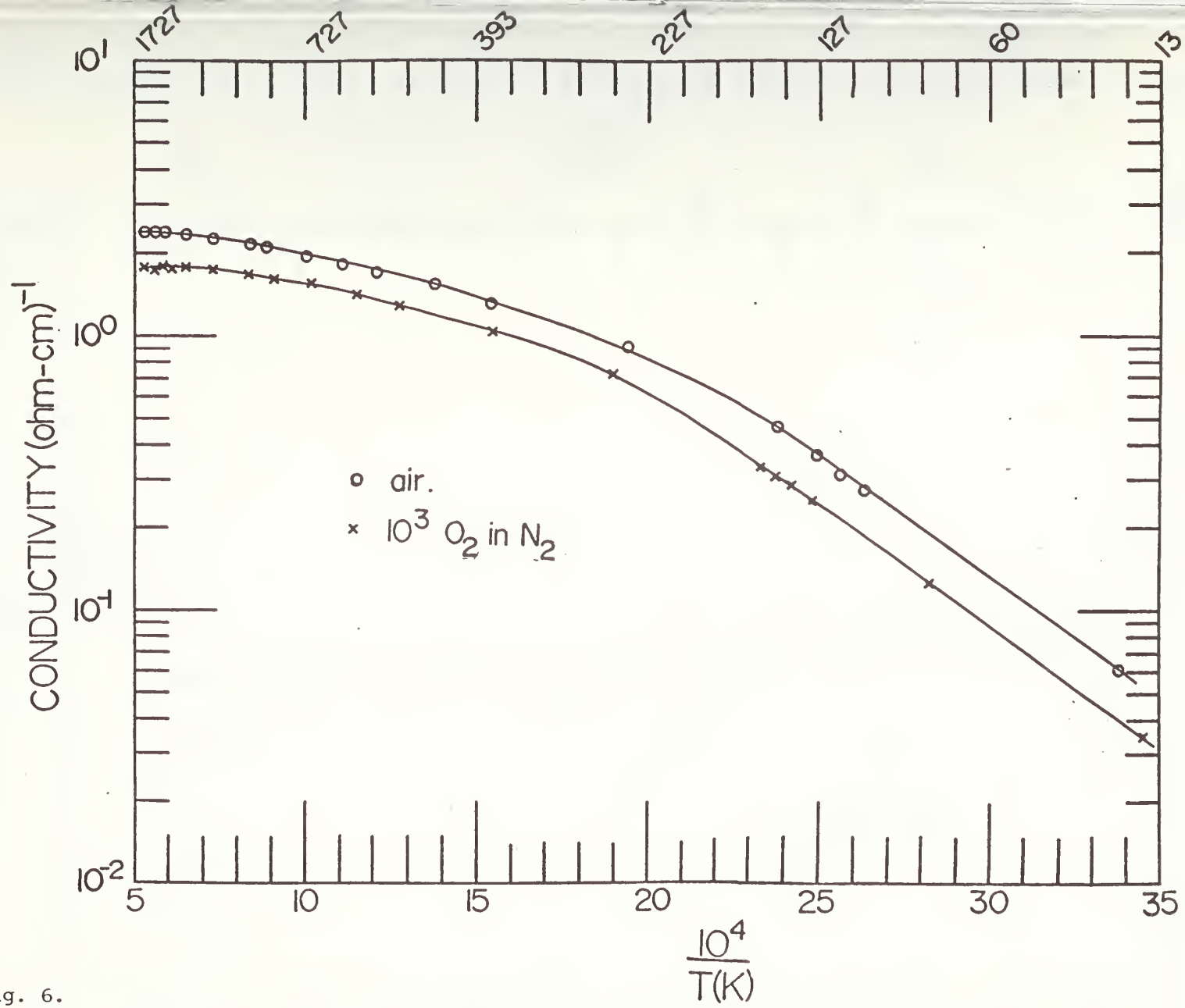

Fig. 6.

Electrical conductivity of $La_{0.95}Mg_{0.05}CrO_3$ as a function of temperature at several partial pressures of oxygen. Hot pressed material made by General Refractories. Preparation details not submitted.

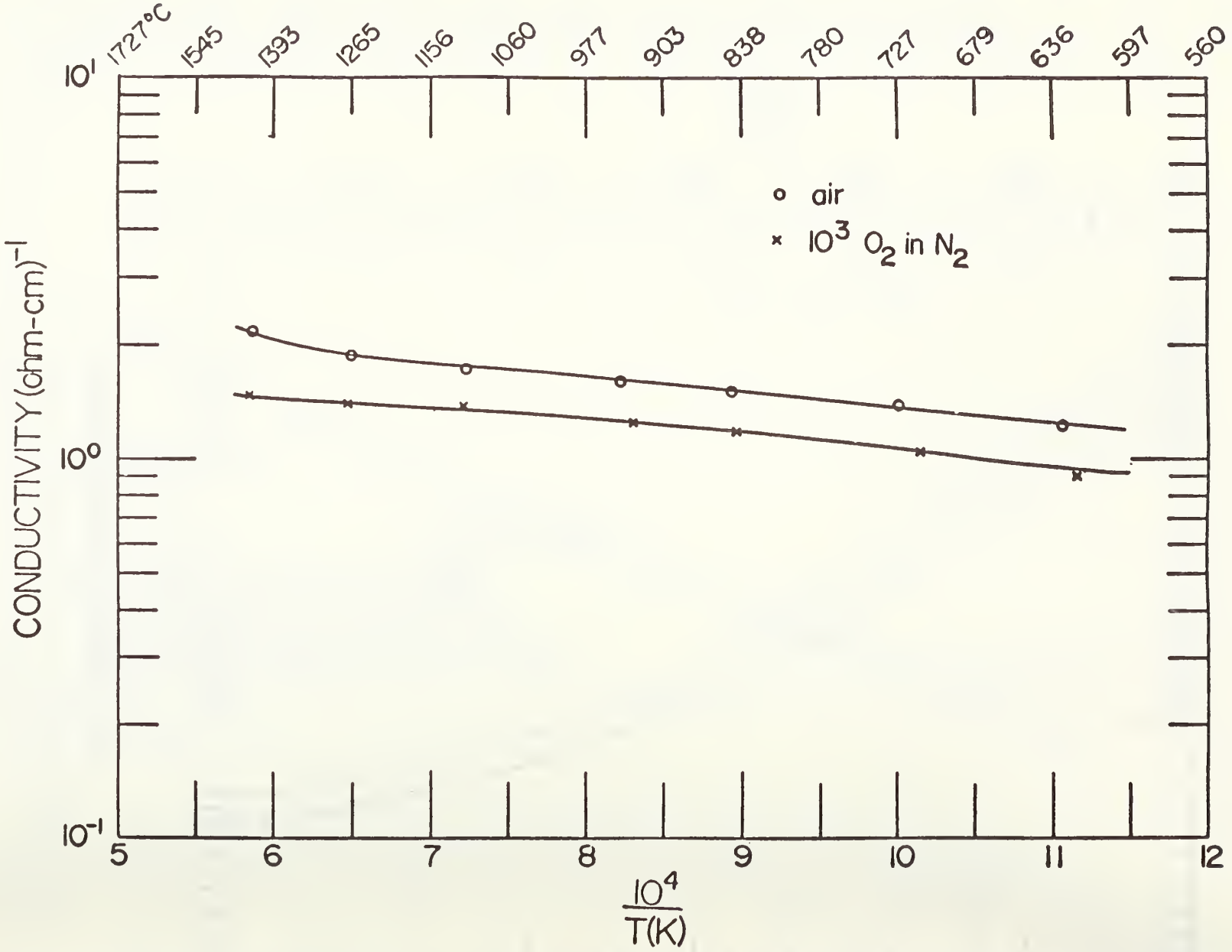

Fig. 7. Electrical conductivity of $YFeO_3$ + 5% $CaZrO_3$ as a function of temperature at several partial pressures of oxygen.

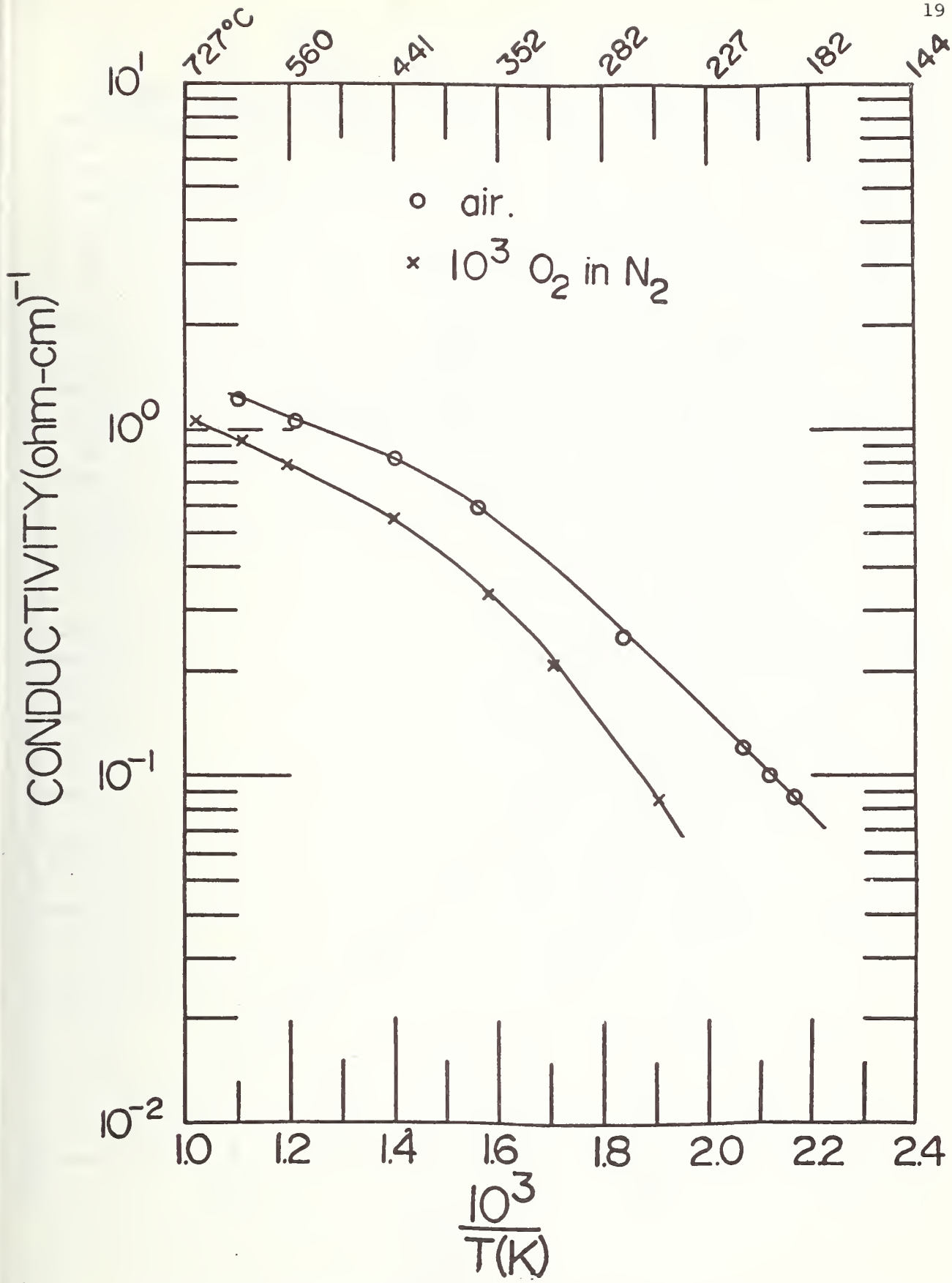

Fig. 8. Electrical conductivity of $YFeO_3$ + 5% $CaZrO_3$ as a function of temperature at several partial pressures of oxygen.

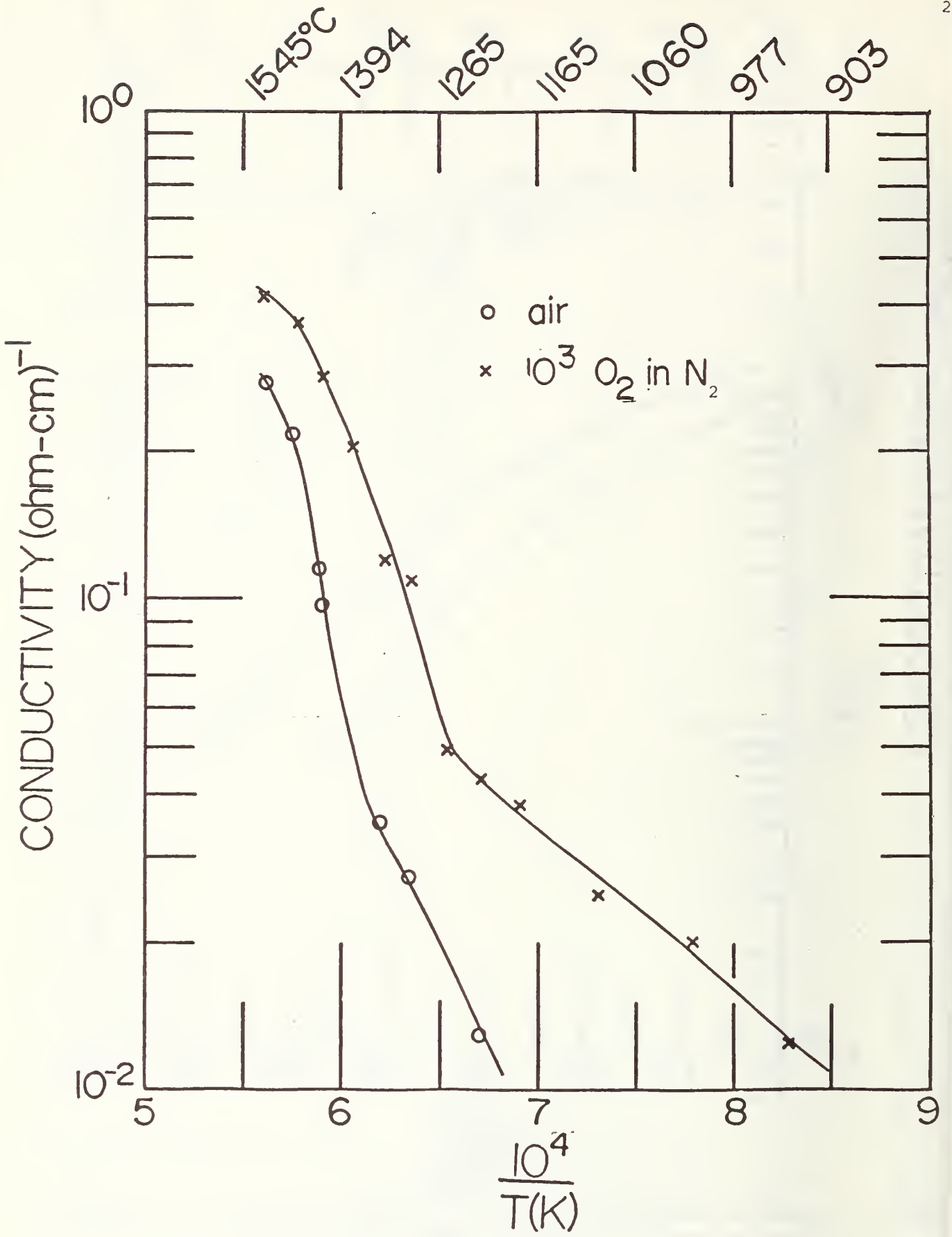

Fig. 9. Electrical conductivity of coal slag unseeded (no added potassium) as a function of temperature at several partial pressures of oxygen. The slag melt was derived from the Bow, New Hampshire power plant fly ash used in the AVCO/NBS slagging test #1.

Scanning Electron Microscopy Examination of $LaCrO_3$ Plus Stainless Steel Wool (A. J. Armstrong)

Attachment of monolithic ceramics to a metal lead-out is a continuing problem in MHD electrode design. Recently, metal meshes especially prepared for a number of materials have been successfully used as electrode attachments either by directly brazing the ceramics to the mesh or by arc plasma spraying the ceramic into the mesh. Dr. Graves of the University of Dayton has attempted to hot press $LaCrO_3$ integral with a stainless steel wool (430) which in turn could be directly brazed to a copper electrode base. Unfortunately, $LaCrO_3$ will not pressure sinter into a dense monolithic body at temperatures below the melting point of the 430 stainless steel. In initial experiments a temperature of 1650 °C was necessary which is well above the melting point of this alloy. SEM examination showed the diffusion of Fe (main constituent) into the $LaCrO_3$ and areas where the stainless steel was intimately bonded to the $LaCrO_3$. This technique appears to have little promise as an attachment mechanism due to the high sintering temperature required for $LaCrO_3$. Use of this technique using other ceramics is under investigation.

3. Vaporization Studies (E. R. Plante)

This section describes measurements of the potassium gas pressure over K_2O-containing compounds or phases. Such data are of critical importance in predicting the interaction of a seeded MHD plasma with construction materials or coal ash using equilibrium thermodynamics. For example, Spencer (1) noted that no activity data existed for interior composition points in the K_2O-Al_2O_3-SiO_2 liquid "slag" system so that his ternary Margules model for predicting K_2O activities had to be based on data extrapolated from the binary systems. The vaporization studies at NBS have been planned to provide some of the lacking data for simple systems as well as to measure K_2O activities in solutions having up to 6 components which will be more closely representative of slags in real MHD systems. In this quarterly report the results of measurements on several K_2O-Al_2O_3-SiO_2-containing phases will be summarized.

K_2O-Al_2O_3-SiO_2 (Glass) Vapor Pressure Measurements

These measurements were carried out using glasses obtained from the Geophysical Laboratories, Washington, DC. They were among the well characterized materials used by Schairer and Bowen (2) for their study of condensed phase relations. Composition data was reported in a previous NBS report (3). Preliminary measurements of the K pressure over several glass compositions were not successful because of insufficient sensitivity of the microbalance system and a tendency for the low melting glasses to creep from the Pt Knudsen cells. Neither of these problems have been apparent in the mass spectrometer work.

Pressure measurements were generally restricted to the temperature range of 1200 - 1600°C but depend to some extent on the pressure generated by the particular sample. Potassium pressures below 10^{-7} atm are more difficult to measure because of a ubiquitous background at mass 39 while pressures above 10^{-4} atm lead to rapid changes in sample composition. In addition, experiments run at temperatures in excess of 1600°C will result in significant loss of Pt through vaporization so that independent measurements of the mass spectrometer calibration constant are necessary. The above temperature range leads to only a short extrapolation into the MHD region where seed slag interaction is expected to be most important.

In this temperature range, the only appreciable pressure is that due to the K_2O dissolved in the glass. The vaporization reaction is

$$K_2O \text{ (dissolved in glass)} = 2K(g) + 1/2\ O_2(g).$$

As vaporization proceeds the K_2O content of the glass gradually decreases while the SiO_2/Al_2O_3 ratio remains constant. The principal source of error in the pressure is the temperature measurement while the mass spectrometer constant is insensitive to errors in temperature.

As a pessimistic estimate, an error of ±50K at 1700K would lead to an error of ±100 percent (a factor of 2) in pressure while the mass spectrometer constant would be in error by only ±1 percent. However, the mass spectrometer constant is also sensitive to the error in the weight loss used in its determination which can be effected by sample impurities as well as weight loss in the Pt effusion cells at temperatures of 1900K and above. For the pressures summarized here, errors in pressure are thought to be less than ±100 percent and errors in composition are less that ±10 percent of the change in composition. Initial compositions are assumed to be exact. Most of the samples have a tendency to absorb moisture and were dried prior to use in air at temperatures from 200 - 500°C for periods of several hours. This may have lead to absorption of CO_2 as evidence by small mass 44 signals during the initial vaporization measurements. It is also possible that small amounts of CO_2 as unreacted carbonate remain in the original glass preparations. This would have a tendency to make the initial K pressures higher than they should be at the starting compositions.

K210 Measurements

The starting composition of K210 was 39.6 wt percent K_2O, 10.0 percent Al_2O_3 and 50.4 percent SiO_2. The effusion cell had a .5mm diameter effusion hole. Vaporization measurements on this sample were carried out until the K_2O composition had been reduced to 15 percent K_2O. Initially, the K pressures were about 3 times as high as the K pressures over 40 wt percent K_2O in silica solutions but were about the same as those over 20 wt percent K_2O in silica by the time the K_2O content of K210 was reduced to 20 wt percent K_2O. Between 20 wt percent K_2O and 15 wt percent K_2O, the pressures decreased by a factor of about 6. This is in sharp contrast to the behavior of K_2O-SiO_2 solutions which showed minor decrease in pressure in this concentration range. It was not determined whether this was due to a rapid decrease in pressure with composition in this concentration range or whether non-equilibrium effects were becoming prominent. This type of behavior would be expected if the rate controlling step for the evaporation is diffusion of the K_2O through the glass and a concentration gradient is established. Below 15 wt percent K_2O other non-equilibrium effects were observed. Here, the K pressure fluctuated by roughly a factor of two at constant temperature. This effect has previously been observed and is thought to result from accumulation of gas in the slag sample with the resultant formation of bubbles which burst through the surface exposing higher concentration regions of K_2O.

Questions concerning non-equilibrium can be answered if the K pressure of glasses having lower K_2O concentrations but the same SiO_2/Al_2O_3 ratio and known to be homogeneous are measured. Two attempts to do this were made using sample K1113 which had an initial composition

of 21.7 wt percent K_2O, 13 wt percent Al_2O_3, and 65.3 percent SiO_2. This composition corresponds closely to the composition K210 would have when its K_2O content was decreased to 21.7 wt percent K_2O. Unfortunately, none of these measurements led to valid data.

K220 Measurements

The starting composition of K220 was 35.2 wt percent K_2O, 20. percent Al_2O_3 and 44.8 percent SiO_2. The SiO_2/Al_2O_3 ratio of 2.2 approximates that for a "typical" Eastern coal and represents a signigicant change from the SiO_2/Al_2O_3 ratio of 5.0 of K210. A Pt Knudsen cell having a .34mm diameter effusion orifice was used. The measured pressures over this sample were much below those for the K210 at similar K_2O concentrations as well as below those of K_2O-SiO_2 solutions having the same K_2O concentration. At a K_2O concentration of 19 wt percent the K pressure is close to an order of magnitude below the K pressure of a K_2O-SiO_2 solution having 10 wt percent K_2O. This data appears to be confirmed from preliminary measurements on K728 which has an initial composition of 14.9 wt percent K_2O, 28 percent Al_2O_3 and 57.1 percent Al_2O_3.

Conclusions

K_2O-SiO_2-Al_2O_3 glasses with an SiO_2/Al_2O_3 wt ratio of 5 appear to have an increased activity of K_2O down to about 20 wt percent K_2O at which concentration the K_2O activity is the same as a K_2O-SiO_2 solution. Glasses with an SiO_2/Al_2O_3 wt ratio of 2 show reduced activity of K_2O from about 32 wt percent K_2O to 19 wt percent K_2O as compared with K_2O-SiO_2 solutions.

Future Work

Future work will include K pressure measurements over selected compositions in the K_2O-SiO_2-Al_2O_3 system to complement the current results. Extension to several K_2O-SiO_2-Al_2O_3-CaO compositions is planned. Comparison of experimental results on the K_2O-SiO_2-Al_2O_3 system with Spencers (1) ternary model will be made.

References

1. F. E. Spencer, Jr., J. C. Hendrie, Jr., and D. Bienstock, VIth International Conference on MHD Power Generation, Washington, DC (1975).

2. J. F. Schairer and N. L. Bowen, Am. J. Sci., 253, 681 (1955).

3. H. P. R. Frederikse, T. Negas and S. J. Schneider, NBS Quarterly Report, September (1975).

Task J. Corrosion and Diffusion

1. The System $CaO-K_2O-Al_2O_3-SiO_2$ (L. P. Cook)

Further experimentation has been directed toward determining the temperature of the invariant melts first appearing within four phase subvolumes in the Al, Si-rich portion of the system $CaO-K_2O-Al_2O_3-SiO_2$. Results are summarized in Table 1, below. These experiments were performed using mixtures of the crystalline end-members indicated. The temperatures given have not been reversibly bracketed by equivalent glass crystallization experiments. However temperatures are believed to be not far from equilibrium, as extensive superheating does not seem likely. Possible exceptions are melts involving $KAlSi_3O_8$ - these are undergoing further study, and results will be given in the next quarterly report.

Table 1. Temperatures at Which Melt First Appears Upon Heating Four-Phase Mixtures in System $CaO-K_2O-Al_2O_3-SiO_2$.

Four Phase Volume [1/]	Phases	Temperature (°C) of Melting
2	$KAlSiO_4$-$CaAl_{12}O_{19}$-$Ca_2Al_2SiO_7$-$CaAl_2Si_2O_8$	1275±20
3	$KAlSiO_4$-$KAlSi_2O_6$-$Ca_2Al_2SiO_7$-$CaAl_2Si_2O_8$	1280±20
4	$KAlSiO_4$-$KAlSi_2O_6$-$Ca_2Al_2SiO_7$-$CaSiO_3$	1260±15
5	$KAlSiO_4$-$KAlSi_2O_6$-Al_2O_3-$CaAl_2Si_2O_8$	1335±15
6	$KAlSi_2O_6$-Al_2O_3-$3Al_2O_3.2SiO_2$-$CaAl_2Si_2O_8$	1370±15
7	$KAlSi_2O_6$-$Ca_2Al_2SiO_7$-$CaAl_2Si_2O_8$-$CaSiO_3$	1235±15

[1/] Refer to previous two quarterly reports.

a. The System $CaO-K_2O-FeO_x-MgO-Al_2O_3-SiO_2$ (L. P. Cook)

With the aid of a statistical analysis of coal ash data in U.S. Bur. Mines Bull. 567, and available channel slag analyses, two compositions, representing hypothetical "Eastern" and "Western" seeded channel slags, have been chosen for experimental study (Table 2). Experiments made under oxidizing conditions ($P_{O_2} \approx 0.21$ atm) show that the melting temperatures of these slags are somewhat higher than the equivalent unseeded slag, due to the presence of refractory potassium aluminosilicates (Figure 1). Initial melting of "Eastern" channel slag occurs in the range 1350-1400°C; liquidus temperature is in the range 1600-1650°C. Equivalent temperatures for "Western" channel slag are 1400-1450°C and 1650-1700°C, respectively. The volume of melt does not become more than 50% until temperatures above 1550°C are reached. Under oxidizing conditions, "Eastern" channel slag melt shows a marked enrichment in Fe at lower temperatures; "Western" channel slag melt shows a similar enrichment in Ca (see Figure 2). Analogous experiments are planned for the same compositions under reducing conditions, more applicable to the cathode side.

In operating MHD channels, there are at least two competing effects which may serve to locally modify the composition of the accumulating slag layer, in addition to the temperature gradient: (1) diffusion of K inward toward the cooler walls along chemical potential gradients, (2) electrochemical migration of mobile species. Limited test data available (e.g. AVCO 1976 100 h test; G.E./AVCO test on 9/27/77) suggest that the electrochemical effect is most important in a zone a few hundred microns wide adjacent to the electrode. Both calcium and potassium appear to diffuse away from the anode. However in the outer zones of the slag layer away from the electrode interface, temperature may exert an important control on melt compositions, if low enough (less than ~1600°C) that solid/liquid interaction occurs.

Table 2. Suggested Average Compositions for Modeling MHD Channel Slag (wt %). 1/

	Western Coal	Eastern Coal
SiO_2	34.78	36.19
Al_2O_3	24.58	25.36
FeO_x as Fe_3O_4	5.32	12.13
CaO	9.27	1.77
MgO	3.33	0.63
K_2O	22.71	23.92
	99.9	100.0

1/ Refer to April-June 1977 Quarterly Report.

1A.

1A.

Figure 1. SEM micrographs of experiments on synthetic "Western" channel slags. Granular outlines are produced by contact with Pt.

A) Eutectic intergrowth (1600 °C), B) Crystal/liquid mixture (1500 °C). Crystals are potassium aluminosilicates, presumably $KAlSiO_4$.

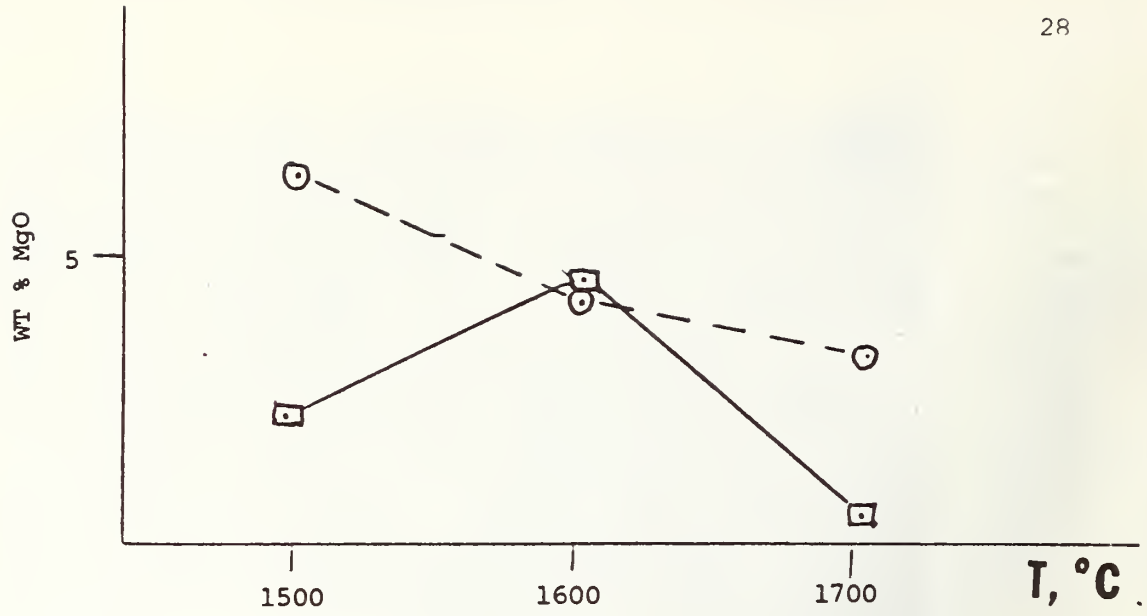

Fig. 2-A

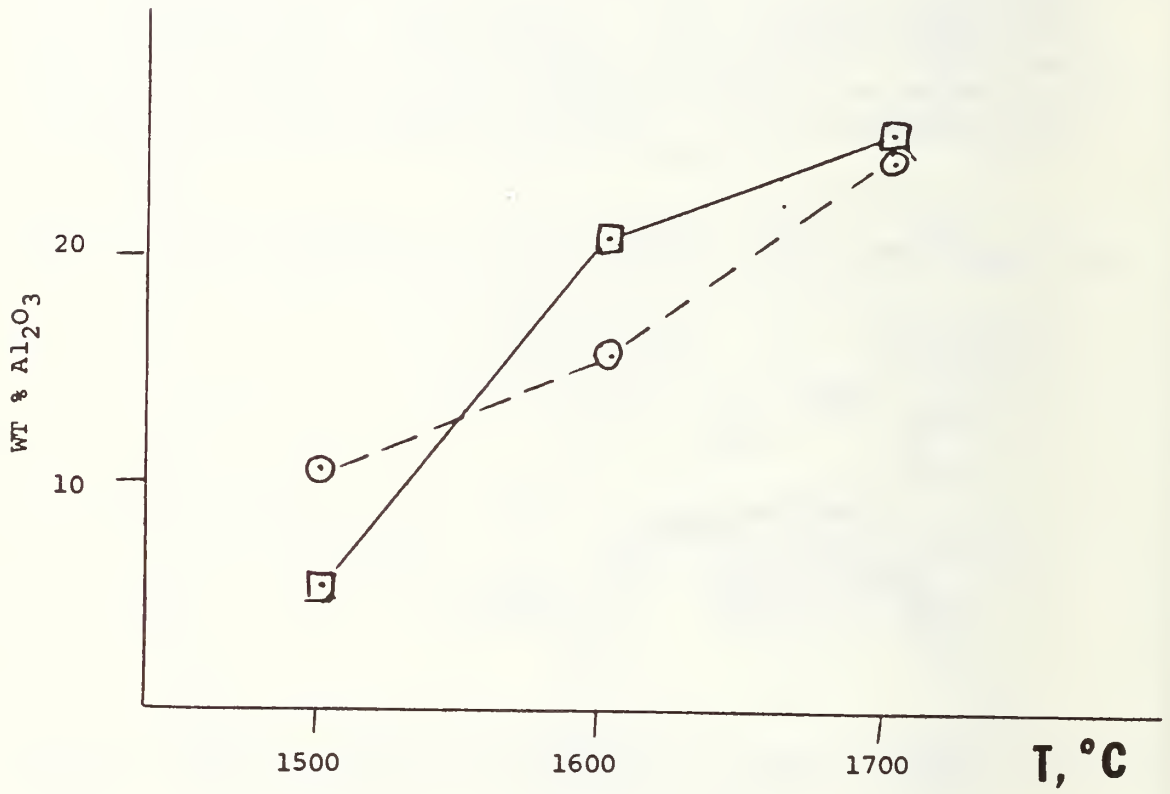

Fig. 2-B

Figure 2. Composition of melt as a function of temperature for six oxides (dashed - Western; solid - Eastern). Vertical axes indicates wt% oxide in melt, as estimated from comparison with completely melted "Eastern" and "Western" glasses. Horizontal axis shows temperature of melting.

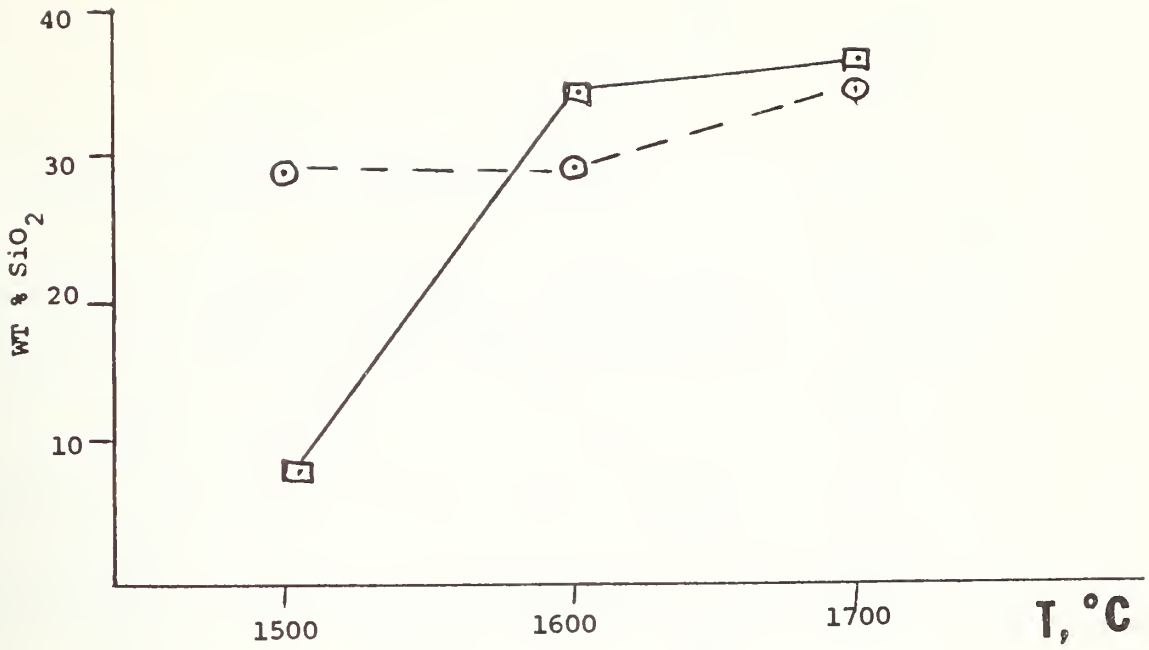
40
30
20
10
WT % SiO_2
1500
1600
1700
T, °C

Fig. 2-C

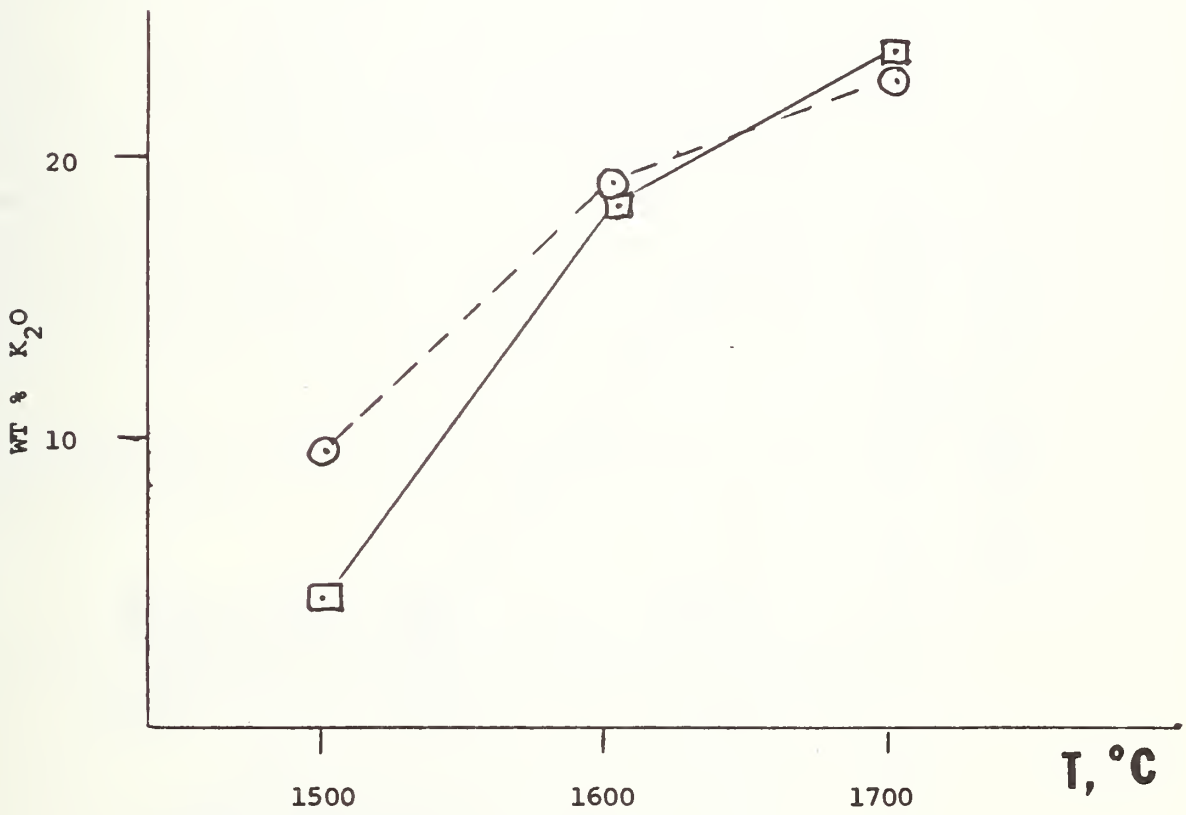
20
10
WT % K_2O
1500
1600
1700
T, °C

Fig. 2-D


30
15
WT % CaO
1500
1600
1700
T, °C

Fig. 2-E

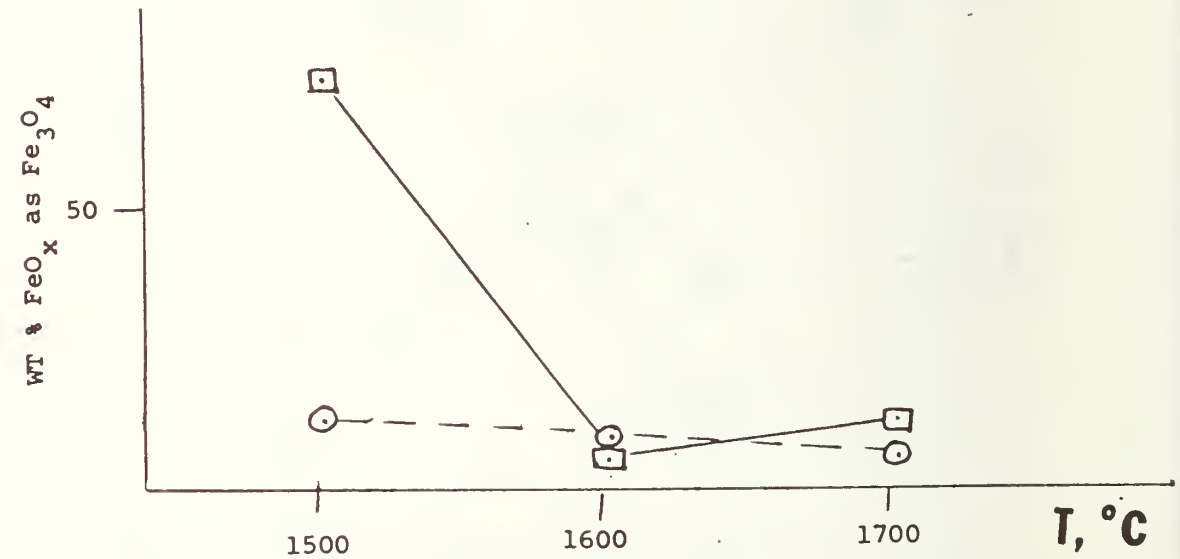
50
WT % FeO_x as Fe_3O_4
1500
1600
1700
T, °C

Fig. 2-F

2. Diffusion in Insulator - Electrode Couples (A. J. Armstrong, E. N. Farabaugh and J. R. Manning)

Investigation of the diffusion of Fe from MAFF31 ($3MgAl_2O_4:1Fe_3O_4$) into various insulator materials is continuing. This investigation should serve to study the possible degradation of the insulating characteristics of the insulator material after exposure to high temperature while in contact with iron spinel electrode material.

During this reporting period electrode - insulator-electrode couples of MAFF31 and SP71 ($MgAl_2O_4$) were made and tested at 1600 °C for 1, 10 and 100 hrs. These diffused couples are shown in Fig. 1a (1 hr.), Fig. 1b (10 hr.) and Fig. 1c (100 hr.). Notice the difference in Fe penetration in the SP71 (insulator) indicated by the dark bands in the SP71 at the insulator-electrode interface. It is seen that the bands become wider with longer time at 1600 °C.

A part of Fe concentration profile from the 10 hr. test is shown in Fig. 2. (This profile is from one electrode-insulator interface. The Fe concentration profile taken across the electrode and through the insulator and into the other electrode material showed very nearly the same shape at each electrode-insulator interface). The profile in Fig. 2 is not as smooth as those profiles obtained from MAFF31-MgO couples (Quarterly Report 9/77). In fact, a small plateau is possibly present in the MAFF31 about 60 μm from the interface. When this 10 hr. test profile is compared to the 10 hr. test profile for the MAFF31-MgO couple (Quarterly Report 9/77), it is seen that the Fe penetration is markedly less in SP71 than in the MgO. The Fe concentration in the SP71 goes to zero approximately 250 μm from the MAFF31-SP71 interface, whereas the Fe concentration goes to zero in the MgO approximately 450 μm from the MAFF31-MgO interface. Thus, it appears that for equal 10 hr. test conditions there was deeper Fe penetration in MgO than in SP71.

Concentration profiles will be obtained from the 1 and 100 hr. tests and during the next reporting period compared to the 1 and 100 hr. MAFF31-MgO tests.

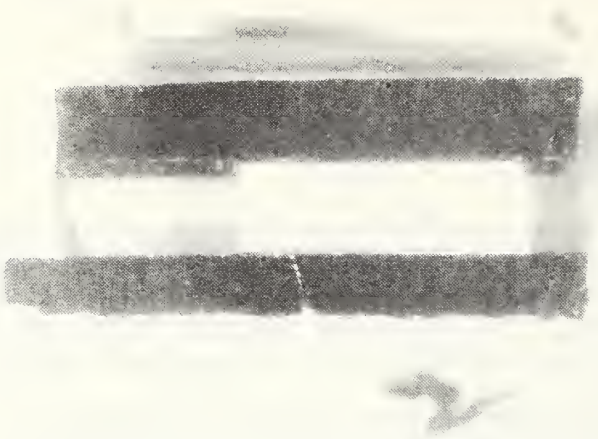

Fig. 1a MAFF31-SP71 Diffusion couple, tested at 1600°C for 1 hr.

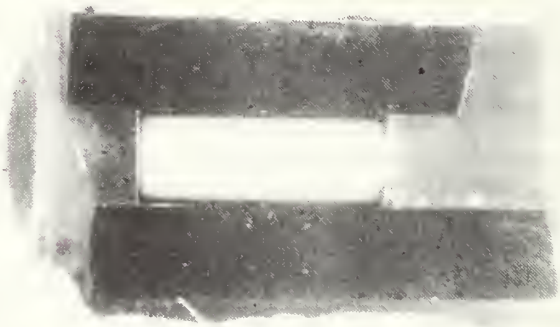

Fig. 1b MAFF31-SP71 Diffusion couple tested at 1600°C for 10 hr.

Fig. 1c MAFF31-SP71 Diffusion couple, tested at 1600°C for 100 hr.

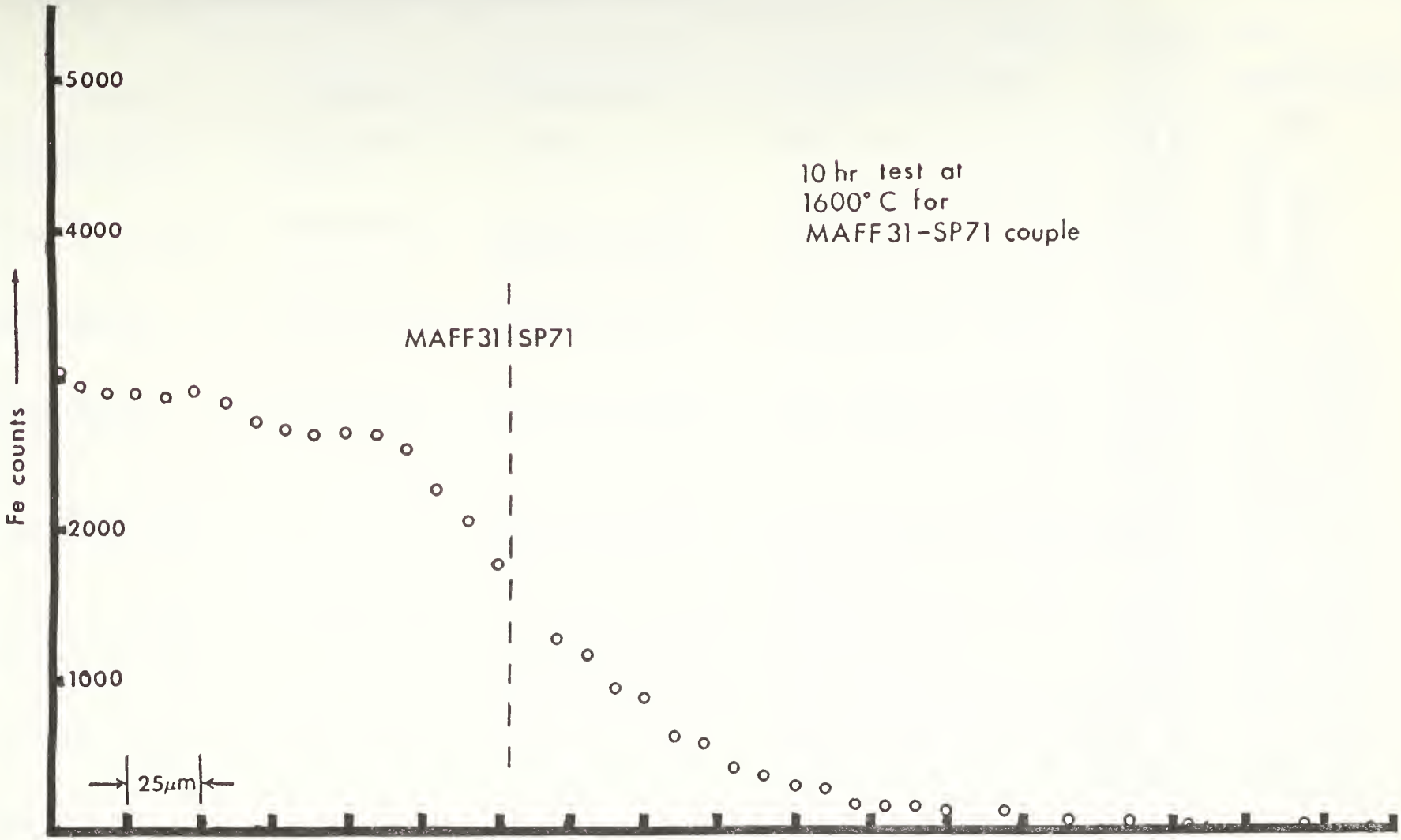

Figure 2. Fe concentration profile for 10 hr tested MAFF 31-SP71 couple.

Task K. Materials Testing and Characterization

1. Structural Analysis of Powdered and Solid Ceramics

a. X-Ray Diffraction of MHD Materials (C.L. McDaniel)

During this quarter we received about 60 materials (powders, dense ceramics, etc.) from various external sources. These were analyzed by x-ray diffraction methods. Data, transmitted to the appropriate source, are shown in Table 1.

Table 1. X-Ray Analysis of MHD Electrode and Insulator Materials

Material	From	Description	X-Ray Diffraction Data: Type Phase Present	X-Ray Diffraction Data: Crystallinity
$85ZrO_2$-$12CeO_2$-$3Y_2O_3$ CZ-CE0201	Westinghouse	Solid	Cubic fluorite solid solution	Poor
$La_{.95}Mg_{.05}Cr_{.85}Al_{.15}O_3$	Westinghouse	Received as solid, powder prepared	Rhombohedral perovskite solid solution	Good
$70La_{.95}Mg_{.05}CrO_3$-$30(12Y_2O_3$-$88ZrO_2)$	Westinghouse	Received as solid, powder prepared	Rhombohedral perovskite solid solution + cubic fluorite solid solution	Good
$60La_{.95}Mg_{.05}CrO_3$-$40(12Y_2O_3$-$88ZrO_2)$	Westinghouse	Received as solid, powder prepared	Rhombohedral perovskite solid solution + cubic fluorite solid solution	Good
$50Sr_{.9}Zr_{.9}La_{.1}Cr_{.1}O_5$-$50Sr_{.1}Zr_{.1}La_{.9}Cr_{.9}O_3$	Westinghouse	Received as solid, powder prepared	Orthorhombic perovskite solid solution + rhombohedral perovskite solid solution	Poor
$50Sr_{.9}Zr_{.7}La_{.1}Cr_{.3}O_3$-$50Sr_{.1}Zr_{.1}La_{.9}Cr_{.9}O_3$	Westinghouse	Received as solid, powder prepared	Rhombohedral perovskite solid solution	Poor
$50Sr_{.9}Zr_{.9}La_{.1}Cr_{.1}O_3$-$50Sr_{.1}Zr_{.1}La_{.9}Cr_{.9}O_3$	Westinghouse	Received as solid, powder prepared	Orthorhombic perovskite solid solution + rhombohedral perovskite solid solution	Poor
$40NiFe_2O_4$-$60Fe_2O_3$ MS 8013	Trans-Tech	Solid	Spinel solid solution	Medium to Good
$95YFeO_3$-$5CaZrO_3$ No. 8011	Trans-Tech	Received as solid, powder prepared	Orthorhombic perovskite solid solution	Good
$95YFeO_3$-$5CaZrO_3$ No. 2	Trans-Tech	Powder	Orthorhombic perovskite solid solution + Y_2O_3 + trace Fe_2O_3	Medium

$64FeAl_2O_4$-$36Fe_3O_4$ No. 1	Trans-Tech	Powder	Fe_2O_3 + Al_2O_3	Poor
$4NiAl_2O_4$-Fe_3O_4 No. 8012	Trans-Tech	Received as solid, powder prepared	Spinel solid solution	Good
Slag A10019 (A)	AVCO	Received as solid, powder prepared	Tetragonal $KAlSiO_4$ ($K_{1+x}Al_{1+x}Si_{1-x}O_4$) + low-orthorhombic $KAlSiO_4$ + trace $K_2CO_3 \cdot 1\ 1/2\ H_2O$	Poor
Slag A10019 (B)	AVCO	Received as solid, powder prepared	Low-orthorhombic $KAlSiO_4$ + Fe_3O_4 + trace unknown	Poor to Medium
Slag A10019 (C)	AVCO	Received as solid, powder prepared	Low-orthorhombic $KAlSiO_4$ + tetragonal $KAlSiO_4$ + Fe_3O_4 + $K_2CO_3 \cdot 1\ 1/2\ H_2O$	Poor
Slag A10019 (D)	AVCO	Received as solid, powder prepared	Low-orthorhombic $KAlSiO_4$ + Fe_3O_4	Poor to Medium
Slag (E)	AVCO	Received as solid, powder prepared	Low-orthorhombic $KAlSiO_4$ + unknown	Medium
Slag (F)	AVCO	Received as solid, powder prepared	Low-orthorhombic $KAlSiO_4$ + tetragonal $KAlSiO_4$ + unknown	Poor
Slag (G)	AVCO	Received as solid, powder prepared	Unknown + tetragonal $KAlSiO_4$ + low-orthorhombic $KAlSiO_4$	Very Poor
$MgAl_2O_4$ (A)	Fluidyne	Received as solid, powder prepared	Spinel + MgO	Good
$MgAl_2O_4$ (B)	Fluidyne	Received as solid, powder prepared	Spinel + MgO	Good

K_2O-$7Fe_2O_3$ (1)	Trans-Tech	Powder	Fe_2O_3 + $KFeO_2$ + β-$KFeO_2$	Medium
K_2O-$7Fe_2O_3$ (2)	Trans-Tech	Powder	Fe_2O_3 + $KFeO_2$ + β-$KFeO_2$	Medium
$95YFeO_3$-$5CaZrO_3$ MS 8015	Trans-Tech	Solid	Orthorhombic perovskite solid solution + unknown	Very Good
$95LaCrO_3$-5MgO	General Refractories	Received as solid, powder prepared	Rhombohedral perovskite solid solution + ∿5% spinel	Good
$LaCrO_3$	APS Inc.	Received as solid, powder prepared	$LaCrO_3$	Poor
Hf-Y-CeO_2 Electrode 108	Westinghouse	Received as solid, powder prepared	Monoclinic solid solution + two cubic fluorite solid solution + perovskite	Poor to Medium
Hf-Y-CeO_2 Electrode 109	Westinghouse	Received as solid, powder prepared	Cubic fluorite solid solution + monoclinic solid solution + Y_2O_3	Medium
HfO_2-CeO_2 Electrode 110 (A)	Westinghouse	Solid	Monoclinic solid solution + cubic fluorite solid solution + perovskite	Medium
HfO_2-CeO_2 Electrode 110 (B)	Westinghouse	Received solid, powder prepared	Perovskite + monoclinic solid solution + cubic solid solution	Medium
HfO_2-CeO_2 Electrode 110 (C)	Westinghouse	Received solid, powder prepared	Perovskite + monoclinic solid solution + cubic solid solution	Medium
$3MgAl_2O_4$-Fe_3O_4 Electrode 105 (A)	Westinghouse	Received solid, powder prepared	Spinel solid solution + Fe_2O_3	Medium
$3MgAl_2O_4$-Fe_3O_4 Electrode 110 (B)	Westinghouse	Received solid, powder prepared	Spinel solid solution + trace Al_2O_3 + trace unknown	Medium

$85YFeO_3$-15CaO No. 1	Trans-Tech	Powder	Orthorhombic perovskite solid solution + trace Y_2O_3 + trace unknown	Medium
$Y_{.90}Ca_{.10}FeO_3$ No. 1	Trans-Tech	Powder	Orthorhombic perovskite solid solution + trace Y_2O_3	Medium
$Y_{.95}Ca_{.05}FeO_3$ No. 1	Trans-Tech	Powder	Orthorhombic perovskite solid solution + ∿5% Y_2O_3	Medium
$95LaCrO_3$-5MgO	Univ. Dayton	Solid	Rhombohedral perovskite solid solution + trace unknown	Medium
$95LaCrO_3$-5MgO	Univ. Dayton	Solid	Rhombohedral perovskite solid solution + ∿5% spinel	Medium
$95LaCrO_3$-5MgO	Univ. Dayton	Solid	Rhombohedral perovskite solid solution + ∿5% unkown	Poor to Medium
$95LaCrO_3$-5MgO	Univ. Dayton	Solid	Rhombohedral perovskite solid solution + ∿5% spinel	Medium
$95LaCrO_3$-5MgO	Univ. Dayton	Solid	Rhombohedral perovskite solid solution	Medium
$95LaCrO_3$-5MgO	Univ. Dayton	Solid	Rhombohedral perovskite solid solution + ∿5% spinel	Medium
$95YFeO_3$-$5CaZrO_3$ MS 8020	Trans-Tech	Solid	Orthorhombic perovskite solid solution + trace unknown	Medium
$95LaCrO_3$-5MgO	Trans-Tech	Powder	Rhombohedral perovskite solid solution + ∿5% spinel	Good
$95LaCrO_3$-5MgO	Trans-Tech	Powder	Rhombohedral perovskite solid solution + trace unknown	Medium to Good

$Y_{.85}Ca_{.15}FeO_3$ MS 8023 (B)	Trans-Tech	Solid	Orthorhombic perovskite solid solution + trace Y_2O_3	Poor
$Y_{.85}Ca_{.15}FeO_3$ MS 8023 (A)	Trans-Tech	Solid	Orthorhombic perovskite solid solution + trace Y_2O_3	Poor
$Y_{.95}Ca_{.05}FeO_3$ MS 8021	Trans-Tech	Solid	Orthorhombic perovskite solid solution + trace Y_2O_3	Poor to Medium
$Y_{.90}Ca_{.10}FeO_3$ MS 8022	Trans-Tech	Solid	Orthorhombic perovskite solid solution + trace Y_2O_3	Poor
K_2O-$7Fe_2O_3$ (A) MS 7611	Trans-Tech	Solid	β-potassium ferrite + Fe_2O_3 + trace β" potassium ferrite	Medium to Good
K_2O-$7Fe_2O_3$ (B) MS 7611	Trans-Tech	Solid	β-potassium ferrite + Fe_2O_3	Very Good
K_2O-$7Fe_2O_3$ (C) MS 7611	Trans-Tech	Solid	β-potassium ferrite + Fe_2O_3	Medium
$La_{.95}Mg_{.05}CrO_3$	Trans-Tech	Powder	Rhombohedral perovskite solid solution	Medium to Good
$Y_{.85}Ca_{.15}FeO_3$ MS 8030	Trans-Tech	Solid	Orthorhombic perovskite solid solution	Poor to Medium
$Y_{.95}Ca_{.05}FeO_3$	Trans-Tech	Powder	Orthorhombic perovskite solid solution	Medium
$Y_{.85}Ca_{.15}FeO_3$	Trans-Tech	Powder	Orthorhombic perovskite solid solution	Medium

2. Thermochemical Effects in Laboratory and in situ Tests (T. Negas, W. HOsler)

a. Introduction

For several years, this laboratory has described features of tested, MHD electrode materials that could be interpreted only by considerations involving electrochemistry (see references 1, 2, for example). More recently, Westinghouse Corp., Stanford Univ. and apparently Battelle Northwest researchers have undertaken laboratory studies which have suggested the potential importance of electrochemically induced phenomena on electrode performance and durability. Although we have been quite aware of these phenomena, this provides us the opportunity to review some of our previous data pertinent to static, electrochemical tests, as well as, to relate some recent data obtained from dynamic, "in-channel" testing of electrodes. These particular data are limited to a slagging system although anionic conductors in a clean-fuel system also reflect well-known and obvious electrochemically-induced features.

Our static tests concentrated first on Pt electrodes in slag at temperatures above the softening point. These provided data for the electrochemical behavior strictly of slag without intervening reactions among slag and other constituents of a more complex ceramic oxide electrode. $LaCrO_3$-based electrodes (arc plasma sprayed) were tested next and other materials, including hot pressed and sintered $LaCrO_3$, are under investigation as time permits. Test parameters and materials include,

a) fly ash from Bow, New Hampshire power plant (AVCO-type), seeded (20 w/o K_2O) and unseeded,

b) isothermal conditions, 1300-1400°C (tests at lower temperatures are reserved for future work),

c) initial current at 250 ma (current density, $\sim$1 A/cm^2),

d) P_{O_2} varied from $10^{-0.68}$ - 10^{-3} atm.

The test-cell temperature was raised without current to the test condition. When thermal equilibrium was attained, a voltage was applied to drive a maximum current of 250 ma in the constant current mode. Data (voltage, current, temperature) were recorded every ten minutes or less. As the test continued, voltage increased (to maintain 250 ma current) to 50 V at which point the power supply was out of compliance and the current decreased over the total test period of $\sim$20 hours. After testing, the electrode/slag assembly was cooled, sectioned, potted in epoxy, polished and examined by SEM/EDX.

For this report, we describe features of Pt- and $LaCrO_3$-slag electrodes without seed and under static conditions. A MIT cathode with flowing slag also is presented. Our next report will include results from static, seeded slag tests plus features of electrodes tested under MHD conditions at AVCO.

b. Electrochemistry at the Pt/Slag Boundary (no seed, $P_{O_2} = 10^{-3}$ atm)

Figure 1 (43X) illustrates the post-test condition of a Pt anode, 20 hours in unseeded slag, 1400°C, $P_{O_2} = 10^{-3}$ atm. The microchemical/microstructural details for this anode correlate well with the macroscopic examination of a Pt/iron oxide-silica "slag" anode described as early as 1954 (3). The spectrum in Figure 2 illustrates the elemental content of our New Hampshire-type slag. Dominant constituents include Al, Si and Fe while K, Ca and Ti are characteristic minor components. This spectrum provides a frame of reference to be compared with ensuing spectra (see below) showing elemental partitioning controlled by thermochemical/electrochemical processes.

Fig. 3A (860X) illustrates the "slag" in contact with the Pt anode within porous zone C, Figure 1. The brightest phase, Pt metal, occurs as domains in intimate contact with "slag" but segregated from the main anode wire. The lack of a sharp Pt/slag interface suggests evolution of gas, probably oxygen, and, possibly, slight oxidation-solution of the Pt wire. The source of oxygen is clearly from the slag. In reference (3), it was demonstrated that molten iron oxide-silica "slags" are primarily ionic conductors. It also was suggested that at the anode, silicate groups (of undefined degree of polymerization) are "discharged" according to,

$$[SiO_4]^{4-} \rightarrow SiO_2 + O_2 + 4e^-.$$

Figures in series 3 and 4 demonstrate that the above anodic process is viable. Figure 3B magnifies (4300X) a portion of Figure 3A. The bright phase is Pt in contact with "phases" 1 and 2. Phase 1 consists predominately of Al and Si, and an appreciable amount of Ti plus traces of Pt, Rh and Fe (Figure 3C). Calcium and K are entirely absent. Phase 2 is similar but contains somewhat more Fe. Figure 4A (4300X) magnifies a typical area in zone C (Figure 1) closer to the undisturbed Pt metal. Pt is associated with partly filled pores (1) and dark domains (2) having a microchemistry depicted by Figure 4B. Very little, if any, Al is present with Si (SiO_2) dominating. The presence of Pt may suggest some oxidation/solution, fine Pt-particles, or interference from adjacent Pt during the analysis at high magnification.

Within the slag (B), Figure 1, dendrites, illustrated in Figure 5 (1720X), are common. These were not observed for cathodic slag. X-ray mapping of these dendrites at high magnification is not precise due to their small size. However, they appear to be enriched in Fe. The

microstructure may develop on cool down of the slag and/or may represent in situ enrichment of the Fe-component in the slag away from the Pt/slag interface.

Figure 6 (43X) contrasts the post-test condition of the pertinent Pt/slag cathode. Considerable damage to the Pt-metal remains obvious. Domains and streamers of Pt are distributed well within the "slag" while dark streamers of "slag" have intruded the remaining Pt cathode. Throughout Figure 6, the Pt is significantly "impure" (in contrast with anodic Pt) having been intruded by and alloyed with Fe. This probably accounts for the apparent degradation of the Pt. Figure 7A (4300X) shows a typical Pt domain (1) in contact with darker "slag" (2). Figure 7B indicates that the metal is enriched with substantial Fe derived from the immediately adjacent slag (2) which is depleted of this component (enriched in Al, Si).

c. Laboratory Experiments Concerning the $LaCrO_3$/Slag Interface (no seed, $P_{O_2} = 10^{-0.68}$ atm)

$LaCrO_3$-based electrodes in slag provide a veritable smorgasbord for the microscopist. Figure 8 (90X) illustrates several well developed, sharply defined interfaces and zones involving arc plasma sprayed $LaCrO_3$ (zone 1) and unseeded slag, without current (1400°C). Chemical partitioning, significantly unlike $LaCrO_3$/slag electrodes with current, occurs within and between each zone. Figure 9A (9100X) shows a blown-up section of the Mg-doped, $LaCrO_3$. The material is somewhat porous and consists of at least two phases (1, 2 Figures 9A, B). The sharp interface between zones 1 and 2 (Figure 8) is magnified in Figure 10 (4500X). Zone 2 marks the first appearance of slag components Al, Si, and Fe. Although similar in microstructure to zone 3 (Figures 8, 11A), zone 2 differs in being enriched in La/Cr-components. Zone 3, Figure 11A (4500X), has apparently densified via reaction between slag and $LaCrO_3$ (Figure 11B). This zone (plus zone 2), probably partly crystalline, constitutes a reaction-diffusion barrier providing the $LaCrO_3$ "protection" from further reaction with slag. Zone 4 (Figure 8), the outermost and thickest portion of this barrier, is magnified in Figure 12A (4600X) to illustrate its "glassy" nature. Chromium is practically absent but La-oxide (plus other rare earths) has dissolved preferentially in the slag (Figure 12B). Adjacent to zone 4 (now occupied by epoxy in Figure 8) typical New Hampshire-type slag (see above) was present but detached with considerable ease.

A $LaCrO_3$ anode in slag is shown in Figure 13. The material (corroded considerably) and surrounding "slag" display noteworthy microstructural and microchemical features. Areas (1), Figure 13, are structureless (glassy ?) and are enriched in the La-component similar to zone 4 (Figure 8, see also Figures 12A, B). Darker areas (2) adjacent to areas (1) consist of irregularly shaped domains within a featureless (glassy ?) matrix, Figure 14A. This matrix has a bulk composition similar to areas (1), Figure 13, while the domains consist of Cr, Fe, Al-oxides (Figure 14B), possibly a spinel or a sesquioxide solid solution depending

on the oxidation state of iron. Similar but better developed crystallites are observed at the cathodic side (see below). The bulk iron content and bulk Al/Si ratio of areas (2), qualitatively, are enhanced in comparison with normal New Hampshire-type slag. Elemental partitioning of this type (not observed without current) suggests solution of $LaCrO_3$ in slag followed by electrochemical migration of the more mobile network modifying cations (such as Cr and Fe) away from the positive anode. Simultaneously, the slag near the anode can be depleted of network-forming, polymerized (n), $[Al,Si]_n^{m-}$ groups which accumulate and discharge oxygen at the anode/slag interface. Similar to Pt/slag anodes but in contrast to cathodes and the "no current" configuration, this interface for $LaCrO_3$/slag is particularly porous suggesting simultaneous solution and gas evolution. Zone A, Figure 13, magnified in Figure 15, is typical of the anode interface. Figure 16A (4500X) includes area 4 of zone A, Figure 13, while Figure 17A (1800X) depicts adjacent areas 3. In Figure 16A, reaction/solution features dominate while partitioning of elements is demonstrated by Figures 16 B, C, D. Dark areas (1) rich in SiO_2 are adjacent to domains of Al, Cr, Fe-rich material (2) similar (but with much less Fe) in chemistry but not morphology to the domains observed in the outer slag, areas 2, Figures 13, 14. The groundmass (3), containing the La-component from the pre-existing $LaCrO_3$, also is similar chemically (but with far less Fe) to area 1 (Figure 13) and the matrix in area 2 (Figures 13, 14). Notably absent in appreciable amounts are K and Ca. Figure 17A of adjacent areas 3 (Figure 13), illustrates the resistive layer developed near the former $LaCrO_3$/slag interface. Microchemistry varies but is dominated by Al/Si-oxides with traces of La, Cr, and Fe (e.g., see Figure 17B). Powder x-ray diffraction data reveal that these deposits consist of silica (tridymite and cristobalite) plus mullite.

Area 5, Figure 13 reflects the processes which degrade this particular $LaCrO_3$ ceramic. Slag apparently intrudes via the available porosity and dissolves the material to produce rounded $LaCrO_3$ islands (1). Figure 18 (4600X). The groundmass consists of dark, Al/Si-rich areas (2) and brighter, Si/La-rich areas (3). Very little Fe, K, or Ca is present. Except for microchemical details, cathodic $LaCrO_3$ degrades in similar fashion (see below).

Figure 19 illustrates a $LaCrO_3$/slag cathode. Areas 1 and 2 summarize the most pertinent features. Figure 20 (48X) shows area 1 which is subdivided into three distinct zones. In contrast with the anode, a porous resistive layer, rich in Si/Al-oxide is clearly absent. Instead, rather sharply delimited reaction zones have developed. Zone A, Figure 20, is magnified in Figure 21A (920X). This zone is typical of the "slag" adjacent to the altered $LaCrO_3$ electrode (zone C, Figure 20). Isolated islands or crystallites (2) plus "stringers" or dendrites (3) are contained within a featureless matrix (1). The crystallites are rich in Cr, derived from the $LaCrO_3$, and Fe, derived from the slag. These may be a Fe/Cr-oxide spinel (plus traces of Mg and Al, Figure 21B). Powder

x-ray diffraction data, indeed, reveal the presence of a spinel phase. The "stringers" (3) are Fe-rich (Figure 21C) and may represent crystallization during cool-down. These were not observed, however, in anodic slag. Microchemistry of the groundmass (1), given in Figure 21B, is similar to area 1, Figure 13 (anode) and area 1, zone 4, Figures 8, 12A (no current). This material, containing the La-oxide component, occurs within cracks and fissures obvious in Figure 20. Noteworthy is the rather high concentration of Ca and K.

Zone B, Figure 20, is magnified in Figure 22 (1900X). Interconnected domains (2), rich in Fe/Cr-oxide (Figure 21B), now enclose a featureless material (1) having "slag" components similar to Figure 21B. Zone C, Figure 20, includes the volume previously occupied by the $LaCrO_3$ electrode. Figure 23A (1840X) is a magnification of this zone. Slag has intruded the ceramic, similar to the anode, to produce a phase assemblage composed of rounded domains of $LaCrO_3$ (2) enclosed within a complex matrix. In contrast to the anode, the matrix consists of several materials showing partitioning of Si, La, Cr and Fe (Figure 23B, C). Phase 4 (Figure 23A, C) appears to be the precursor for the Fe/Cr-rich domains in area B, Figures 20, 22. The bulk Ca, K and Fe contents are significantly higher than for corresponding anodic areas, Figure 18. Within the "neck" (2) of the $LaCrO_3$ in Figure 19, slag again has penetrated, probably via the available porosity, Figure 24. Although $LaCrO_3$ particles are more numerous the phase assemblage is identical with that observed in Figure 23.

d. MIT Electrodes

We received from W. R. Cannon, MIT, two electrodes (designed, fabricated and tested in their laboratories) for microstructural examination. Both are identical in terms of initial materials, design and fabrication. One was subjected to current (number S4048) while the other (S4055) apparently was tested only for thermal behavior. Test conditions and materials included,

a) 304 stainless steel base, grooved,

b) 36% Fe_3O_4-64 $FeAl_2O_4$, nominal composition (plasma-sprayed?) originally 0.030" above grooves followed by,

c) hercynite ($FeAl_2O_4$, 0.20" thick),

d) surface temperature 1360°-1390°C before introduction of slag,

e) $\sim$ 1650°C slag surface temperature,

f) $\sim$ 2 hrs slag time with 1 hr current as cathode (40 min at 1 1/2 A/cm^2),

g) $\sim$ 2 1/4 hrs slag plus seed with no current, and

h) the upper hercynite layer was completely dissolved off.

SEM/EDX examination revealed that insulation is $MgAl_2O_4$ while the specified "304 stainless steel" base is nearly pure Fe (mild steel ?) with traces of Mn. Figure 25 (15X) illustrates the basic features of the MIT electrodes. Pertinent microstructure and microchemistry to be documented for the electrode tested without current should be compared with corresponding areas of the cathode (see below). A rather sharp interface exists between ceramic and vesicular slag as suggested in Figure 26A. The pre-existing hercynite layer was sacrificial, having been dissolved by the slag. The slag (S) layer is characterized by domains (e.g. 1 and 2, Figure 26) within a structureless matrix. The spectra in Figure 26B indicate that these domains are enriched with respect to Si, K, Ca and Fe components while the groundmass is predominately a vitrified potassium aluminosilicate plus some iron oxide. This partitioning of elements, not evident closer to the slag surface, may have developed during cool-down or during testing in response to crystallization controlled by the inherent thermal gradients. If the latter situation prevailed, the segregation of Fe within discontinuous domains could diminish the electrical conductivity of the slag significantly.

The uppermost portion of ceramic (C), Figures 25, 26 is illustrated by Figure 27 (5000X). A two-phase mixture clearly is evident. The brighter domains are rich in Fe-oxide, low in Al-oxide (a spinel ?) while the darker matrix is rich in Al-oxide, low in Fe-oxide (plus potassium). This layer may be the remains of the altered hercynite layer (see above) intruded by K or may be recrystallized ceramic similar in bulk composition to that existing below the original hercynite layer. The bulk of the ceramic (C), Figure 25, is shown in Figure 28A (2000X). Variation in the microchemistry is reflected by the varigated nature of the ceramic. Bright areas correlate with Fe-rich zones which grade into darker bands containing variable Al/Fe contents (Figures 28B, C). This microchemistry developed either during fabrication (plasma spraying of Fe/Al-oxide ?) or via oxidation of the ceramic during testing.

Features related to the slag/ceramic interface of the electrode tested without current are well defined and not particularly complex. The corresponding cathode, having similar materials and thermal conditions but with current, differs substantially. Figure 29 (200X) illustrates the slag-ceramic interface for much of this cathode. Within the slag (3) and in interface (2), bright domains (A), magnified in Figure 30A, are evident. These are not abundant near and at the surface of the slag. In contrast to the domains in the slag of the electrode without current (see above), these have different morphology and are particularly enriched in Fe. The featureless groundmass (B), however, has a similar composition (Figure 30B, with apologies). Interface (2), Figure 29, extends but widens toward the $MgAl_2O_4$ insulator. Figure 31 (90X) illustrates interface (2) within several type-areas (5, 6, 7) are evident. Areas (6) "intrude" the insulator (4) and contain domains (5) of a Ca-rich material. Area 7

includes domains of the Fe/Al-oxide ceramic undergoing reaction with slag components. Figure 32A (2000X) magnifies a typical portion of areas (6). Bright, Fe-rich domains (1), are contained within a matrix (2) of Al, Si, K and Fe components (Figure 32B). Chlorine and Zn from unknown sources are also present within areas (6) as well as in porous zones of insulator (4) adjacent to area (6), Figure 31.

The microstructure within interface (2), Figures 29 and 31, are illustrated in Figure 33A (900X). Fe-rich segregations (1), Figure 33B, are confined within a K/Al/Si-rich (2) matrix (Zn often present).

Cathodic reduction and segregation of iron (as reduced oxide or even metal) mixed with "slag" has been observed previously (reference 3). For a Pt cathode (see above) available Fe reacts with the noble metal provided temperature is high enough. In this Fe/Al-oxide cathode, dissolution of the ceramic by slag probably enhances the concentration and segregation of Fe-rich material. $LaCrO_3$-based cathodes (see above) provide chrome to the slag and this component reacts with the available Fe to precipitate crystalline Fe/Cr-oxide, probably a spinel containing reduced iron. Thus, the chemistry at a slag/metal or slag/ceramic interface is controlled not only by cathodic reduction of iron in the slag electrolyte but, obviously, by temperature and bulk chemistry of the electrode.

Microstructural and microchemical features of the Fe/Al-oxide ceramic below the slag are of two types. Figure 34A (2000X) illustrates the ceramic immediately adjacent to interface (2), Figure 29. A two-phase assemblage (Figure 34B) is characterized by bright domains rich in Fe and Al (a spinel ?) plus darker intergrowths rich in Al, K, and Fe (K/Al/Fe-oxide, β-alumina ?). The bulk of the ceramic below this zone of apparent interaction with K remains relatively unaltered and is identical with Figure 28A (tested without current).

e. AVCO/NBS Slagging Test 1

Post test analysis and materials characterization of these electrodes is in progress and will be reported at a later date. Some delay has been caused by the urgency for characterization of electrode systems from the proof tests carried out at Westinghouse Research and Development Labs. in preparation for the U-02 Phase III test in Moscow early next year.

f. NBS/AVCO Slagging Test 2

Another set of electrodes has been designed and is partially constructed for eventual testing at AVCO. This set will consist of $LaCrO_3$ and/or platinum as the electrode materials. Careful attention has been paid to the bond line temperature between platinum and slag or $LaCrO_3$ and slag. Experiments reported elsewhere in this report were designed to give information concerning the electrochemical effects expected at these boundaries. These experiments are continuing.

Details of the electrode construction will be given at a later date.

g. NBS/APS Electrodes

A set of six electrodes (3 anodes and 3 cathodes) have been constructed. The set is composed of arc plasma sprayed $LaCrO_3$ (Mg) attached through a cermet to a nickel ion plated copper base. A cap of $85ZrO_2$-$3Y_2O_3$-$12CeO_2$ (aps) is attached through a grade to the $LaCrO_3$. The insulator consists of $MgAl_2O_4$ arc plasma sprayed over the entire side of each electrode and ground flat.

Two thermocouples are built into the electrode set; one in a cathode and one in an anode. The electrodes are designed for a heat flux of 100 w/cm^2 and a surface temperature of 1650 °C. Stress relief slots are cut into the surface at 20 mm intervals. Fig. 35 (p. 77) shows a schematic diagram of the electrode. Testing of this electrode has been delayed due to the extensive renovation of the MIT test bed facility. The proposed test program has been submitted to Prof. J. Cordero of MIT and the test should be conducted during the next reporting period.

h. Conclusions

Several conclusions and speculations can be derived from the electrodes examined for this report and from those (including seed, static and dynamic slagging conditions) to be reported for the next quarter,

1. Molten slag (certainly, New Hampshire-type) has a significant ionic component to its bulk electrical conductivity.

   a) This probably includes <u>both</u> anion (oxygen) and cation (Fe, Ca, K) current carriers which are manifested by,

   b) Partitioning of elements particularly at the slag/electrode interface.

   c) Resistive Al_2O_3/SiO_2- or SiO_2-rich deposits develop at the anode interface regardless of the electrode material (e.g. Pt or $LaCrO_3$), and these are accompanied by enhanced porosity due to evolution of gas, presumably oxygen; network-forming, polymerized $[(Al,Si)O_4]_n^{m-}$ groups appear to be one source of available oxygen discharged.

   d) Mobile network-modifying cations, especially Fe^{n+}, K^+, and Ca^{2+} are displaced away from the anode and enhanced at the cathode.

   e) Over and above these phenomena, several related effects have been observed:

1) Pt cathodes react (alloy) with the available iron while,

2) $LaCrO_3$ and the MIT Fe/Al-oxide (spinel) cathodes develop Fe-rich deposits at the ceramic/slag interface, the chemistry being controlled by the cathodic material itself plus thermal and electrochemical factors.

For MHD electrodes, the following recommendations can be formulated:

1. Pt appears to be a reasonable anodic material although build-up of resistive layers could inhibit current transfer and contribute to accelerated arcing and degradation.

2. Pt at the cathodic side probably should be operated cold or with an appropriate design to prevent degradation via Fe-diffusion.

3. Porous $LaCrO_3$-based electrodes are subject to considerable solution/reaction at both anode and cathode.

a) $LaCrO_3$, nevertheless, develops resistive oxide layers at the anode.

b) Fe/Cr-oxide (probably spinel) develops adjacent to $LaCrO_3$-cathodes to preclude deposition of highly conductive Fe-rich zones,

4. When slag is molten at the cathodic side, Fe-enrichment near or at the electrode/slag interface could contribute to axial shorting in an MHD channel.

a) Pt prevents this enrichment in short-term experiments by alloying with Fe.

b) $LaCrO_3$ provides Cr-oxide which interacts with the iron to precipitate spinel.

c) Fe/Al-oxide may aggravate the formation of axially conductive layers by providing additional Fe to the cathode/slag interface.

5. Spinels containing Fe-oxide may be desirable anodic materials; dissolved Fe could diminish the build-up of Al/Si-oxide resistive layers.

Problems (build-up of resistive or conductive layers) associated with the electrochemical behavior of slag could be diminished by:

1. Operating "cold" metal or oxide cathodes at temperatures such that thin, crystalline and, hopefully, conductive (electronic) deposits develop at the electrode/slag interface.

2. Develop "hot" ceramic/metal electrodes with thin, passivated (equilibrium) but conductive layers at the electrode/slag interface; this entails detailed chemical/electrochemical studies of slags combined with candidate oxides.

References

1. W. R. Hosler, T. Negas, S. W. Petty, 15th Symposium, Proceedings on Engineering Aspects of MHD, Philadelphia, PA, May 24-26, 1976.

2. Final Report on the Joint U.S.-U.S.S.R. Test of U.S. Electrode System in the U-02 Facility-Phase I, ERDA 1976.

3. M. T. Simnad, G. Derge, I. George, Trans. AIME 200, 1386 (1954).

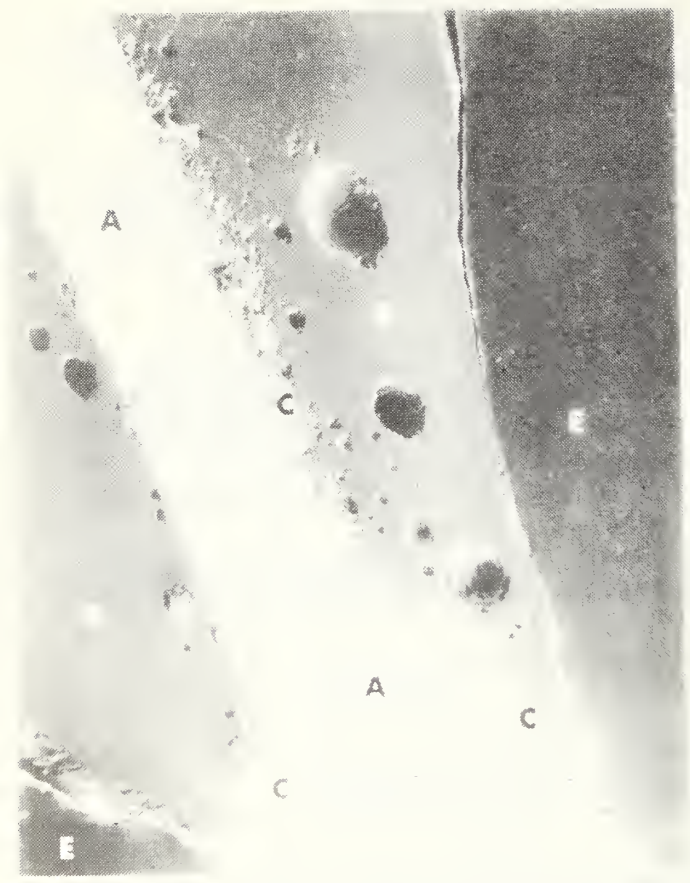

Figure 1. SEM micrograph (43X) of a Pt anode (A) in slag (B); E = epoxy, C = porous Pt/slag interface.

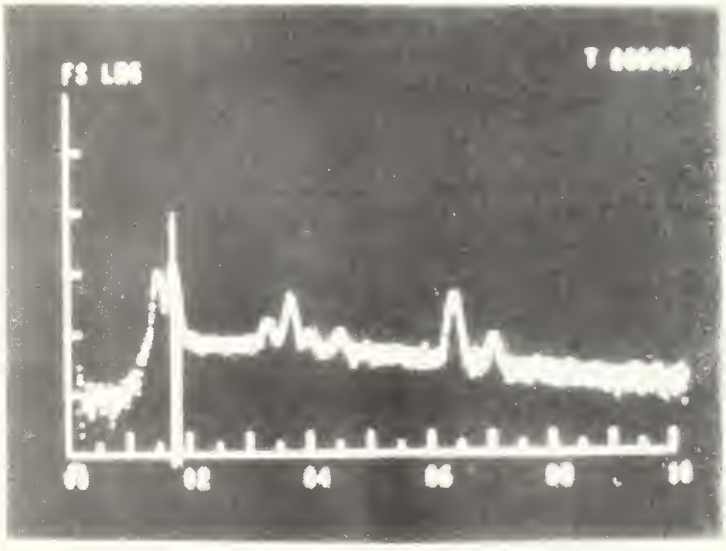

Figure 2. EDX spectrum for New Hampshire-type slag. Elements from left to right are Al, Si (long vertical markers superimposed), K, Ca, Ti and Fe.

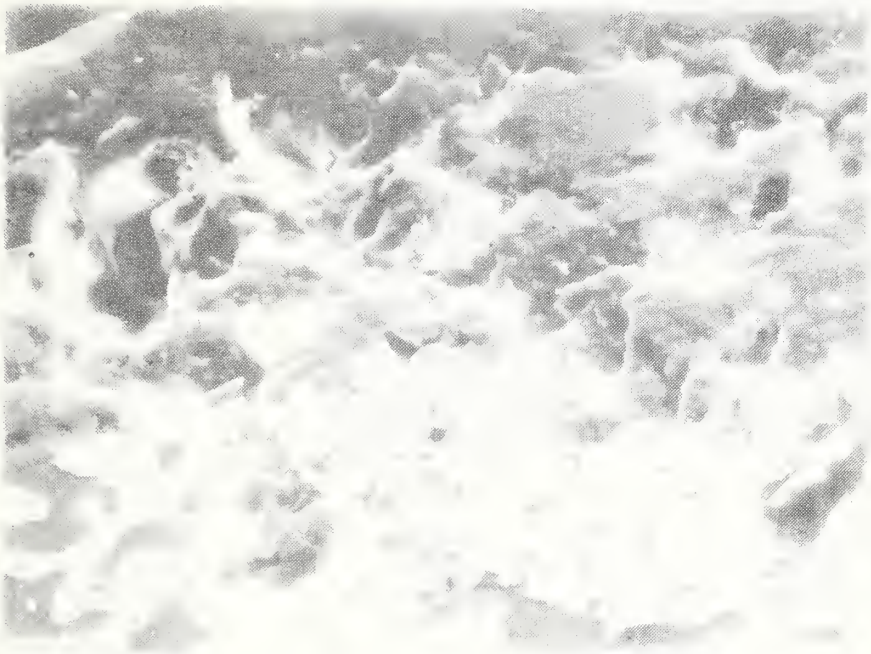

Figure 3A. SEM micrograph (860X) of porous Pt/slag interface C, Figure 1. Bright domains are Pt.

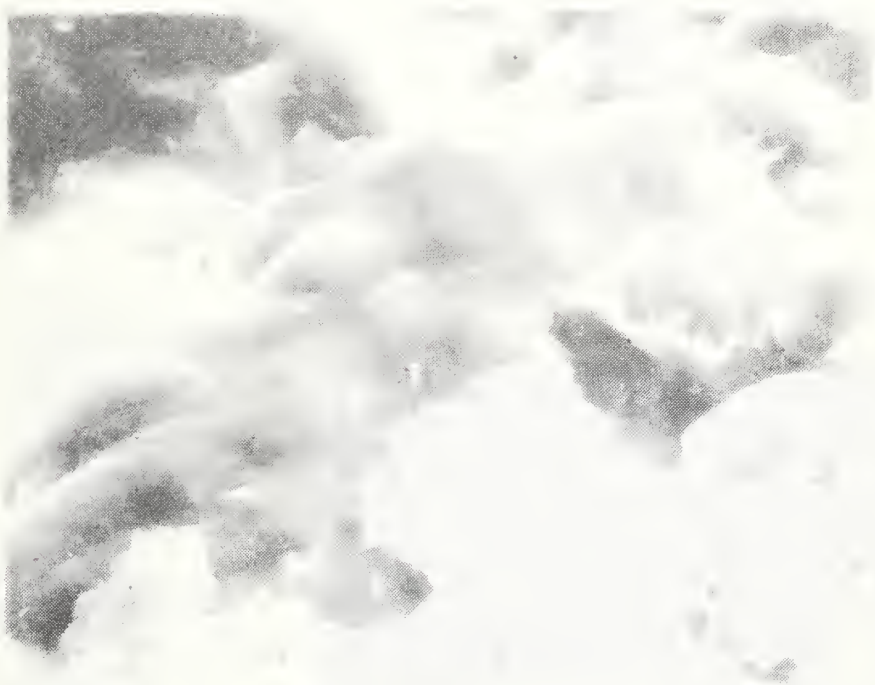

Figure 3B. Magnification (4300X) of porous Pt/slag interface C, Figures 1 and 3A.

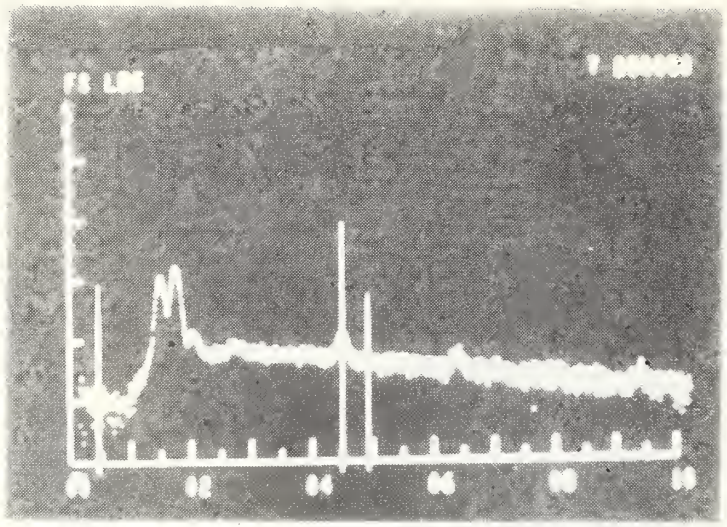

Figure 3C. EDX spectrum for "phase" 1, Figure 3B. Al, Si dominate with smaller amounts of Pt, Rh, Ti (superimposed vertical markers) and Fe.

Figure 4A. SEM micrograph (4300X) of zone C, Figure 1, near the undisturbed Pt metal.

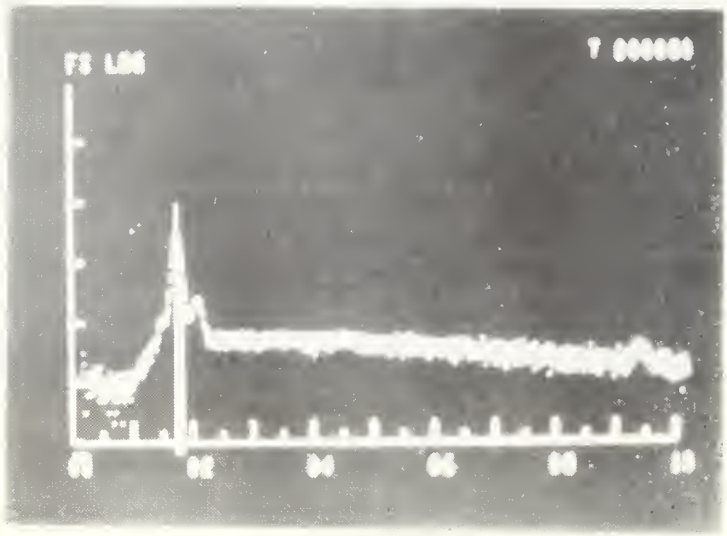

Figure 4B. EDX spectrum for "phases" in (1) and (2) of Figure 4A. Si (superimposed vertical markers) dominates with some Pt also present.

Figure 5. SEM micrograph (1720X) of slag (B), Figure 1. Dendritic growth of an iron-rich phase is apparent (see text).

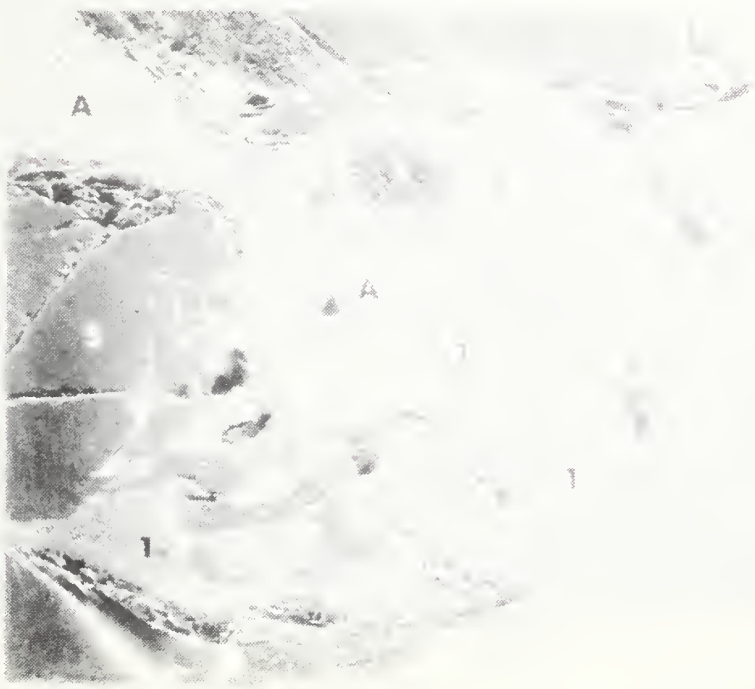

Figure 6. SEM micrograph (43X) of Pt (A)/slag (S) cathode. E = epoxy; areas 1 are "slag" intrusions and/or Pt/"slag" domains.

Figure 7A. SEM micrograph (4300X) of a typical Pt domain (1) in contact with "slag" (2).

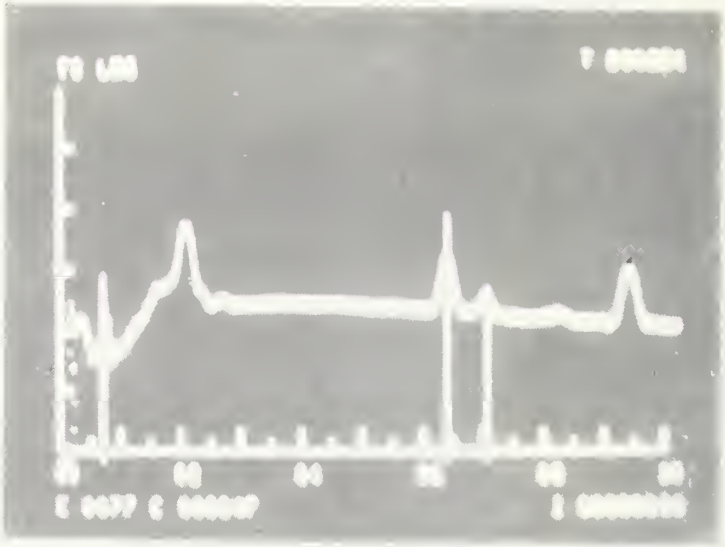

Figure 7B. EDX spectrum for typical Pt in Figures 6, 7A. Pt dominates but is alloyed with Fe (superimposed vertical markers).

Figure 8. SEM micrograph (90X) of $LaCrO_3$/slag, 1400°C, without current. E = epoxy; Zone 1 = $LaCrO_3$; Zones 2, 3 and 4 develop from slag/$LaCrO_3$ interactions (see text).

Figure 9A. SEM micrograph (9100X) of $LaCrO_3$ (doped with MgO) in zone (1), Figure 8.

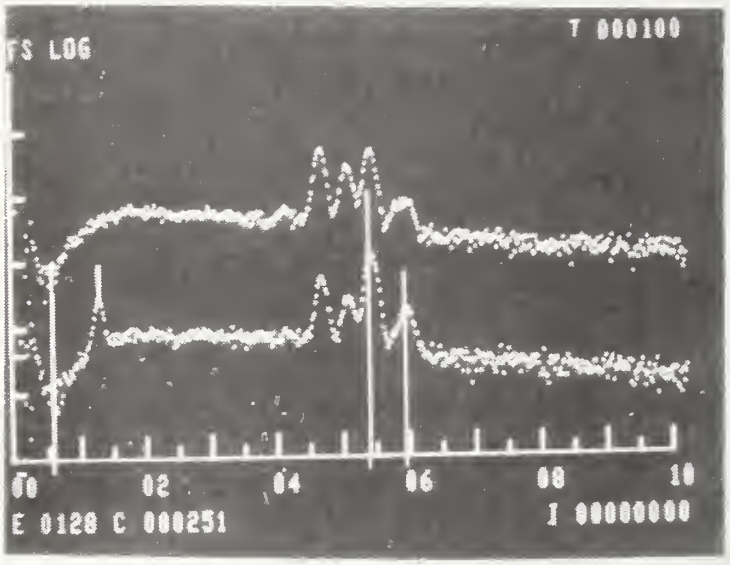

Figure 9B. Upper EDX spectrum, brighter irregularly shaped domains (1), Figure 9A; $LaCrO_3$ (plus a trace of Sc and other rare earths judging from the diffuse nature of the last line, CrKβ). Lower spectrum, darker matrix (2), Figure 9A; Mg (short vertical marker), La (weaker than in upper spectrum), Cr (long vertical markers).

Figure 10. SEM micrograph (4500X) of interface area between zones 1 and 2, Figure 8. Zone 1 is $LaCrO_3$ while zone 2 contains slag components plus $LaCrO_3$ (see text).

Figure 11A. SEM micrograph (4500X) of zone 3, Figure 8. See Figure 11B.

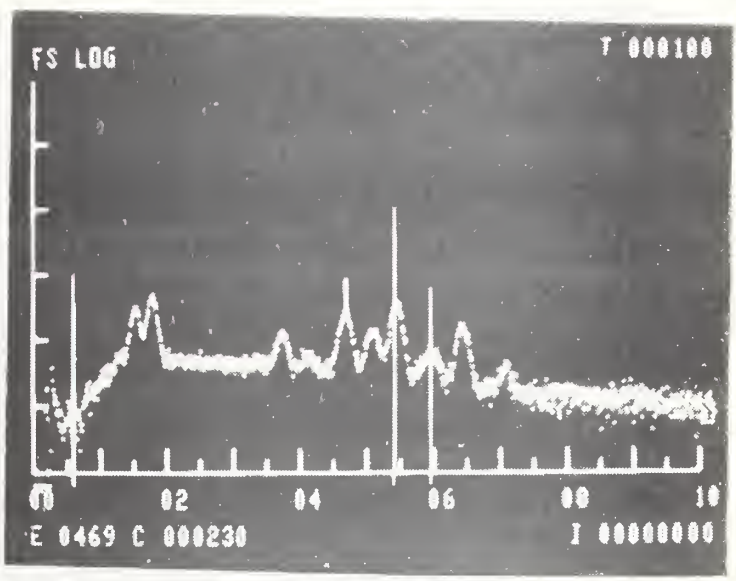

Figure 11B. EDX spectrum for entire area, Figure 11A; Al, Si, Ca, La (short vertical markers), Cr (long vertical markers), Fe. Darker phase 1, Figure 11A, is enriched in Al/Si and depleted in La/Cr which are concentrated in phase 2.

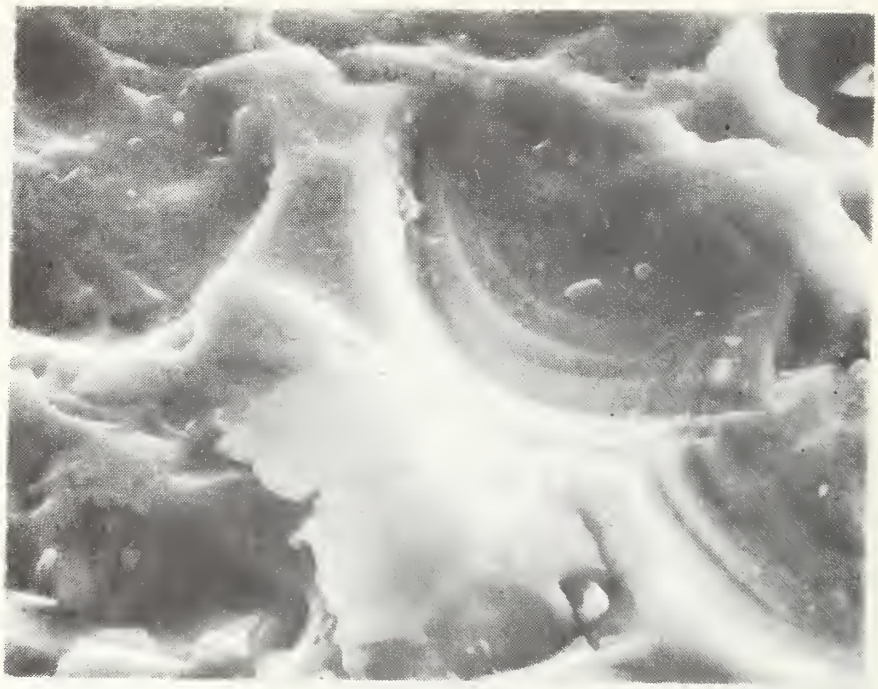

Figure 12A. SEM micrograph (4600X) of zone 4, Figure 8.

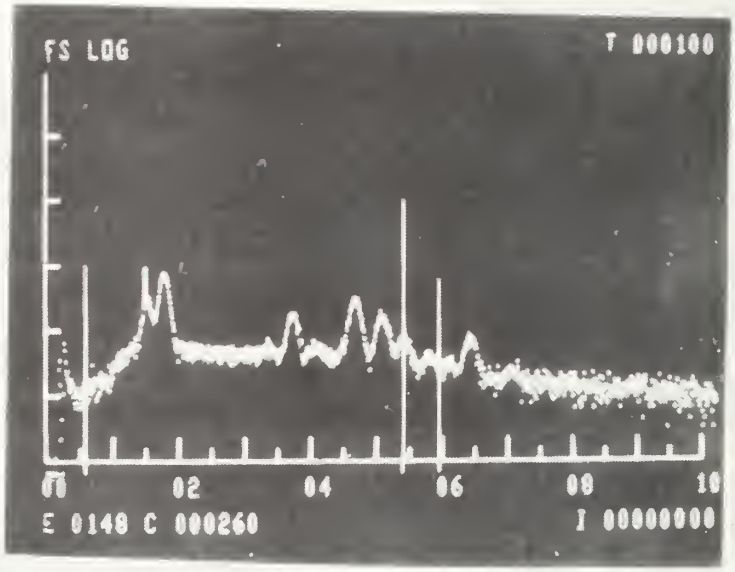

Figure 12B. EDX spectrum for entire area in Figure 12A. Very little, if any, Cr is present as the CrKβ line is absent (third long vertical marker). The CrKα line superimposes with other rare earths; Al (short vertical marker), Si, Ca, La + rare earths, Fe.

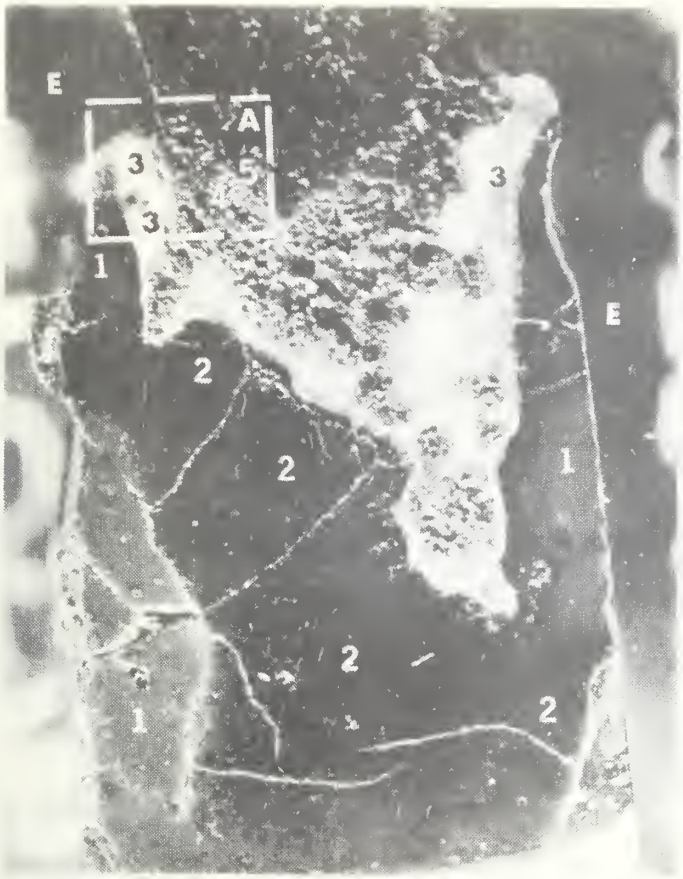

Figure 13. $LaCrO_3$/slag (no seed) anode (4-5X). Numerals refer to typical areas examined by SEM/EDX; E = epoxy.

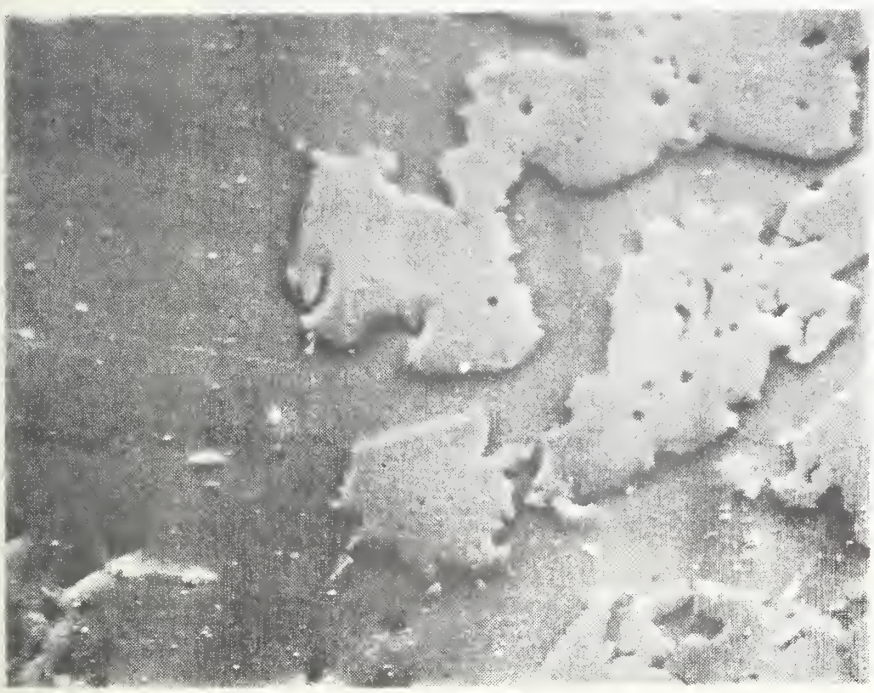

Figure 14A. SEM micrograph (1760X) of areas (2), Figure 13.

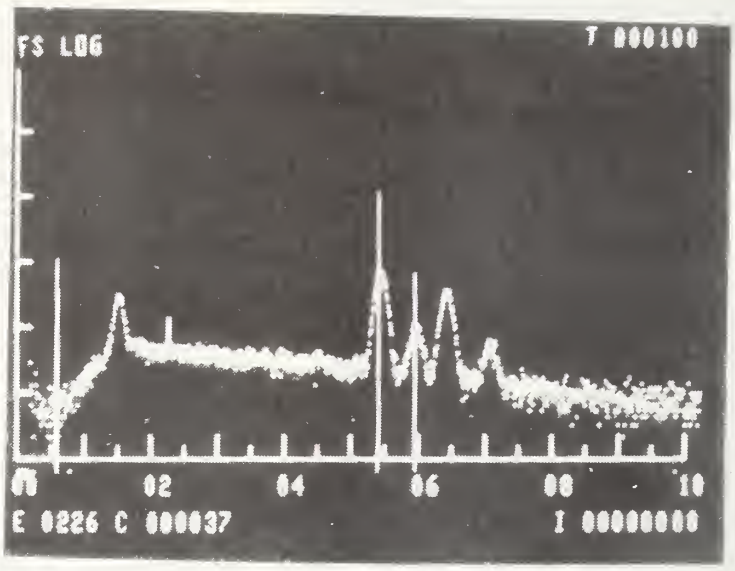

Figure 14B. EDX spectrum for irregularly shaped domains in Figure 14A; Al, Cr (long vertical markers), Fe.

Figure 15. SEM micrograph (47X) of zone A, Figure 13. L = $LaCrO_3$ anode; S = modified slag; E = epoxy. Areas 3, 4 are typical of areas 3, 4 shown in Figure 13.

Figure 16A. SEM micrograph (4500X) of area 4, Figures 13, 15.

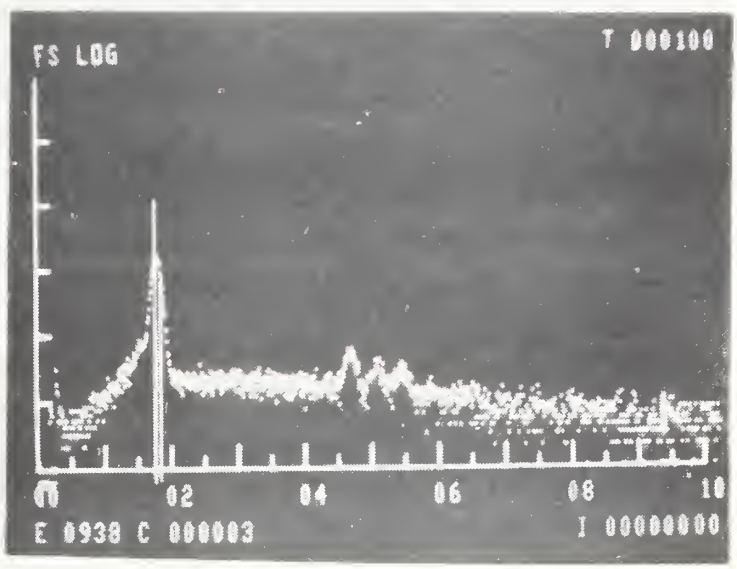

Figure 16B. EDX spectrum for phase 1, Figure 16A; Si (long vertical) markers plus traces of La, Cr.

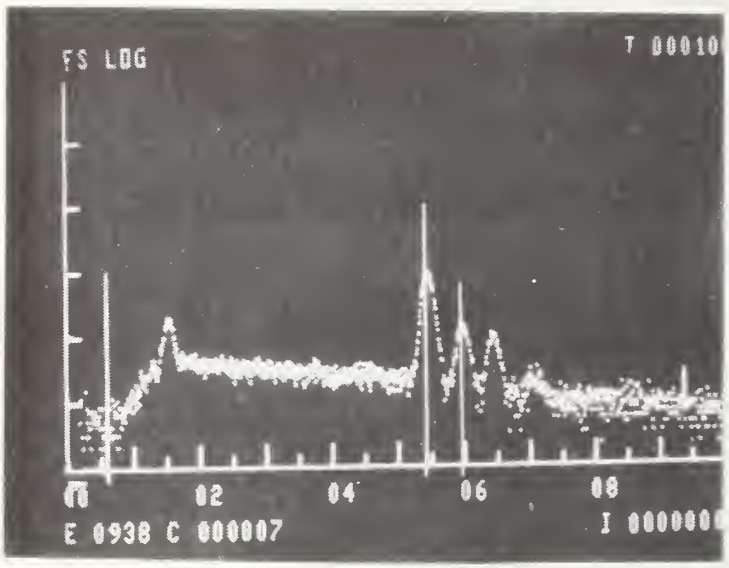

Figure 16C. EDX spectrum for areas 2, Figure 16A; Al, Cr (long vertical markers), Fe.

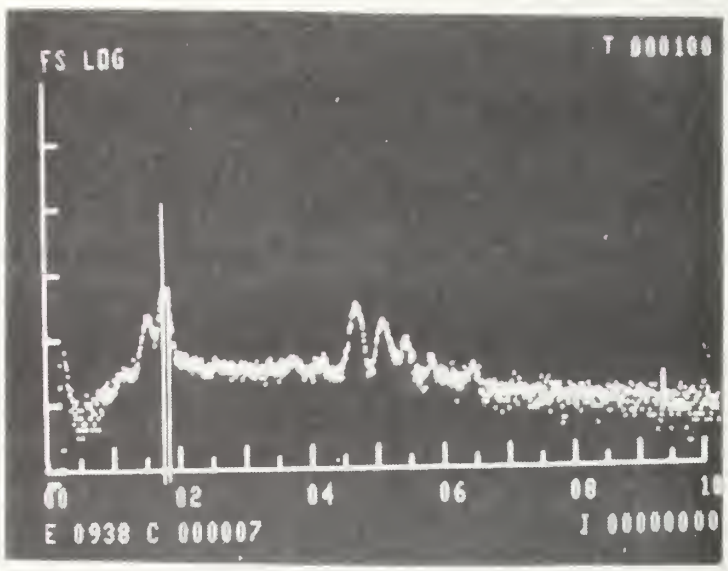

Figure 16D. EDX spectrum for matrix 3, Figure 16A; Al, Si (long vertical markers), Ca (trace), La (plus rare earths), Fe (trace).

Figure 17A. SEM micrograph (1800X) of areas 3, Figure 13.

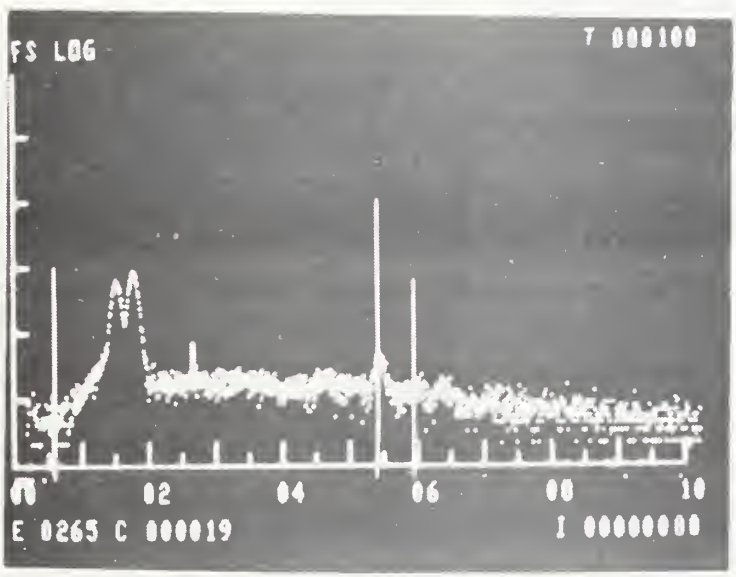

Figure 17B. EDX spectrum for Figure 17A; Al, Si, plus traces Cr (long vertical markers), Fe.

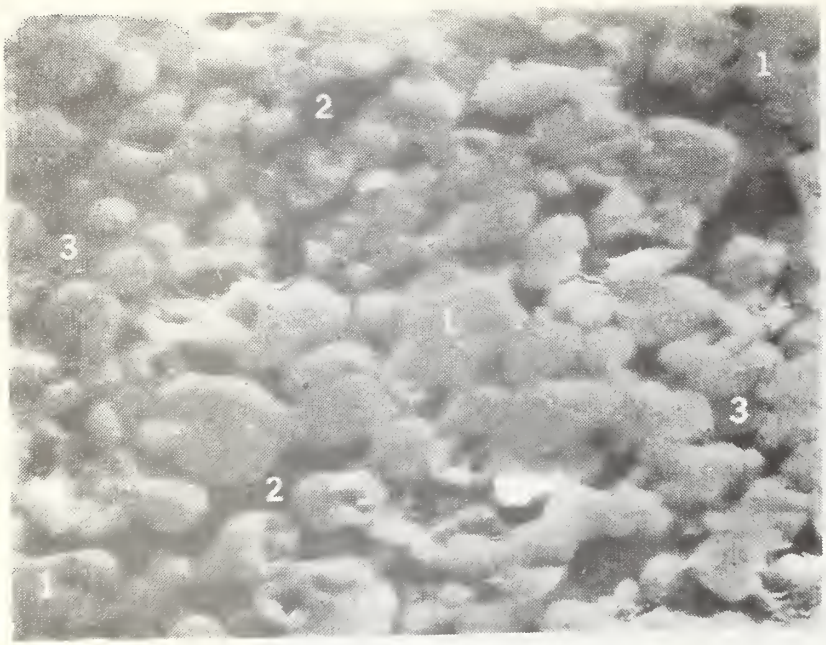

Figure 18. SEM micrograph (4600X, poor focus) of area 5, Figure 13.

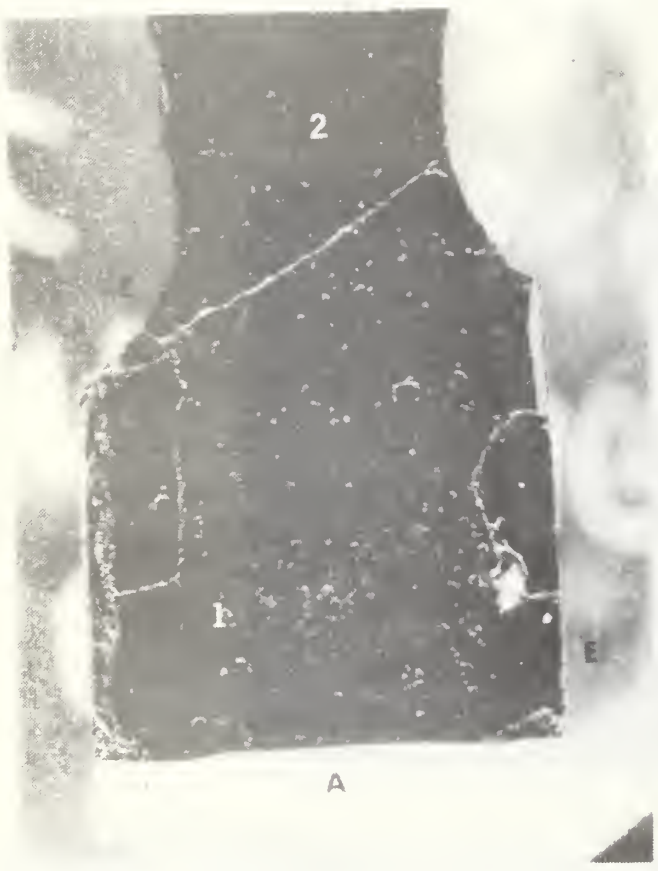

Figure 19. $LaCrO_3$/slag cathode (∿4-5X), no seed. Numerals refer to typical areas examined by SEM/EDX. A = portion of Al_2O_3 boat containing the slag; E = epoxy.

Figure 20. SEM micrograph (48X) of area 1, Figure 19. A, B, C zones subdivide this area (see text and figures below).

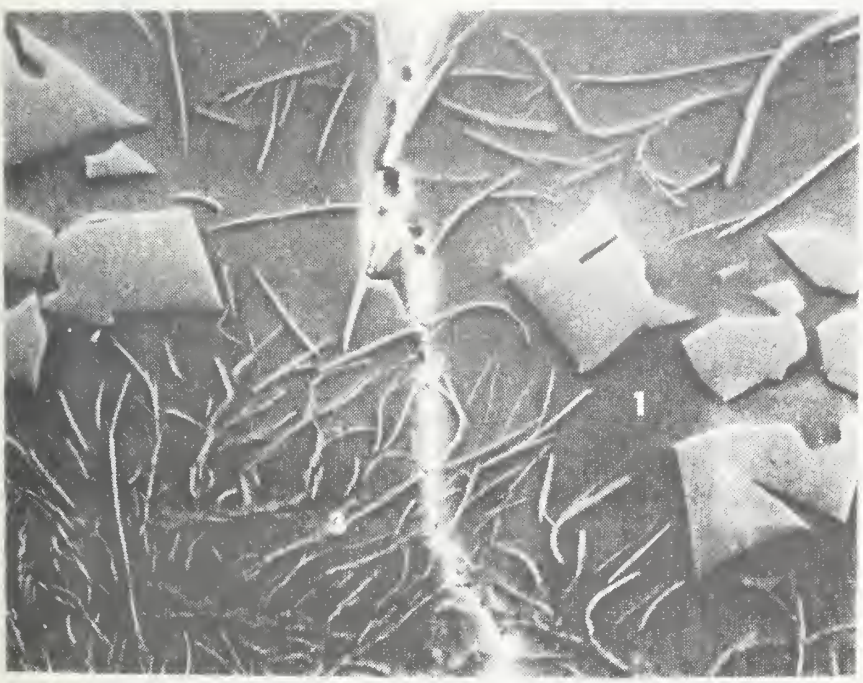

Figure 21A. SEM micrograph (920X) of zone A, Figure 20.

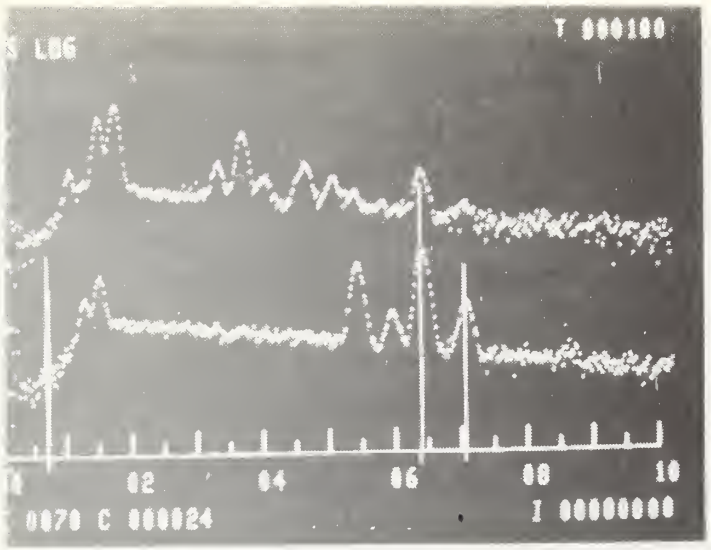

Figure 21B. EDX spectra for phases in Figure 21A. Upper spectrum for groundmass (1); Al, Si, K, Ca (strong) La (plus rare earths), Fe (long vertic markers). Lower spectrum for crystal-lites (2); Mg, Al, Cr, Fe.

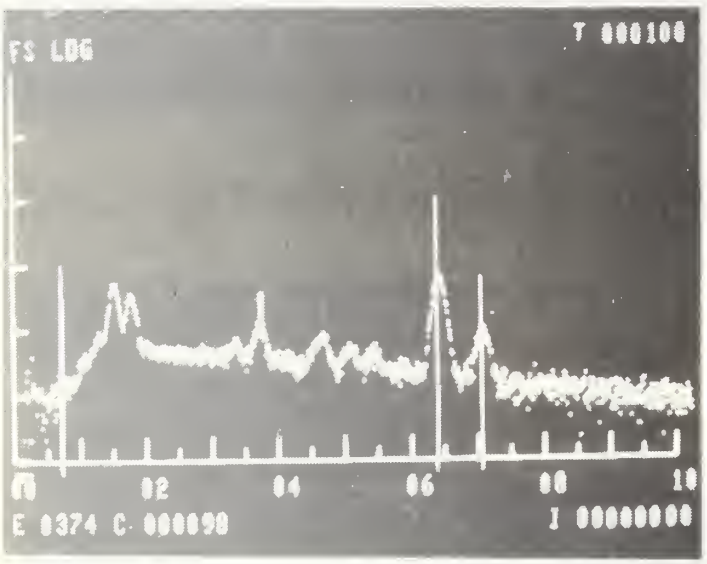

Figure 21C. EDX spectrum for "stringe (3), Figure 21A; Al, Si, K, Ca (short vertical marker), La (plus rare earths Fe (strong, long vertical markers).

Figure 22. SEM micrograph (1900X of zone B, Figure 20 (see text). Areas 1, 2 are identical with are 1, 2, Figure 21A.

Figure 23A. SEM micrograph (1840X) of zone C, Figure 20.

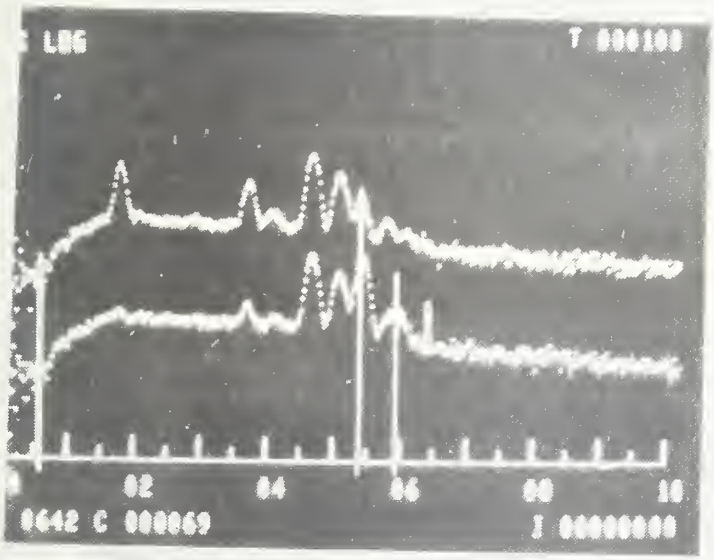

Figure 23B. EDX spectra for phases in Figure 23A. Upper spectrum, phase 1; Si, Ca, La (plus rare earths). Lower spectrum, phase 2, $LaCrO_3$; Ca, La (plus rare earths), Cr (long vertical markers).

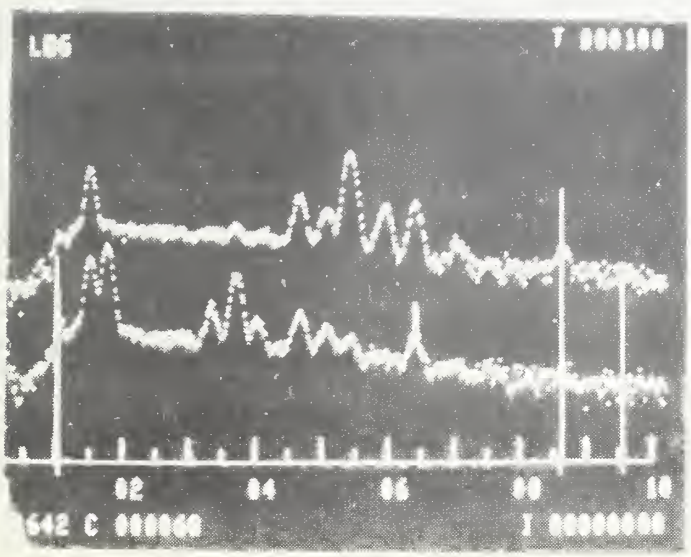

Figure 23C. EDX spectra for phases in Figure 23A. Lower spectrum, phase 3; Al, Si, K, Ca, La (plus rare earths), Fe (short vertical marker). Upper spectrum, phase 4; Si, Ca (trace), La, Cr (strong), Fe, Zn (long vertical markers).

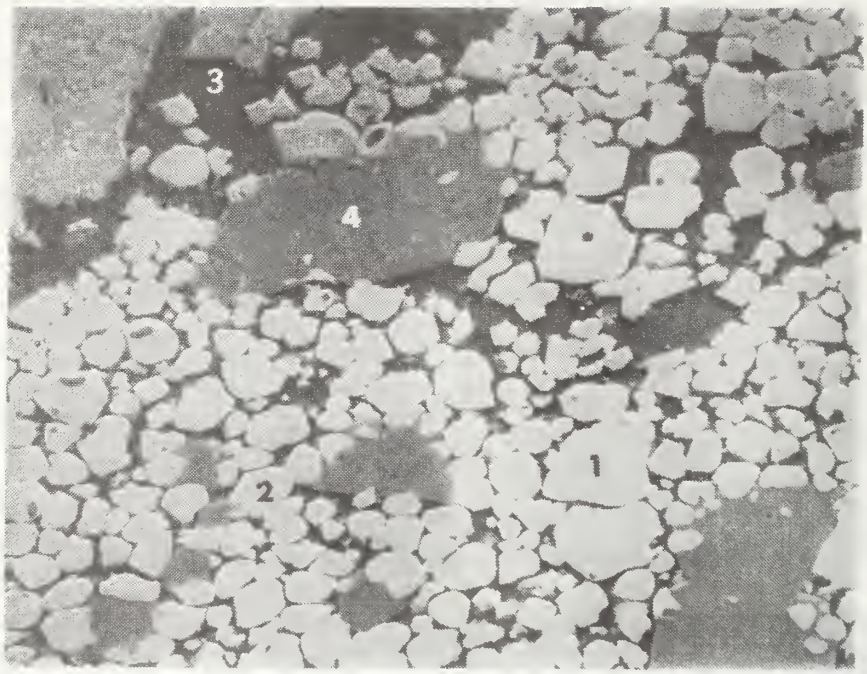

Figure 24. SEM micrograph (910X) of area 2, Figure 19, within the "neck" of the $LaCrO_3$ cathode. Phases indicated are identical with those in Figure 23.

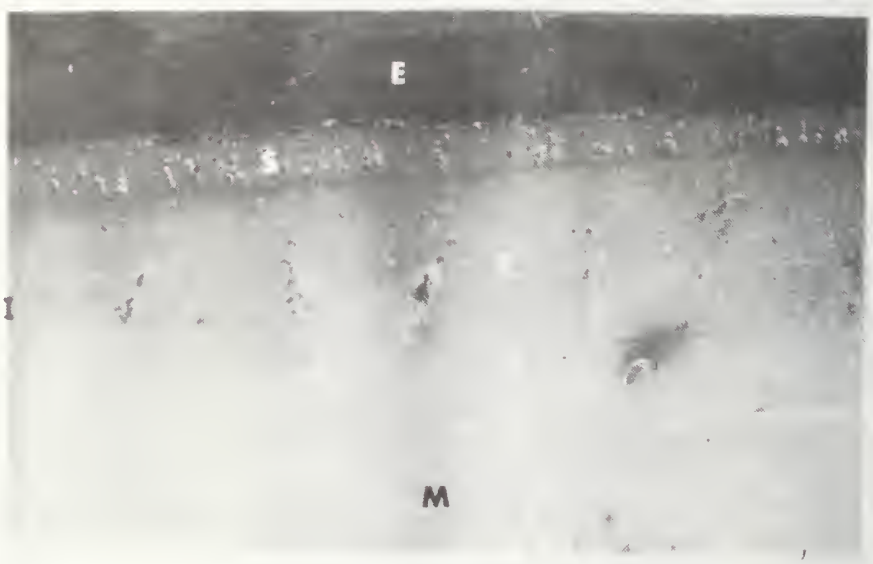

Figure 25. SEM micrograph (15X) of a portion of the cross-section of MIT electrode (S4055, tested without current). M = grooved Fe metal; C = ceramic, Fe/Al-oxide, see text; S = slag; I = insulation; E = epoxy.

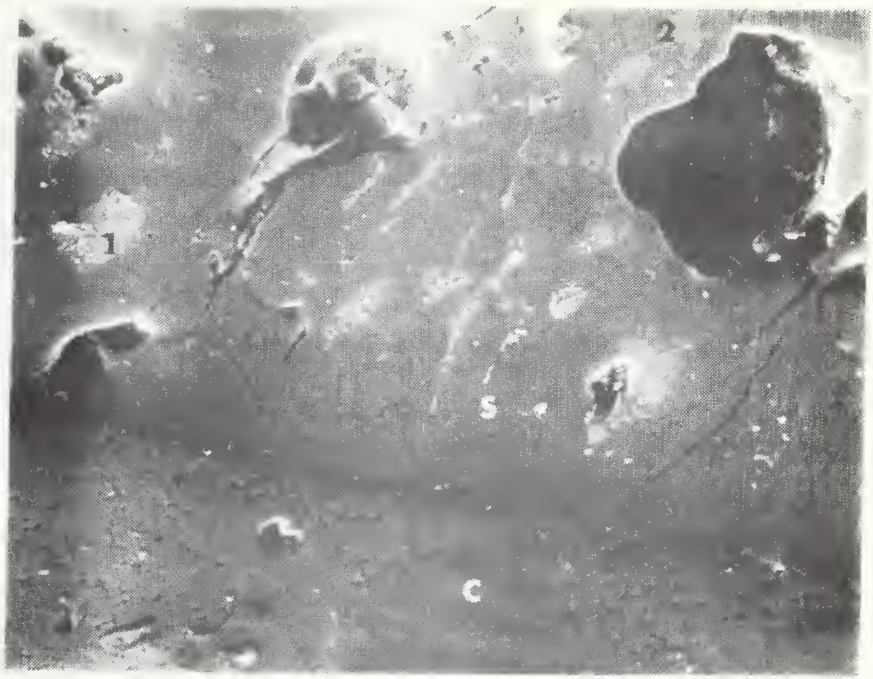

Figure 26A. SEM micrograph (500X) of slag (S) - ceramic (C) interface of Figure 25.

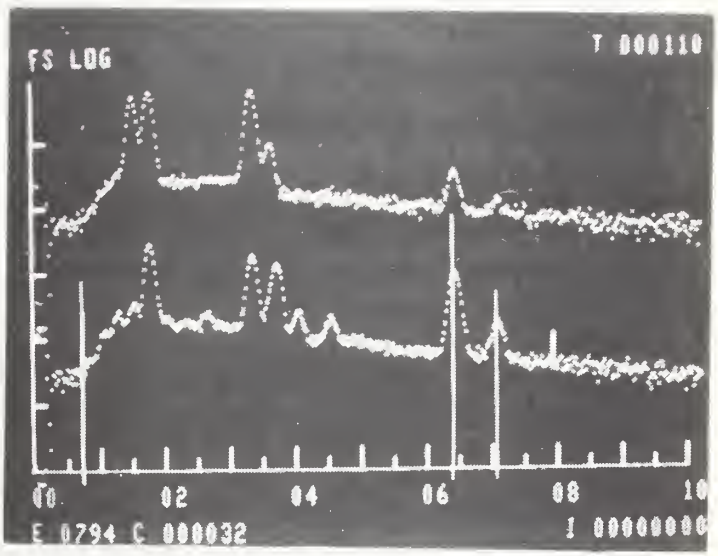

Figure 26B. Lower EDX spectrum typical of domains 1, 2, Figure 26A; Mg, Al (traces), Si (strong), K, Ca, Ti and Fe (superimposed vertical markers). Upper spectrum is for the main slag groundmass, Figure 26A; Al, Si, K (strong), Fe (weak).

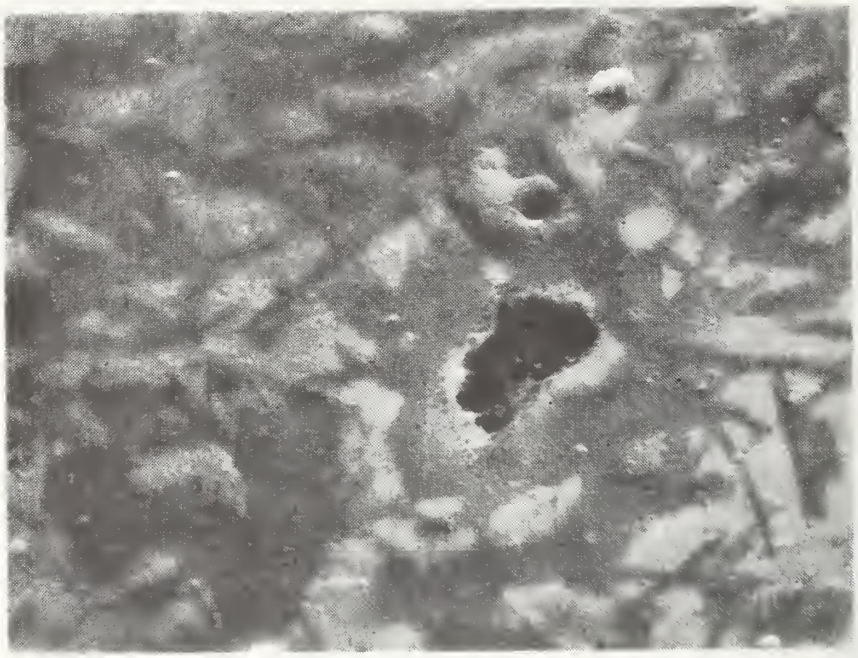

Figure 27. SEM micrograph (5000X) of the uppermost portion of ceramic (C), Figure 26 (see text).

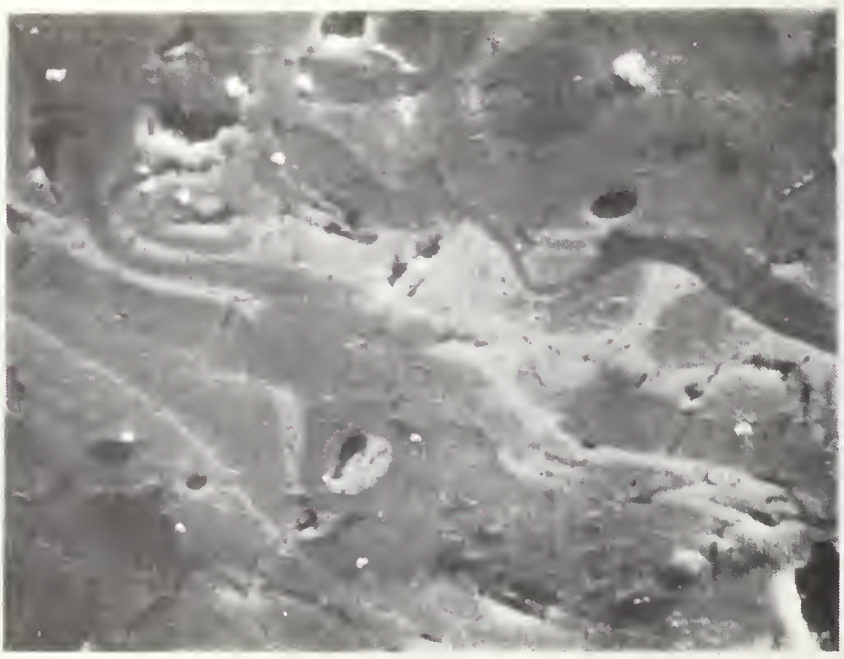

Figure 28A. SEM micrograph (2000X) of Fe/Al-oxide ceramic (C), Figure 25. Metal substructure and slag are located, respectively, above and below this figure.

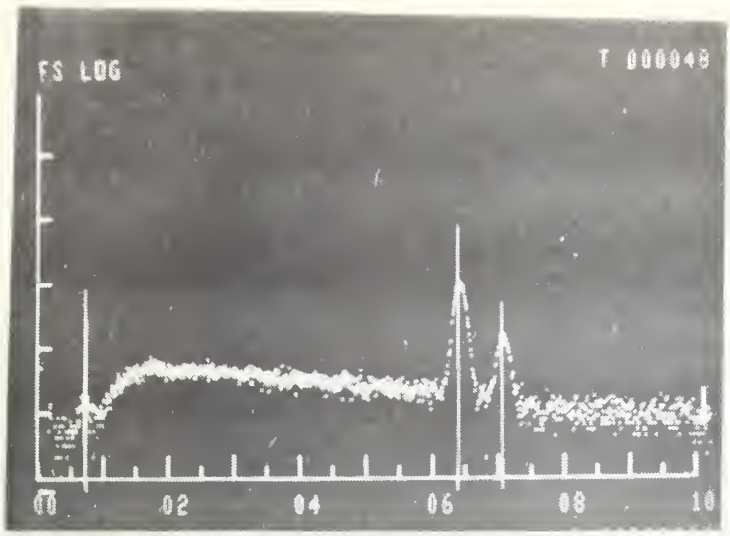

Figure 28B. EDX spectrum for brightest areas, Figure 28A; Fe (iron oxide) only.

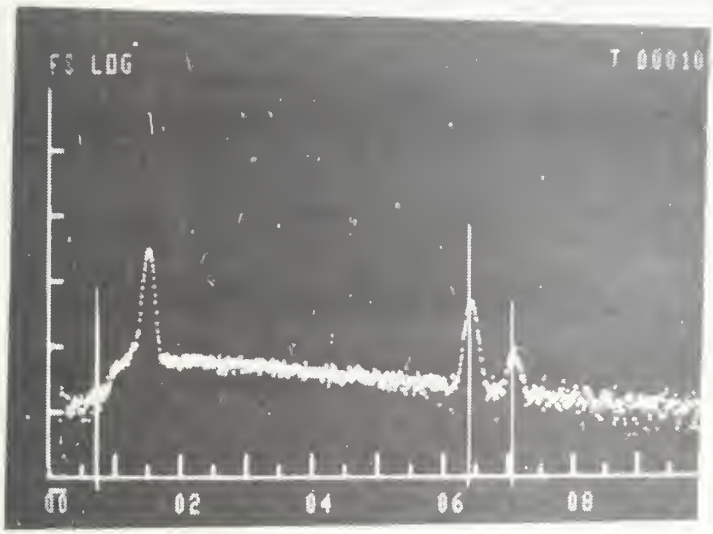

Figure 28C. EDX spectrum of darker areas, Figure 28A; Al (strong) plus Fe (superimposed vertical markers).

Figure 29. SEM micrograph (200X) of the ceramic (1) - slag (3) interface (2) for an MIT cathode (see text).

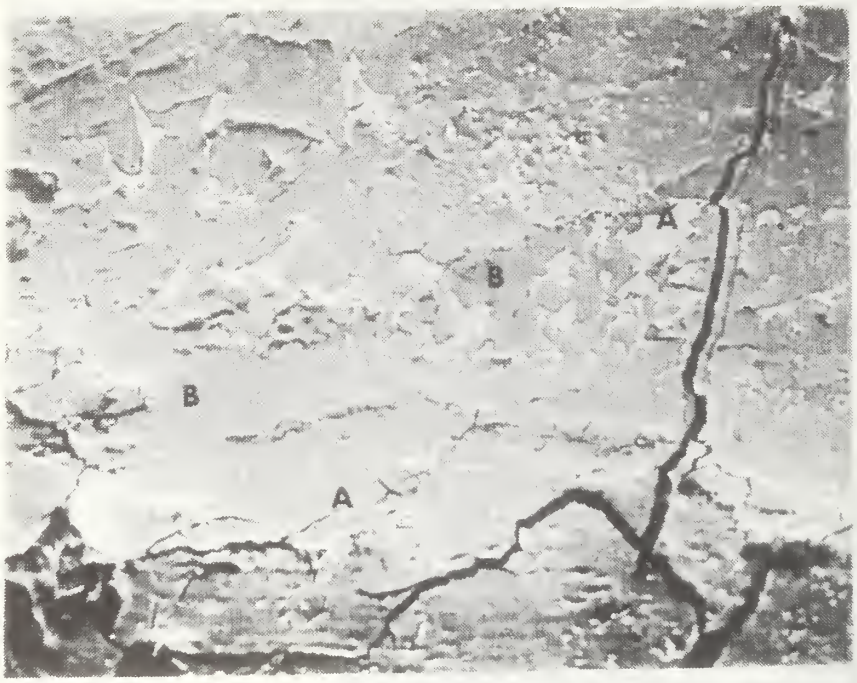

Figure 30A. SEM micrograph (450X) of slag, Figure 29, showing domains (A) within groundmass (B).

Figure 30B. Lower EDX spectrum for domains A, Figure 30A; predominately Fe plus traces of Mg, Al, K. Upper spectrum for groundmass (B), Figure 30A; Al, Si, K (strong), Fe.

Figure 31. SEM micrograph (90X) of MIT cathode. M = Fe metal fin; 1 = slag with inclusions (see Figures 29, 30A); 2 = slag/ceramic interface; 3 = Fe/Al-oxide ceramic; 4 = $MgAl_2O_4$ insulation; 5 = Ca-rich domains; 6 = Fe-rich zones and intrusions; 7 = zone of ceramic within slag.

Figure 32A. SEM micrograph (2000X) of areas (6), Figure 31.

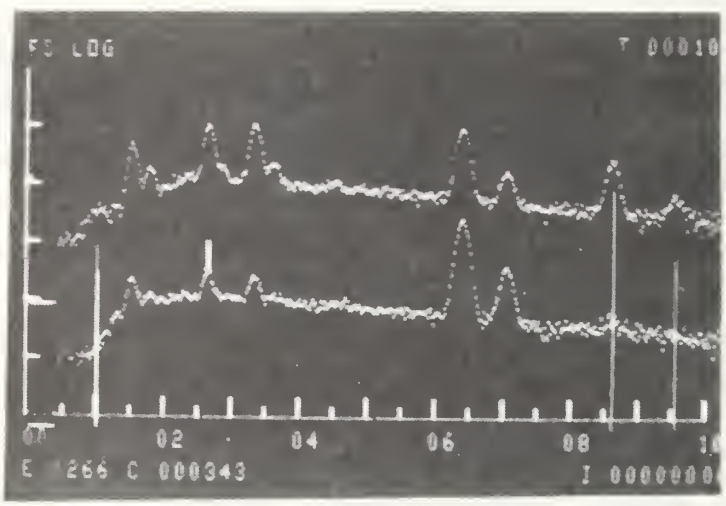

Figure 32B. Lower EDX spectrum, phase (1), Figure 32A; traces of Al, Si, Cl (?, short vertical marker), Fe dominant. Upper spectrum, phase (2), groundmass, Figure 32A; Al, Si, Cl (?), K, Fe plus Zn (long vertical markers).

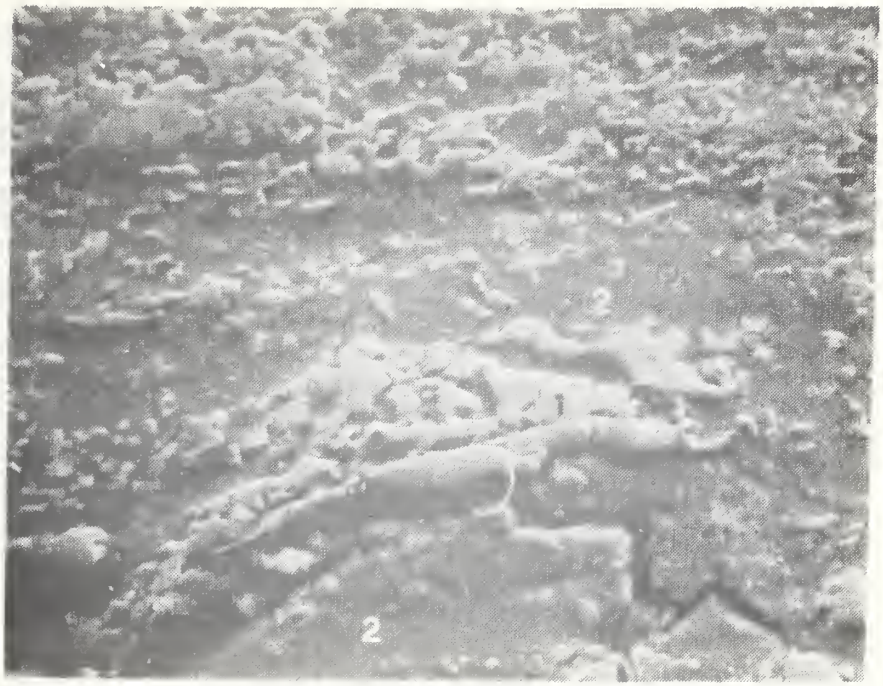

Figure 33A. SEM micrograph (900X) of slag/ceramic interface (2), Figures 29 and 31.

Figure 33B. EDX map, FeKα, for Figure 33A.

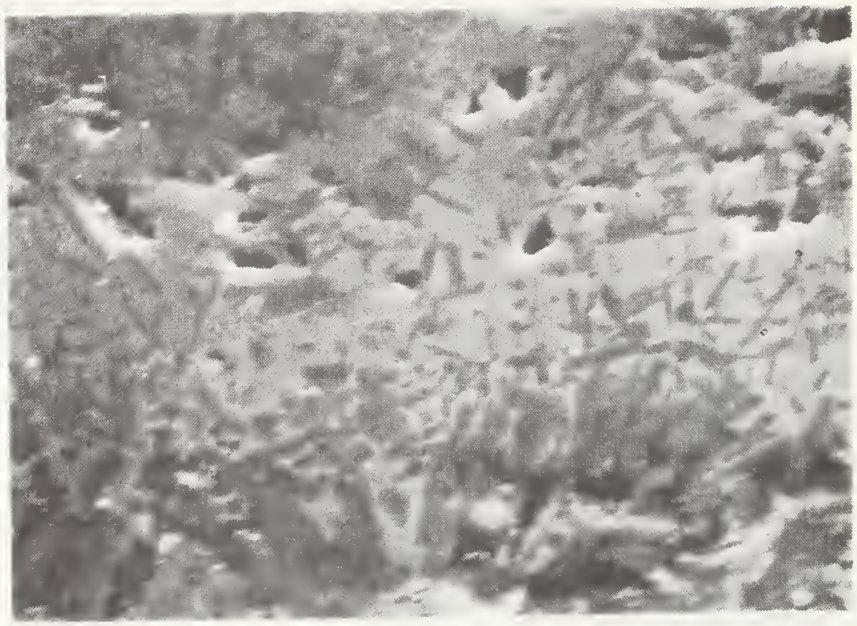

Figure 34A. SEM micrograph (2000X) of ceramic adjacent to interface (2), Figure 29. Microscope difficult to focus here.

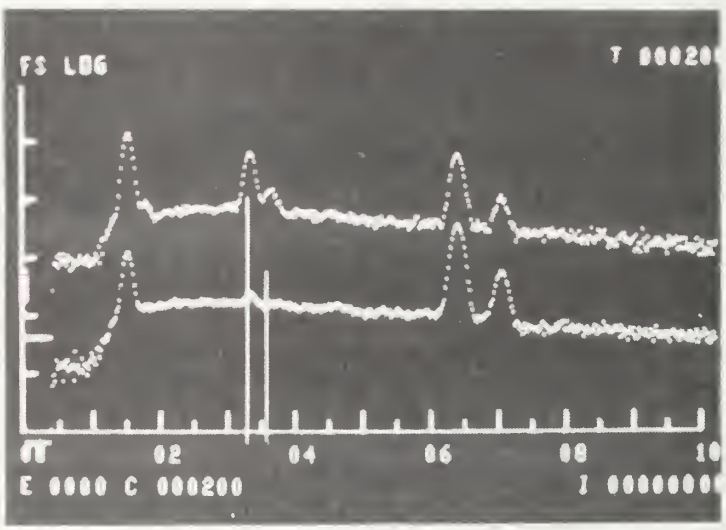

Figure 34B. Lower EDX spectrum, bright domains, Figure 34A; Al, trace K, Fe (strong). Upper spectrum, darker intergrowths, Figure 34A; Al (strong), (Si-trace ?), K (vertical markers), Fe.

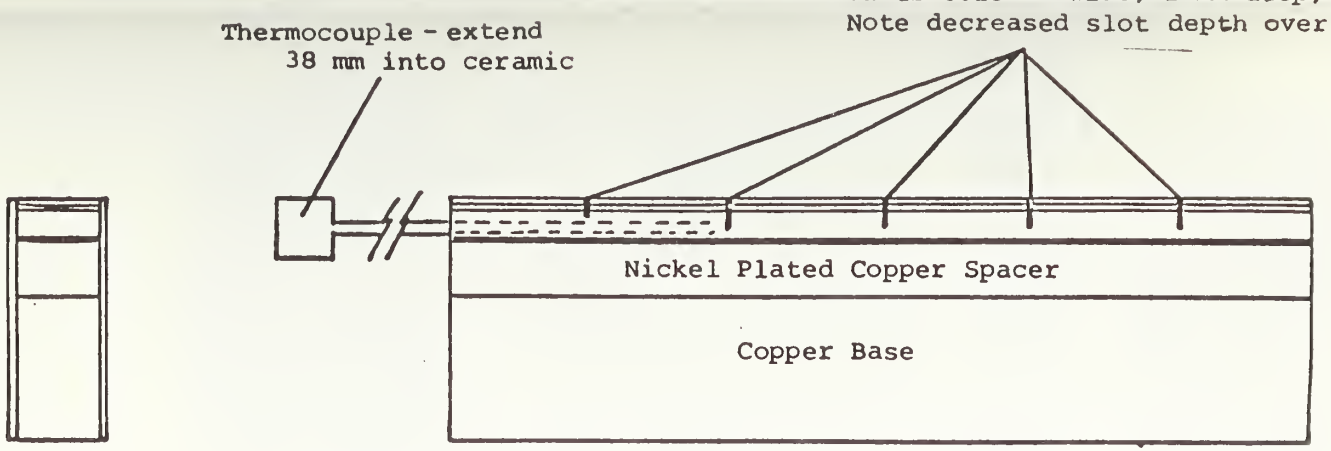

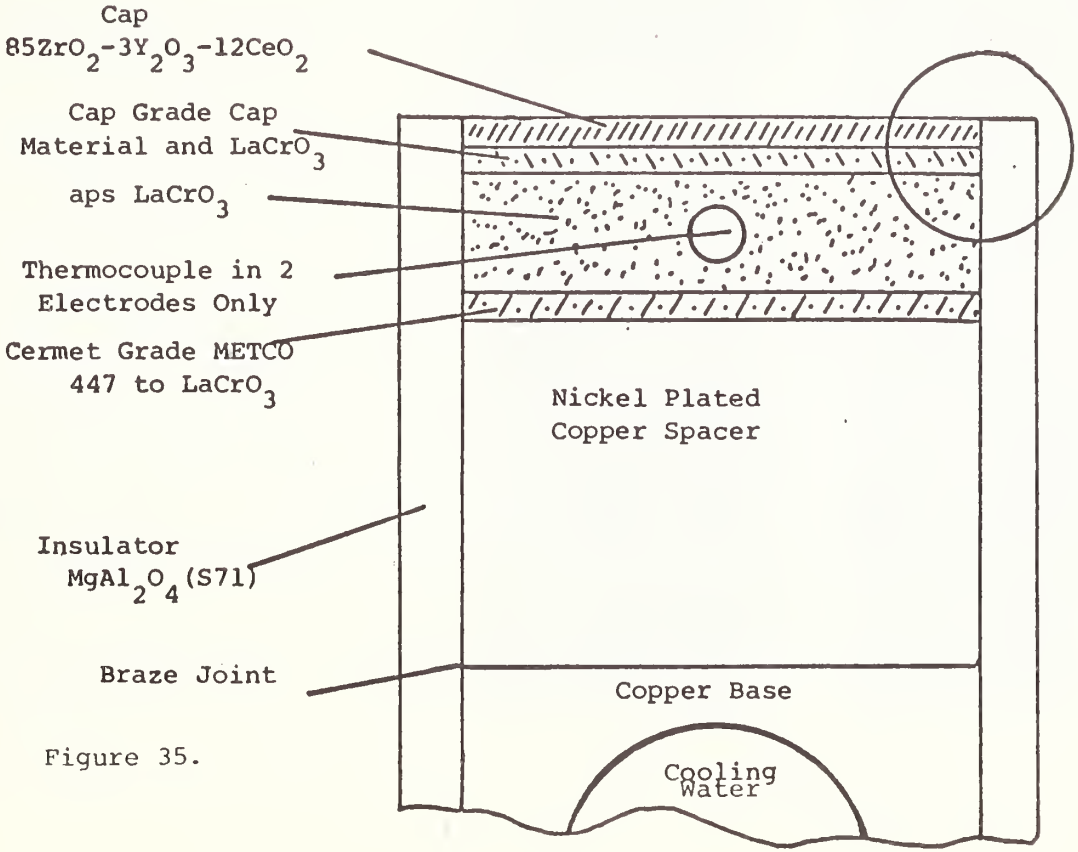

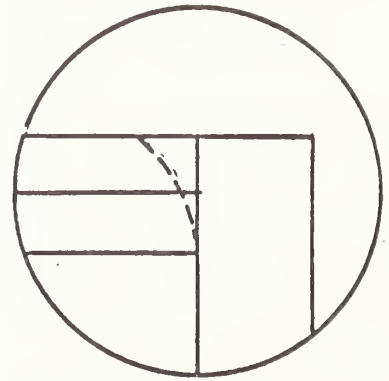

Insert showing possible electrode roll off and fill with insulator

Figure 35.

3. Proof-Test I for U-02 Experiment Phase III (T. Negas, L. P. Cook and W. R. Hosler)

A. Electrode Systems and Component Materials

The first proof test of candidate electrode systems for Phase III of the U-02 experiment series was carried out at Westinghouse Electric Systems Test Facility (WESTF) on October 10 and 11, 1977. The experiment was designed primarily to verify several electrode system designs incorporating several materials and attachment mechanisms. The heat fluxes and temperature gradients through the electrode systems were similar to those expected in the U-02 test facility.

Fig. 1 (p. 84) is a schematic diagram showing the nine electrode pairs included in this test with one upstream guard and two downstream guards composed of $LaCrO_3$. These guard electrodes were supplied by Westinghouse.

The first three upstream pairs were composed of magnesium aluminate ferrous ferrite attached to a "flex bed" lead-out. This attachment and flex bed lead-out is propriatary and was supplied by General Electric Company. The next three anode systems (downstream from the GE electrode pairs) were composed of arc plasma sprayed magnesium aluminate ferrous ferrite (MAFF-31) spray-attached to a Brunsbond pad which was, in turn, brazed to the copper base. These were prepared by Technetics Division of the Brunswick Company under the guidance of Westinghouse. The three corresponding cathode pairs were again composed of arc plasma sprayed MAFF-31 attached through a nickel-MAFF-31 cermet to a Brunsbond pad which was brazed to the copper base. These systems were prepared by Arc Plasma Spray Materials, Inc. under the guidance of Westinghouse.

The last three downstream electrode system pairs were composed of two different materials and attachment mechanisms. One design included a nichrome mesh base while the other used a Brunsbond pad base. In each case the lower portion (cold side) of the mesh contained no ceramic but was attached to copper via a gold/nickel bond. Further toward the hot side the ceramic was integral with the mesh and finally pure ceramic material served on the plasma side. 9.7 Y_2O_3 + 16.3 CeO_2 + 74 HfO_2 ceramic was used with the nichrome mesh while 18 CeO_2 + 82 HfO_2 ceramic was used with the Brunsbond pad (mesh composed of Hoskins alloy 875). Electrodes 108, 109, 208, 210 were composed of Y, Ce, Hf ceramics while 110, 209 were composed of the Ce, Hf ceramics only.

B. Post Test Handling of the Electrode Modules

Each module (anode and cathode) was cut through the center in a plane parallel to the plasma flow and perpendicular to the plasma-electrode surface. Half of each module was given to Battelle NW and half was retained by NBS for analysis. Subsequent sectioning was done as shown in Figure 2. Disposition of the sectioned electrodes is also shown in the figure. All cutting was done after the systems had been potted in an epoxy resin, using a diamond saw of appropriate diamond concentration with water as a coolant. Not shown in Figure 2 is the sectioning of the individual slices after polishing for examination using the scanning electron microscope. Figures 3 and 4 are representative anode and cathode wall cross sections, respectively. These slices illustrate the arrangement of materials for purposes of orientation. The photographs were taken of the surface as cut.

C. Analytical Methods

This proof-test was concerned with electrode design, performance and endurance under conditions closely approximating those for U-02. Implicit were the availability and development of candidate materials which were selected and "woven" by various contractors into a "best-effort" configuration. Thus, the test did not strictly involve development and optimization of materials. For this reason, and as specific pre-test electrodes were not available for comparison purposes, our characterization efforts are limited to gross features rather than being detailed and comprehensive. Furthermore, the $LaCrO_3$-based "guard" electrodes (one upstream and two downstream), although in relatively good condition, were not scrutinized. Proof-test II for U-02, Phase III will emcompass these materials whereupon they will be subject to analysis.

Electrodes were investigated using SEM/EDX and x-ray diffraction methods. Low magnification (<500X) optical micrographs can be effectively used for orientation purposes and for detecting gross features such as bond detachments. For this set of electrodes, most important chemical/microstructural features could be observed only at magnification greater than ~500X. Low magnification orientation-type photographs provided, herein, are not intended to convey scientific evidence.

D. General Electric Electrodes

1. The overall integrity of both the anode and cathode assemblies appears to have been fairly well preserved in spite of extensive corrosion. An estimated 35 - 50% corrosion has occurred at the anode and 20 - 35% at the cathode, using $LaCrO_3$ electrodes 101, 201 for comparison and assuming all electrodes were at the same level at start-up. Penetration of seed has caused severe weakening of the interior of the ceramic at the cathode; seed has penetrated the interior of the anode only along cracks, some of which appear to have healed themselves. Cracking has occurred in all electrodes near the base along the tips of the (Ni,Cu) lead-outs.

2. Recrystallization of a zone of spinel a few mm in from the surface occurs to a certain extent in all electrodes and appears to be associated with a significant K content -- possibly this represents the K_2CO_3 condensation isotherm. Such recrystallization is locally much more intense in the anode, where evidences of a K, Fe-rich intergranular phase were noted.

3. The insulators were also subject to alteration by (K, Fe) but primarily along the deeper parts where cracking has occurred. The anode insulators underwent corrosion by melting in the upper parts and were bridged by a (Fe, Ni)-containing phase (a spinel?).

4. Untested specimens were not available for comparison, and certain features seem best related to the initial fabrication process: narrow zones of Ca and Mg-rich oxides at the junction between electrode and insulator; interspersed (La, Zr) oxides within the electrode spinel in a regular zone several mm from the surface; Si in the electrode spinel.

5. Melting is difficult to estimate and interpret because of the complexity of the interaction with upstream components; Zr has obviously reacted with the spinel, possibly to produce a melt. The fact that shut-down was gradual further complicates the interpretation of microstructure. It is estimated that melting has occurred at one time or another in a surface zone of variable thickness $\sim$1-5 mm. Melting appears to have been much more extensive at the anode. As would be expected, spinel immediately adjacent to the plasma shows significant Fe-depletion.

E. Argonne Electrodes

1. Pre-test, virgin electrodes were not available for purposes of comparison (especially for the interpretation of thermochemical/electrochemical phenomena).

2. The microstructure, microchemistry and macro-scale phase distribution particularly for the HfO_2-Y_2O_3-CeO_2 materials varies considerably. This was done either intentionally or unintentionally during fabrication. Alumina is a significant contaminant for all of these materials. It, generally, resides within a groundmass containing other elements of the ceramic bulk composition. Within this matrix is coarser-grained ceramic. This contaminant may compromise the very refractory nature of HfO_2-based materials, contribute to a lowering of the electrical conductivity and provide reaction paths for seed. "Bloating" of these materials during electrical measurements above 1600°C (see above) could, in part, reflect formation of a fluid phase initiated by the presence of Al_2O_3. Original ceramic powders may include this contaminant or it might have been introduced during a "ball-milling" procedure prior to final fabrication.

3. HfO_2- based materials retain substantial anionic conductivity. Electrochemical reduction of the cathodic ceramic near and above the mesh was demonstrated. This does not appear to cause severe mechanical degradation in the short duration test. The melting temperature of the metal leadout and pertinent oxidation products, are particularly important for anode metal meshes combined with anion conductors. Oxidation of the metal is accelerated due to directed oxygen-electron transfer. Anodic oxidation/dissolution of metal could lead to formation of a resistive phase assemblage around the wires and loss of thermal/electrical contact. These ultimately would result in destruction of the anode. Evidence for these events, including melting, is suggested. Platinum, by far, has been demonstrated to be superior for use with anionic, anode ceramics wherein leadouts are required at relatively high temperatures.

4. The refractory nature of HfO_2-based ceramics also is compromised by using $MgAl_2O_4$-based insulation. Melting can occur at temperatures near roughly 1700°C (but much lower with Fe-contamination). If HfO_2-based electrodes are to be operated above 1700°C (surface), a margin of safety would be provided by using MgO insulation.

F. Brunswick Anodes and Arc Plasma Sprayed Materials, Inc. Cathodes

1. Pre-test electrodes were not available for purposes of comparing post-test features.

2. Metal-ceramic bonds basically retained thèir integrity.

3. This spinel is sensitive to contamination (internal or external in origin). At elevated temperature, certainly above 1600°C, this Fe-containing material may be subjected to plastic flow and, combined with interactions with the insulation will bridge adjacent electrodes. The material is sensitive to oxidation, alteration by seed and electrochemical activity particularly at the cathodic side. The G.E. spinel is similar in many respects. However, of electrodes fashioned from plasma sprayed spinel, this particular set out-performed all others tested in other facilities utilizing clean fuel. This reflects the excellent design considerations provided by Westinghouse.

4. Microstructure and microchemistry at the anodic side reveal considerable evidence for melting/recrystallization.

G. CONCLUSIONS

An extensive report with 74 figures has been submitted to Westinghouse Corp. but will not be reproduced herein. A summary, however, of pertinent conclusions is provided below.

Bonding among various components associated with leading-out ceramics to a metallic substructure survived this test remarkably well. Designs were well-conceived, utilizing available thermal and electrical conductivity and thermal expansion data effectively. Only the downstream electrodes (8 through 10) showed evidence for significant detachment between metallic components. All ceramics revealed some fissuring above the metallic leadouts.

During the test, heat fluxes ran consistently higher for the anode. Post-test inspection of the anode wall surface suggested deep erosion particularly of the last six materials including the terminating two, $LaCrO_3$-based guard electrodes. Although morphologies and microchemistry, consistent with melting/recrystallization are obvious for both electrode walls, "melting" phenomena are more extensive at the anode. Furthermore, ZrO_2:Ca as a contaminant from upstream is much more evident at the anode wall. Available evidence suggests that anodes 208, 209, and 210 were subjected to extensive surface melting, perhaps accelerated by interaction of the HfO_2-based materials with Fe-containing upstream electrodes. Conceivably, zirconia from upstream more easily could be entrapped, digested and retained within anode areas containing an extensive, pre-existing fluid phase. Hence, the apparent partitioning between electrode walls. Other explanations for the phenomena observed at the anode must reside in unusual plasma conditions which are beyond the realm of these analysts.

This brings up a question involving the general philosophy of materials testing. Within this report, it is quite clear that in a test involving a multitude of differing materials, the probability of degradation due to interactions among adjacent (but unlike) materials and upstream constituents is maximized. Ideally, similar (and basically compatible) materials should be incorporated within one test section. Apparently, Proof-test II for U-02, experiment (Phase III) will have such a configuration.

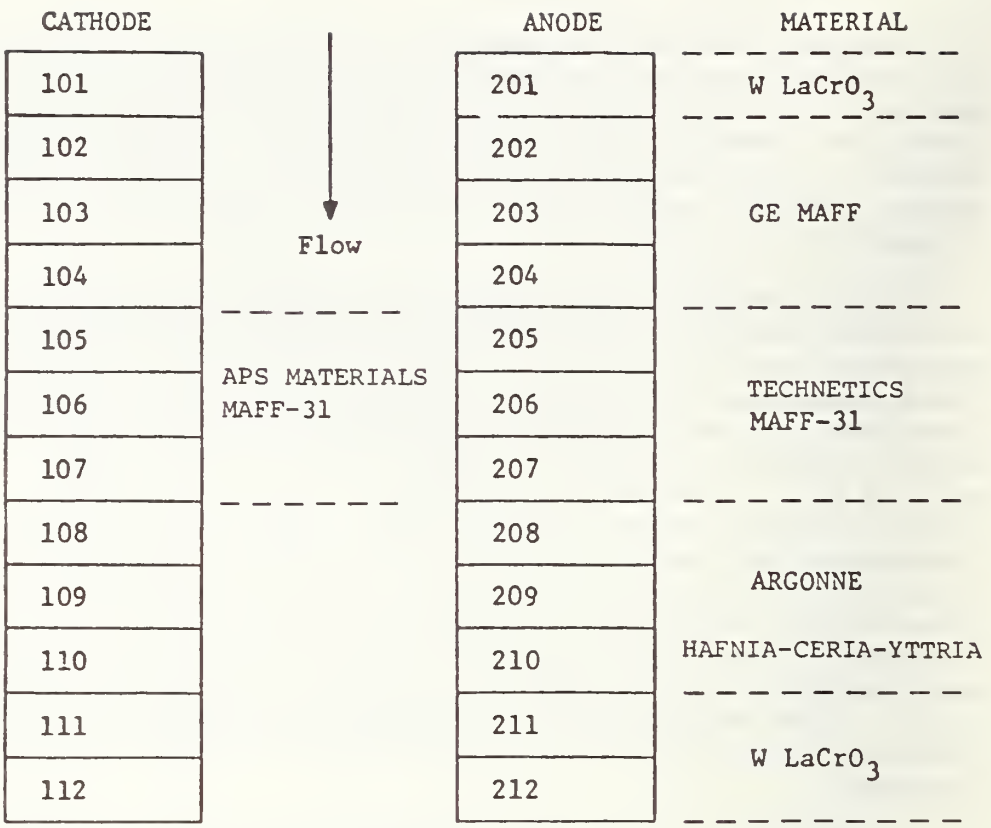

Figure 1. SCHEMATIC DIAGRAM SHOWING ELECTRODE PAIRS

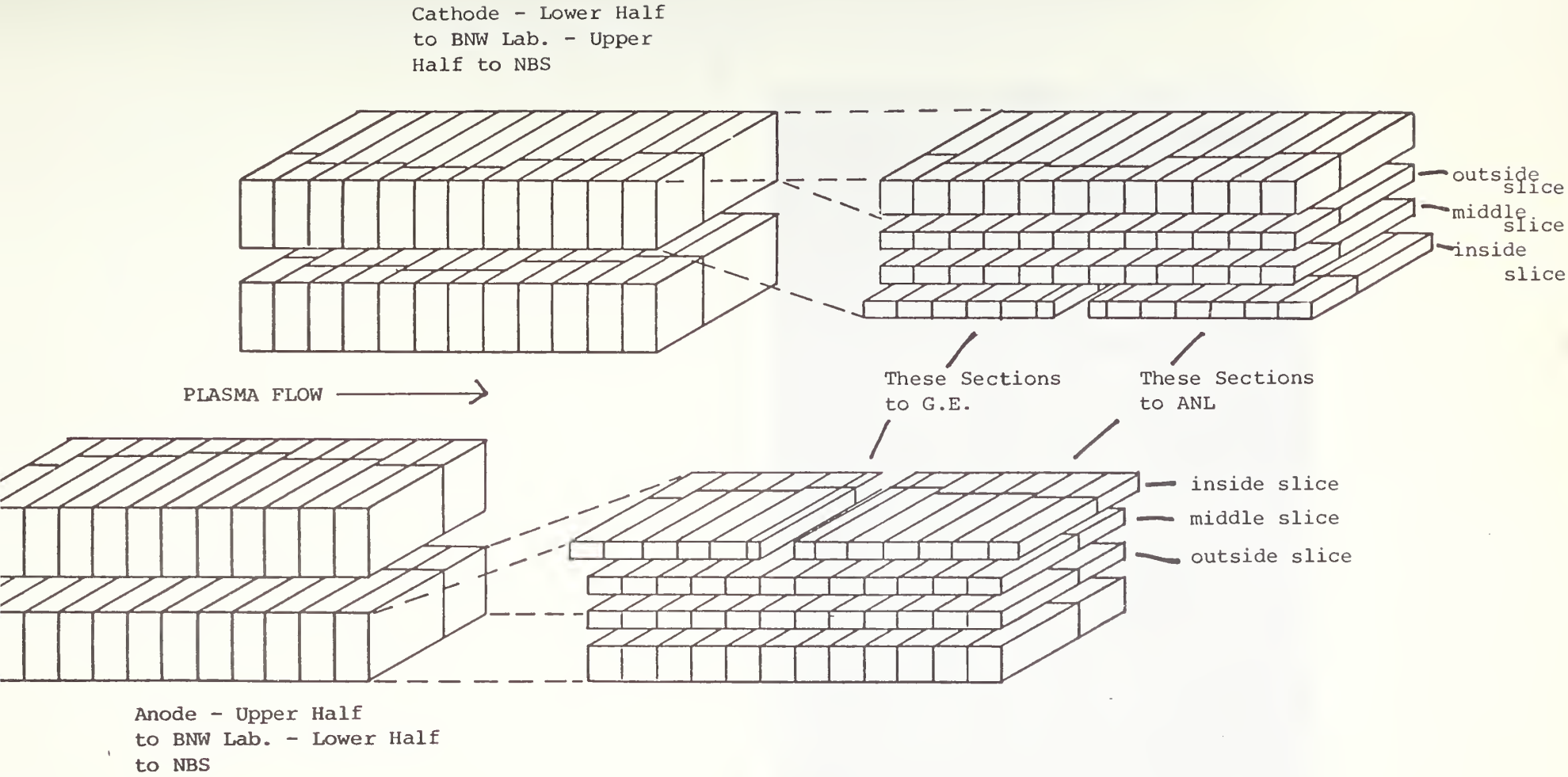

Figure 2. SCHEMATIC DIAGRAM SHOWING NBS SECTIONING OF ELECTRODES FROM PHASE III-U-02 - PROOF TEST 1

Figure 3. Representative anode wall cross sections.

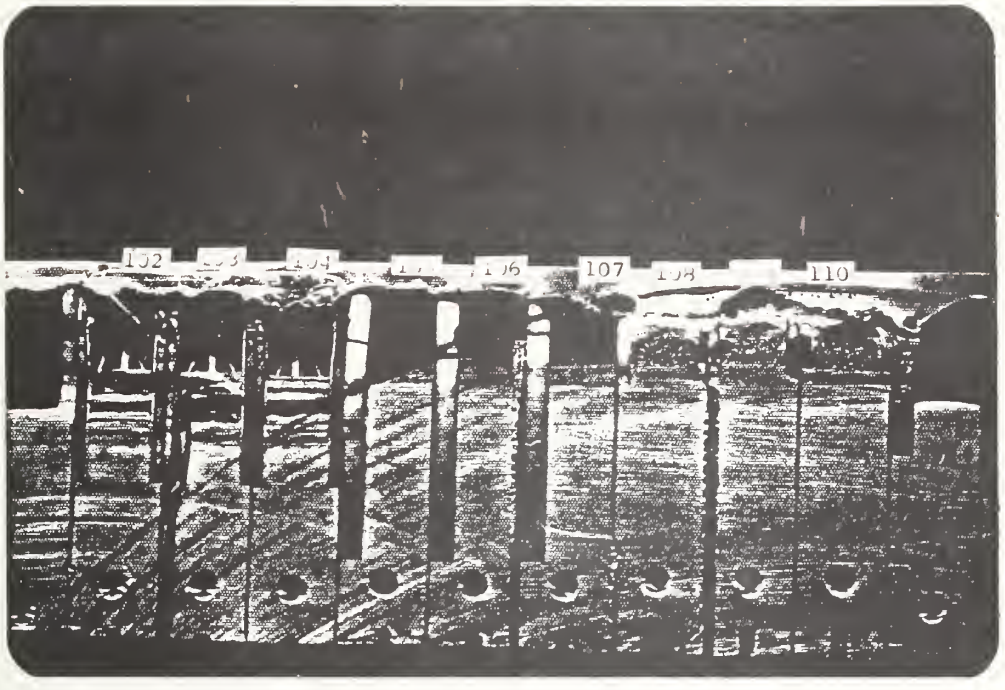

Figure 4. Representative cathode wall cross sections.

TASK L. ASSESSMENT OF STEAM PLANT COMPONENTS (J. R. Cuthill and J. Smit)

This is the 10th quarterly progress report since the initiation of Task L. The following two items will be taken up in the quarterly progress report: [1] Construction of hot corrosion test rig for the evaluation of candidate materials for the steam super heater tubing, and [2] Summary and update of requirement, test results, and material recommendations for steam super heater tubing.

Laboratory Hot Corrosion Screening Program

At the start of this quarter, as a part of Task L, a laboratory hot corrosion screening program was undertaken. The stated goals of this program are to develop a test for and to test candidate materials for downstream MHD components under conditions closely simulating anticipated service conditions.

Under Task L much work has been done thus far on evaluating the suitability of various metals and alloys to function as steam boiler tube materials in the MHD downstream super heaters. These evaluations are made on the basis of data available in the materials literature, e.g., research papers, handbooks and producer bulletins. It is from these studies that specimens are to be selected for further evaluation in the laboratory screening program. The laboratory test conditions are to be as close as possible to the calculated MHD downstream state point conditions as determined by Gilbert Associates and STD Research Corp. To perform these tests and as a first step in the execution of the screening program the design and construction of a hot corrosion burner rig was undertaken.

The burner rig, which is about 80% complete, consists of a verticle chamber housing a combustion tube, a pressurized seed or seed-slag injector, a four jet propane-oxygen burner, a specimen support and an exhaust vent. An instrument panel is mounted externally on the chamber. The chamber, constructed of steel framing and sheet aluminum, in 2.44 M high and 0.61 M square. It contains, mounted vertically along and about 1.5 M up the center axis, the 0.4 M long combustion tube which is directly under the pressurized injector. The four jet burner is positioned over the combustion tube and under the injector. The specimen holder is located immediately beneath the combustion tube. Flow meters for propane and oxygen are located on the instrument panel along side the regulator for pressurizing the injector. The exhaust vent is located in the lower third of the chamber. In operation, after gas stream ignition, the solid seed will leave the injector, follow a mid line down the four jet burner (the nozzles are pointed down the combustion tube), traverse the combustion tube in the hot gas stream and exit with the gas stream onto the specimen being evaluated.

In the next quarter the burner rig will be completed, debugged and characterized. Among other things gas temperature profiles for various propane and oxygen flow rates will be obtained as will combustion tube exit temperatures and gas velocities as a function injector pressure. With this completed, the screening program proper will begin.

Summary and Update of Requirements, Test Results, and Material Recommendation for Steam Superheater Tubing:

This is an appropriate time to summarize and update the requirements, test results and material recommendations for the steam superheater tubing because (1) there were new and encouraging test data revealed at the 1st International Conference on Materials for Coal Conversion and Utilization this past October (ref. 1), and (2) the imminent availability of a test rig to test the selected alloys under simulated steam heat-exchanger tube conditions.

The steam superheater unit in the Baseline Plant Design (Ref. 2) has a gross cross section of 45 x 30 ft. and is 32 ft. long. The 80 looped heat exchanger tubes are 3.18" O.D. and hang vertical on 6.5 inches center to center making the net cross section about two-thirds of the gross cross section for the flow of flue gas through the unit. This configuration of the superheater unit is shown schematically in Figure 1 together with the reported temperature, flue gas velocity and calculated quantity of K_2SO_4/hr-in^2 of gross cross section entering the unit. The outside surface of the heat exchanger tubing is estimated to be about 650 °C, which is even below the melting point of the K_2SO_4 so it is expected to condense out as a solid* on the leading surface of the tubing.

An attempt was made, in a recent Task L quarterly progress report, (for the period ending March, 1977), at a relative ranking of materials from best to worst on the basis absolute life expectancy based on fragmented data in the literature. At the top of the list was the INCOCLAD 671/800H. This INCO 671 (approx. 48 Ni, approx. 52 Cr) had not only been considered by the investigator but by others to be among the best if not the best alloy to resist the hot corrosion attack that would be experienced by the steam superheater tubes. It was of particular interest therefore to note the report from INCO, at the recent Materials Conf. for Coal Conversion at NBS, (Ref. 1), that in laboratory tests simulating such conditions INCO alloy 814, which has the nominal composition,

32Cr, 15.6 Fe, 3.5 Al, .35 Ti, .6 Mn, .2 Si, bal Ni

showed significantly less attack than INCO 671.

INCO considers this alloy to be a semi-commercial alloy. It is in limited production but if tubing can be obtained, it will be included in our hot corrosion test program.

References

1. First International Conf. on Materials for Coal Conversion and Utilization, (Abstract), Oct. 11-13, 1977, Gaithersburg, MD, Conf-771025 UC-90h, NTIS, Dept. of Commerce, 5285 Port Royal Rd., Springfield, VA 22161.

2. Baseline Plant System Design Description, issued June 30, 1977, a report to ERDA by Gilbert/Commonwealth Co., and STD Research Corp.

*Providing, of course, that only pure K_2SO_4 condenses; solutions between K_2SO_4, K_2CO_3 and KOH would freeze at a considerably lower temperature.

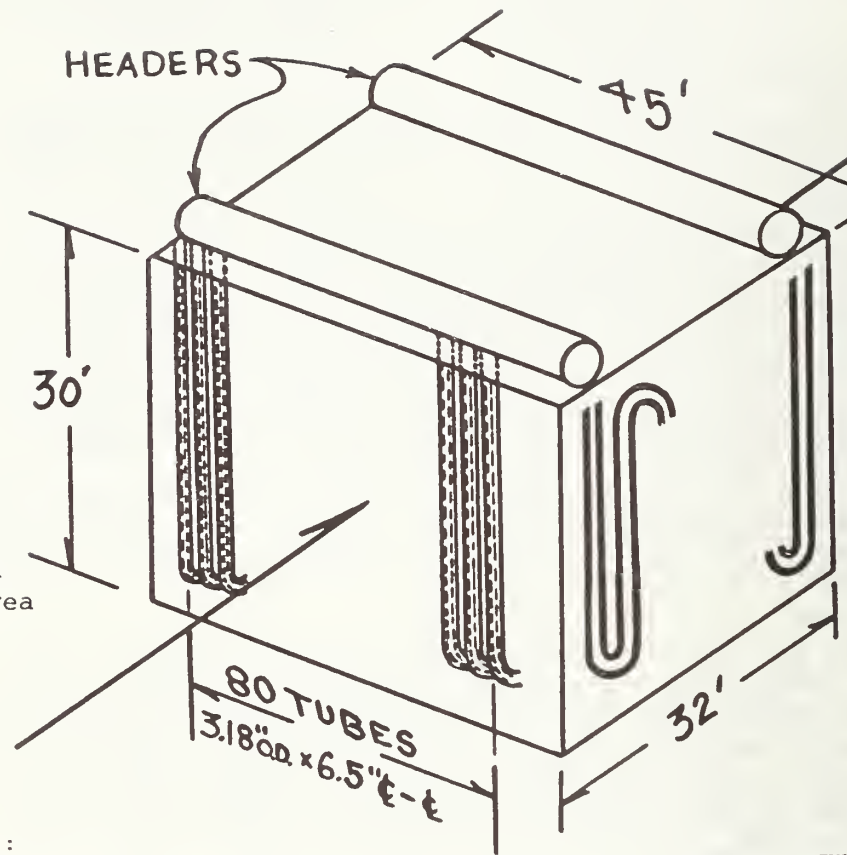

Flue Gas

locity 4400 net area
t/min) 6700 gross area

mperature: 2430 °F
(1605 °K)

ss flow rate of K_2SO_4:
.6 lb./hr-in^2 of gross area

w point of K_2SO_4:

2250 °F
(1505 °K)

Steam Temperature: 1025 °F
Outside Tube Temp: 1200 °F
(920 °F

Figure 1. Schematic of Steam Superheater Unit (Data from Baseline Plant Design, Ref. 2).

TASK M. INFORMATION AND DATA ON MATERIALS FOR MHD-POWER SYSTEMS

1. Data Center for MHD Materials Properties and Performance (H. M. Ondik, A. Perloff, and J. R. Cuthill)

The new MHD Materials Properties and Performance Data Center has the responsibility for designing and maintaining a data bank containing properties of materials for use in MHD applications. The program of the Center should provide for more rapid transfer of evaluated laboratory data and technological information, obtained by DOE-supported MHD materials research, to designers of systems, materials researchers, and operating plants. The initial sources of information to be entered in the data bank are DOE contractors' reports of test data. Data from other sources will be added as appropriate. The data in the contractors' reports will be evaluated and summarized so as to provide the users with as much hard data in as brief a form as is possible. The information in the MHD materials properties data bank can be made available to DOE and the MHD community in a variety of ways -- reports, handbooks, and by direct query of the Data Center. Designing suitable means of distributing the information is listed among the duties of the Center.

During this first quarter, the effort of the Center has been concerned with reviewing some of the contractors' reports in order to plan the Center library, become familiar with the types of information which must be handled, and define the requirements for a suitable computer system. A computer data management system is needed which is open-ended in order to provide for the addition of new types of information as well as possible multiple entries from different sources for similar information. The system must have a matrix-type storage to provide for combination searches on varying sets of items so as to be responsive to users' needs and answer a variety of questions. There are package programs available with the necessary capabilities offered by various commercial groups. These groups are highly competitive and care must be taken to choose the best system. The system must be capable of handling numerical and textual information. Possibilities for storing and retrieving information in graphical form have been investigated and the flexibility available in terms of software and equipment is very encouraging. Enough of the data are in graphical form to make this feature desirable, even necessary.

Plans: Means for distributing up-to-date MHD materials information to the MHD community in the form of brief memos or bulletins are to be investigated and a sample item submitted for DOE approval. The Center library is to be established and review of reports to begin.

Unified Numbering System

Implementation of the U.N.S. designations this quarter in the designation of MHD candidate alloys is particularly timely because the second edition of the Unified Numbering System manual (Ref. 1) was published this quarter. This second edition includes for the first time most of the alloys that are of concern to the MHD program. In the two years since the first edition was published the numbering system has been receiving wide acceptance. It now appears likely to really become the universal system of alloy designation that it was intended to be, even supplanting completely some other specification systems. The Unified Numbering System activity is a joint effort by ASTM, SAE, various metal producer trade associations, and government agencies involved in standards activities including the National Bureau of Standards.

The Unified Numbering System was introduced in some of the early Task L quarterly reports but enough of the alloys had not been entered into the system at that time to pursue its use in the MHD application. Now all of the alloys in the list of Selected Wrought Alloys from the quarterly report for September 30, 1977 have been assigned UNS designation. See Table 1, Chemical Compositions of Selected Wrought Alloys, reproduced from the previous quarterly progress report with the UNS alloy designations added.

It will be noted that each alloy designation consists of a capital letter followed by five digits. The primary series of UNS designations are given in Table 2, and the secondary division of those series that cover the alloys and grades of more than one primary metal and which are of interest in the MHD program are given in Table 3. For a complete description of the system see Reference 1.

Ref. 1. Unified Numbering System for Metals and Alloys, 2nd ed. SAE, HS1086a, ASTM DS-56A, Soc. Automotive Engrs., Inc. 400 Commonwealth Drive, Warrendale, PA 15096.

Table 1. Chemical Compositions of Selected Wrought Alloys

Item No.	Mfgr. Designation	Cr	Ni	Co	Fe	Al	Ti	Nb	Ta	Mo	W	Mn	Si	C	Other
	Stainless Steels														
1 S30400	304 S.S.	18-20	8-12	-	bal	-	-	-	-	-	-	2.0	1.0	0.08*	0.045P .03S
2 S31000	310 S.S.	24-26	19-22	-	bal	-	-	-	-	-	-	2.0	1.5	0.25*	0.045P .03S
3 S31600	316 S.S.	16-18	10-14	-	bal	-	-	-	-	2.0-3.0	-	2.0	1.0	0.08*	0.045P .03S
4 S44600	446 S.S.	23-27	0.50*	-	bal	-	-	-	-	-	-	1.5	1.0	0.35*	0.04P .025N
	Ni & Fe-Ni Base Alloys														
5 N10276	Hastelloy C-276	14.5-16.5	bal	2.5*	4-7	-	-	-	-	15-17	3-4.5	1.0*	0.05*	0.02*	0.35V .03P*
6 N06002	Hastelloy X	20.5-23.0	bal	0.5-2.5	17-20	-	-	-	-	8-10	0.2-1.0	1.0*	1.0*	1.15*	0.02La 0.2N
7 **	Haynes 556	22.0	20.0	20.0	bal	0.3	-	0.1	0.9	3.0	2.5	1.5	0.40	0.10	0.02La 0.2N 0.02Zr
8 N06601	Inconel 601	23.0	60.5	-	14	1.35	-	-		-	-	0.5	0.25	0.05	0.5Cu* 0.007S
9 N06617	Inconel 617	22.0	54	12.5	-	1.0	-	-		9.0	-	-	-	0.07	--
10 N07718	Inconel 718	17-21	50-55	1.0	bal	0.2-.8	0.9	(4.75-5.5)[a]		3.0	-	0.35	0.35	0.08	0.3Cu* 0.006B
11 N07750	Inconel X750	14-17	70 min.	-	5-9	0.4-1.0	2.5	(0.7-1.2)[a]		-	-	1.0	0.5*	0.08	0.5Cu 0.01S
12 ***	Incoclad 671/800H	see below for compositions of cladding (671) and substrate (800H)													
13	Inconel 671	48	bal	-	-	--	0.35	-	-	-	-	-	-	0.05	--
14 N08810	Incoloy 800H	21	32.5	-	46	0.38	0.38	-	-	-	-	0.75	0.50	0.1	0.38Cu -.008S
15 N08800	Incoloy 800	21	32.5	-	46	0.38	0.38	-	-	-	-	0.75	0.50	0.05	0.38Cu -.008S
16 N08802	Incoloy 802	21	32.5	-	46	-	--	-	-	-	-	0.80	0.40	0.35	0.4 Cu
17 N07500	Udimet U500	15-20	bal	13-20	4.0*	2.5-3.2	2.5-3.2	-	-	3.0-5.0	-	-	--	0.15	0.008B
	Cobalt Base Alloys														
18 R30605	Haynes HS25	19-21	9-11	bal	3.0*	--	--	--	--	--	14-16	1-2	1.0*	0.10	--
19 R30188	Haynes 188	20-24	20-24	bal	3.0*	--	--	--	--	--	13-16	1.25	0.2-0.5	.05-.15	0.05-.15La
	Low-Alloy High Strength Steels														
20	Croloy 9M	8-10	--	--	--	--	--	--	--	0.9-1.1	-	0.3-0.6	.25-1.0	0.15*	0.03P 0.03S
21 +	HCM 9M (Japan)	8-10	--	--	--	--	--	--	--	1.8-22	-	0.3-0.7	.50*	0.08*	0.03P 0.03S

* = max

a() = Nb + Ti

* = max

**Developmental Alloy

***Clad products are not given a separate UNS designation

+Foreign alloys are not included

Table 2. Primary Series of UNS Designations

UNS Series	Metal
Non-ferrous metals and alloys	
A00001 - A99999	Al and Al alloys
C00001 - C99999	Cu and Cu alloys
E00001 - E99999	Rare earth and R.E.-like metals and alloys
L00001 - L99999	Low melting metals and alloys
M00001 - M99999	Misc. metals and their alloys
N00001 - N99999	Ni and Ni alloys
P00001 - P99999	Precious metals and alloys
R00001 - R99999	Reactive and refractory metals and alloys
Z00001 - Z99999	Zinc and zinc alloys
Ferrous metals and alloys	
D00001 - D99999	Spec. mech. property steels
F00001 - F99999	Cast irons
G00001 - G99999	AISI & SAE low alloy steel
H00001 - H99999	AISI H-steels
J00001 - J99999	Cast steels
K00001 - K99999	Misc. steels
S00001 - S99999	Stainless steels
T00001 - T99999	Tool steels

Table 3. Secondary Division of Reactive and Refractory Metal Series

R00001 - R99999 Reactive and refractory metals and alloys	Metals
R01001 - R01999	Boron
R02001 - R02999	Hafnium
R03001 - R03999	Molybdenium
R04001 - R04999	Rhenium
R05001 - R05999	Tantalum
R06001 - R06999	Thorium
R07001 - R07999	Tungsten
R08001 - R08999	Vanadium
R10001 - R19999	Beryllium
R20001 - R29999	Chromium
R30001 - R39999	Cobalt
R40001 - R49999	Niobium
R50001 - R59999	Titanium
R60001 - R69999	Zirconium

NBS-114A (REV. 7-73)

U.S. DEPT. OF COMM. BIBLIOGRAPHIC DATA SHEET	1. PUBLICATION OR REPORT NO. FE-3800-13	2. Gov't Accession No.	3. Recipient's Accession No.

4. TITLE AND SUBTITLE

"MATERIALS RESEARCH FOR THE CLEAN UTILIZATION OF COAL"
Quarterly Progress Report, July 1 - September 30, 1977

5. Publication Date: October 1977

6. Performing Organization Cod: NBSIR 77-1296

7. AUTHOR(S)
Samuel J. Schneider

8. Performing Organ. Report No

9. PERFORMING ORGANIZATION NAME AND ADDRESS

NATIONAL BUREAU OF STANDARDS
DEPARTMENT OF COMMERCE
WASHINGTON, D.C. 20234

10. Project/Task/Work Unit No.

11. Contract/Grant No.
E-(49-1)-3800

12. Sponsoring Organization Name and Complete Address *(Street, City, State, ZIP)*
Department of Energy
20 Massachusetts Avenue, N.W.
Washington, D. C. 20545

13. Type of Report & Period Covered Quarterly Progress Report

14. Sponsoring Agency Code
Dist. Cat. UC-90C

15. SUPPLEMENTARY NOTES

16. ABSTRACT *(A 200-word or less factual summary of most significant information. If document includes a significant bibliography or literature survey, mention it here.)*

This progress report covers work on metal corrosion, metal erosion, ceramic deformation, fracture, erosion, and chemical degradation as related to coal gasification systems. This report also covers the failure avoidance program for DOE coal conversion pilot plants.

17. KEY WORDS *(six to twelve entries; alphabetical order; capitalize only the first letter of the first key word unless a proper name; separated by semicolons)* Ceramic corrosion, ceramic erosion, ceramic fracture, chemica degradation, coal gasification material, failure avoidance, metal corrosion, metal erosion, and vaporization processes.

18. AVAILABILITY ☐ Unlimited

☒ For Official Distribution. Do Not Release to NTIS NBS will not submit to NTIS; DOE will submit after approval.

☐ Order From Sup. of Doc., U.S. Government Printing Office Washington, D.C. 20402, SD Cat. No. C13

☐ Order From National Technical Information Service (NTIS) Springfield, Virginia 22151

19. SECURITY CLASS (THIS REPORT)	21. NO. OF PAGI
UNCLASSIFIED	
20. SECURITY CLASS (THIS PAGE)	22. Price
UNCLASSIFIED	